Stepwise Commissioning

- of a Steam Boiler

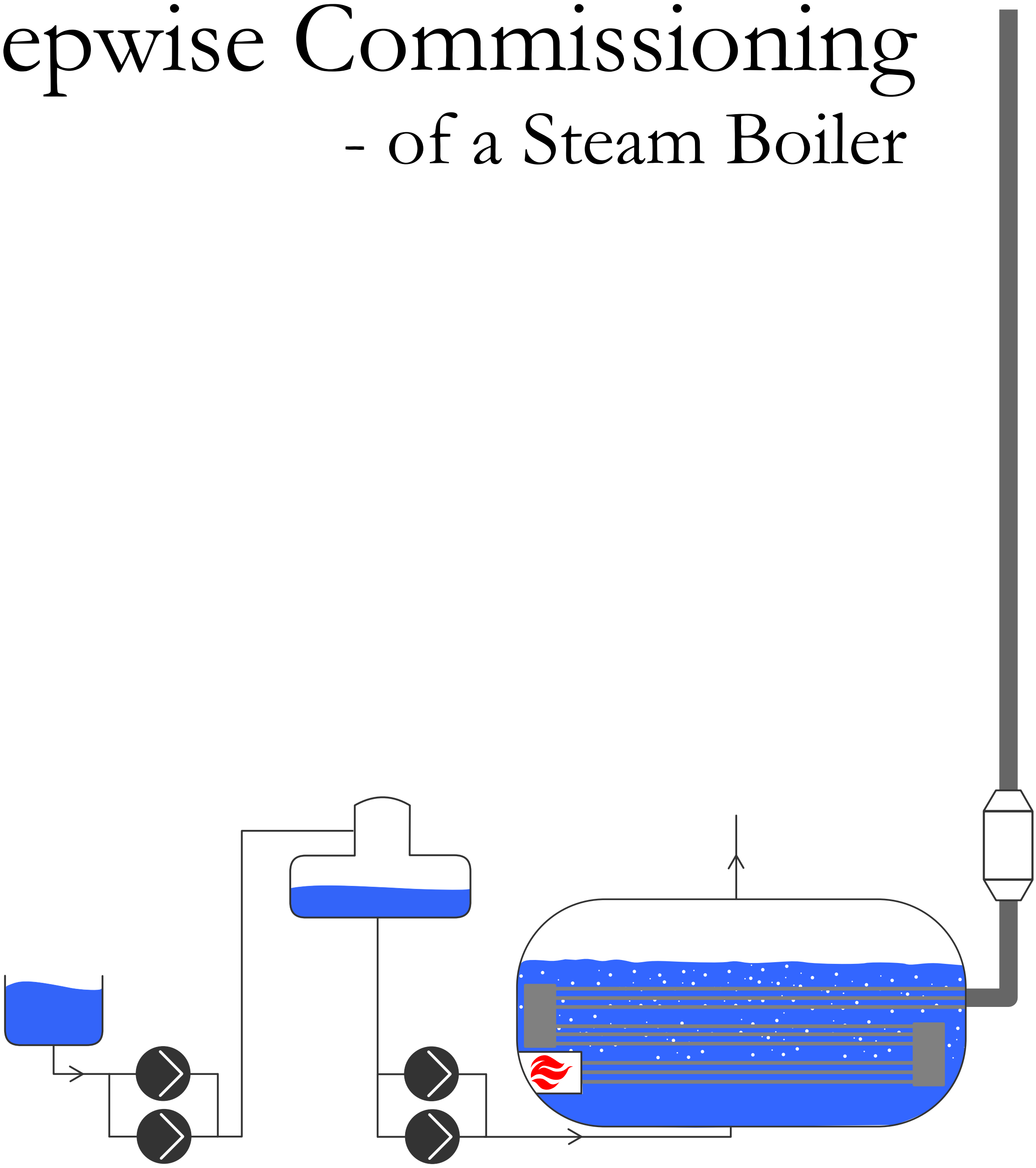

AALBORG UNIVERSITY

School of Information and Communication Technology

Control and Automation \\ Group 1036

Short Termination Master Thesis \\ June 2015

School of Information and
Communication Technology
Fredrik Bajers Vej 7
9220 Aalborg Øst
Phone 99 40 86 00
Fax 99 40 98 40
http://www.es.aau.dk

Title: Stepwise Commissioning

Project period: Feb. 2nd – June 3rd 2015.

Project group: 1036

Participant:

Simon Vestergaard Johansen

Supervisors: Carsten Skovmose Kallesøe
Jan Dimon Bendtsen
Palle Andersen

Existing copies: 5
Pages: 93
Appendices: 10 pages of appendices
Attached: 1 CD

Abstract:

This project deals with the startup of multiple input multiple output (MIMO) controllers for industrial MIMO systems. It aims to make the commissioning of a MIMO controller more straight forward by gradually commissioning it from a set of single input single output (SISO) controllers, after the system has been started.

For this purpose a stepwise commissioning strategy based on the Youla-Kucera parameterization has been developed. It allows for the gradual transition between any two controllers amongst a set of stabilizing controllers in a controlled manner while guaranteeing nominal stability. The only additional requirements imposed is that it requires a plant model and any additional stable and stabilizing controller.

To test if this strategy works in practice on a real industrial system, a case study has been conducted in collaboration with Grundfos of a steam boiler located at Danish Crown in Sønderborg. The objective was to design a feed water controller and control the water level in the steam boiler, which makes the controller a multiple input single output (MISO) controller. A model has been adopted from a previous student project which focuses on the same system. A parameter identification has been carried out with data gathered in the same project.

Based on this model, both a PI and an optimal MISO controller has been designed and used in the developed stepwise commissioning strategy. This controller has been implemented on a control platform and has been tested on the real steam boiler. It shows that the gradual stepwise commissioning between the two controllers occurs very similar to the theoretical one, which makes the developed strategy very promising.

Preface

Reading Guide

The report is structured in three parts. In each part different aspects of the project are analyzed.

- Part I Stepwise Commissioning
- Part II Case Study: Steam Boiler
- Part III Discussion

A symbol- and acronym list, which features all acronyms used in the report, is found at the beginning of the report. At the very end of the main report, a literature list is found, which contains all references used in the report. References are indicated by the Harvard method with ["author", "year"], books with ["author", "year", "page"]. In the literature list books are indicated with author, title, publisher and year. Web pages are indicated with author, title, year and URL. Web pages at the time of usage is downloaded and can be found at the attached CD in Appendix C.

Appendices are found after the main report and on an attached CD. The appendices contain calculations, explanation of software, measurement logs, system diagram, and other materials, which are not important for the understanding of the main objective of the report. The CD also contains a digital version of the report.

All figures, tables and equations are referred to by the number of the chapter, where they feature, followed by a number indicating the number of figure, table or equation in the specific chapter. Hence each figure has a unique number, which is also printed at the bottom of the figure along with a caption. The same applies to tables and equations, the latter of which have no captions, though. Appendices are referred to by capital letters instead of chapter numbers, i.e. A, B etc., equivalently followed by a sub-counter.

Acknowledgements

The author wishes to thank industrial application manager Søren Mortensen at Grundfos for sharing his insights on boiler feed systems and his assistance during the practical test at Danish Crown in Sønderborg.

Contents

Nomenclature

Acronyms

DCF	double coprime factorization
FS	flow sensor
HWL	highest permissible water level
LC	level controller
LQO	linear quadratic observer
LQR	linear quadratic regulator
LS	level sensor
LWL	lowest permissible water level
MIMO	multiple input multiple output
MISO	multiple input single output
NPSH	net positive suction head
NPSHR	net positive suction head required
PC	pressure controller
PS	pressure sensor
SCC	stepwise commissioning controller
SIMO	single input multiple output
SISO	single input single output
TS	temperature sensor
YK	Youla-Kucera
YKP	Youla-Kucera parameterization

Symbols

$\hat{y}$	estimated output	
Q	the Youla-Kucera (YK) parameter	
a	air to fuel ratio	
A	area	$\left[\mathrm{m}^2\right]$
K	controller	
I	cost	
Σ	covariance matrix	
ρ	density	$\left[\mathrm{kg/m}^3\right]$
$\mathcal{F}$	discrete time feedback law	
$\mathcal{O}$	discrete time observer gain	
$\mathcal{H}$	enthalpy	$[\mathrm{J}]$
$\hat{x}$	estimated state vector	
$\hat{e}$	estimation error	
g	gravitational constant	$9.82\left[\mathrm{m/s}^2\right]$

H	pump head	[m]	δ	small signal value	
Q	heat flow	[J/s]	h	specific enthalpy	[J/kg]
$\mathbf{R}$	input cost matrix		c_p	specific heat capacity	[J/(kg °C)]
u	input vector		$\mathbb{S}^-$	the set of all real, rational, stable and proper transfer function matrices of appropriate dimensions	
U	internal energy	[J]	$\mathbb{S}$	the set of all real, rational and proper transfer function matrices of appropriate dimensions	
l	length	[m]	$\mathbf{Q}$	state cost matrix	
L	level	[m]	x	state vector	
$\dot{m}$	mass flow	[kg/s]	T	temperature	[°C]
m	mass	[m]	τ	time constant	[s]
k	opening degree	$\left[\mathrm{kg}/\left(\mathrm{s}\sqrt{\mathrm{Bar}}\right)\right]$	$\mathcal{J}$	total cost	
P	plant		V	volume	$\left[\mathrm{m}^3\right]$
p	pressure	[Bar]			
n	sample number				

Subscripts

a	air	m,f	furnace and flue gas pipes
atm	atmospheric	$b \rightarrow s$	steam bubbles to steam
fw	feed water	b	steam bubble
fg	flue gas	s	steam
fu	fuel	$w+b$	water and steam bubble
$m,f \rightarrow w$	furnace and flue gas pipes metal to water	w	water

PART I

STEPWISE COMMISSIONING

Chapter 1

Introduction

This project deals with the startup of multiple input multiple output (MIMO) controllers for industrial MIMO systems. A description of MIMO systems as well as general control strategies will be introduced. An analysis of the general difficulties in introducing MIMO controllers into the industry will then be carried out. Based on this, a MIMO startup strategy will be selected.

1.1 MIMO systems and general control strategies

A MIMO system is characterized by having multiple inputs and outputs, while a single input single output (SISO) system only has a single input and output. The control challenge involved in MIMO system control is significant compared to those of SISO systems, as it is important to meet multiple control objectives. This is difficult due to internal cross-couplings between the inputs and outputs, which are depicted with transfer functions on Figure 1.1. This complicates the task of controlling the outputs y_1 and y_2, as they both depend on the inputs u_1 and u_2.

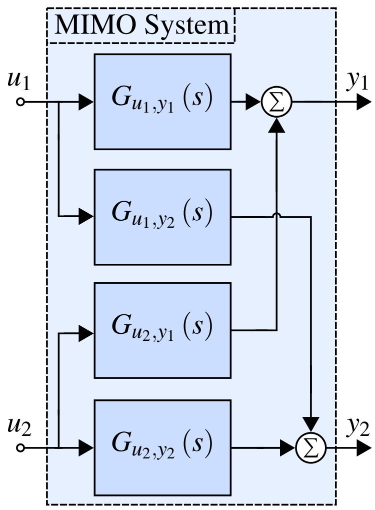

Figure 1.1: MIMO system with cross couplings.

Classical control theory approaches both MIMO and SISO systems with a divide and conquer like strategy. The system is divided into a set of input-output pairs, which individually is controlled by a SISO controller that have no knowledge of the inputs and outputs of the other controllers. This is depicted in Figure 1.2.a, where the MIMO system is divided into two input-output pairs. This ultimately leads to decreased performance, as the individual controller introduces disturbances to the other controllers through the cross-couplings. Each individual SISO controller must be additionally better at suppressing disturbances generated by the other controllers, which results in decreased system performance.

MIMO controllers approach the same control problem in a global fashion, where all the system inputs are determined from the system outputs as depicted on Figure 1.2.b. This allows for direct compensation of the cross-couplings by design. Hence, MIMO controllers are the better choice in terms of performance.

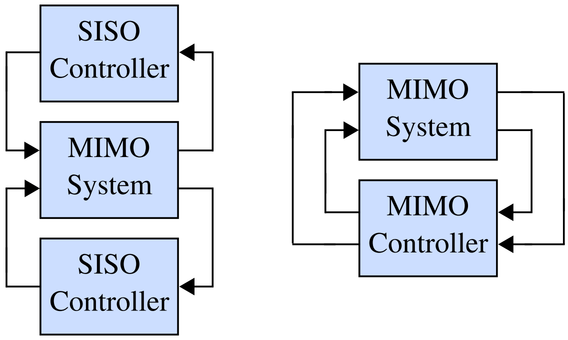

Figure 1.2: SISO (a, left) and MIMO (b, right) controller strategy.

However, MIMO controllers have a naturally higher development cost, as they must be model-based in order to predict and compensate for the cross-couplings. This also results in a more complex controller, which require specialized knowledge and experience in order to design and tune such systems.

1.2 Difficulties in introducing MIMO controllers in the industry

Most MIMO systems in the industry are controlled by a number of SISO controllers as described by the classical control theory approach. This is believed to primarily be due to two reasons:

Reason 1. The majority of implemented controllers in the industry are PID based, which is a SISO type controller. Consequently, the technicians maintaining MIMO systems are familiar with standard SISO controllers.

Reason 2. The full single-loop control system can be set into operation sequentially loop by loop, which is perceived as a safe commissioning procedure compared to setting the whole system into operation in one step.

The increased development cost of MIMO controllers will not be considered in this analysis, as it is relative to the added value of a MIMO controller for the specific system.

The conditions of **Reason 1** can be satisfied by making MIMO controllers simpler to operate and maintain. To understand the conditions of **Reason 2**, further analysis into the typical startup procedures of MIMO control systems need to be investigated. Lets consider two startup scenarios, namely when the system have to be started from a powered off and initialized state. An initialized state refers to the system being close to its intended operating point, while a powered off state refers to the system having settled (steady state) after being powered off. These scenarios will be called hot startup and cold startup, respectively.

In practice, a cold startup procedure is often empirically established from guidelines and regulations specific to the individual system. This is perceived to be motivated by a desire for the technician to be in charge of the startup phase, as it is considered safety critical especially for large scale industrial systems.

For instance, the startup phase of a steam boiler puts great thermal stress on the boiler itself due to large internal temperature differences, compared to that of its normal operation. This drastically decreases the lifespan of such a system and promotes mechanical failures. Consequently, the focus of the startup phase of steam boilers is placed on minimizing thermal stress, which is done by a slow and constant rate of startup [Vedsted, 2008,pp. 279-298, 394]. It has the added bonus of giving the technician room to systematically evaluate the state of the system, and abort if signs of errors appear.

Hence, it is considered very difficult to automate a cold startup procedure, as it requires human interaction and special attention to different aspects compared to normal operation. On the other hand, it is substantially more straightforward for a controller to perform a hot startup, as it basically is a matter of turning the controller on. For this reason, the focus will be to introducing MIMO controllers as the primary controller, in a hot startup scenario. To satisfy **Reason 2** and have a control system that sequentially activates loop by loop, two cases are considered:

Case 1. The SISO controllers are sequentially activated before the MIMO controller is turned on.

Case 2. The system is manually controlled in open loop before the MIMO controller is sequentially activated.

The difference being which controller performs the sequential activation, in **Case 1** it is the SISO controllers and in **Case 2** it is the MIMO controller. One way of sequentially activating a MIMO controller is to mimic the sequential activation of SISO controllers, as explained in Example 1.1.

Example 1.1 (Sequential MIMO activation)
This can be illustrated on Figure 1.3, where a two input and two output MIMO system is controlled by two SISO controllers (left) or a MIMO controller (right). The two SISO controllers form the two loops A and B. The MIMO controller is activated in the same way as the SISO controller, by adding the corresponding actuators and sensors for the loop to the MIMO controller. This might require a dedicated MIMO controller depending on the activated loops. However, it has the same operational interface as the SISO controllers, which plays very well with **Reason 1**.

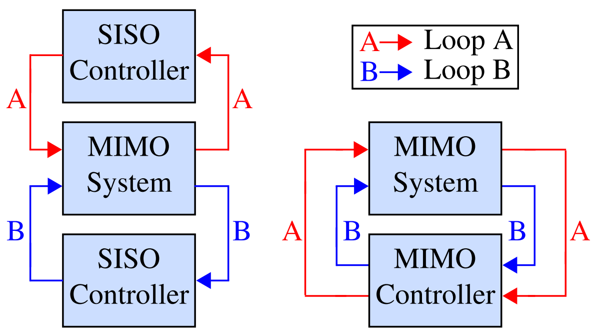

Figure 1.3: SISO (a, left) and MIMO (b, right) sequential controller activation.

Lets assume that a cold startup is performed before the hot startup procedure is engaged. This allows for different initial system states for the hot startup, such as:

- The system is controlled by a series of SISO controllers.
- The system is manually controlled in open loop.

On Figure 1.4, the discussed cold startup elements and the two MIMO incorporating cases are depicted. As **Case 2** works for both cases, it will be favored over **Case 1**. It requires an upgrade of an existing SISO-controller-based MIMO system to a MIMO controlled one, which is not a new concept and has been demonstrated with great success. For instance, [Mortensen et al., 1998] describe a MIMO controller upgrade of a boiler controller for a power plant by complementing the existing SISO controllers.

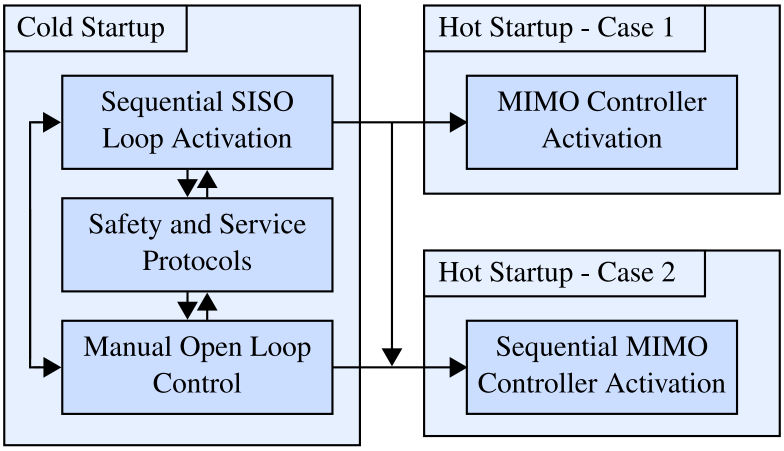

Figure 1.4: MIMO controller startup strategies.

Regardless of the selected strategy, it requires switching of controllers, which in turn requires the transition itself to be carried out in a controlled manner. For this reason, possible controller switching strategies are investigated.

1.3 Controller Switching Strategies

In classical control theory, controller switching is done through bumpless transfer, which is a reference handling scheme. The reference is gradually moved from the initial system state at the switch, to the desired reference state, which ensures a smoother transition.

Another approach to such a problem is to apply the Youla-Kucera parameterization (YKP), which can ensure stability throughout the transition. According to [Bendtsen et al., 2013] it allows for a smooth transition between two different controllers, as it retains closed loop stability throughout the transition, which should not cause large transient responses like the bumpless transfer. If the system is open loop stable, a switch from no controller to a controller is possible. Hence, it can be used in conjunction with both of the hot startup scenarios if the system is open loop stable. The transition is controlled by a single scalar parameter, which provides the added benefit of making the transition reversible. This allow for a stepwise commissioning of a MIMO controller loop by loop, by gradually turning each loop on in a hot startup scenario.

This is a rather lucrative property, as it might allow for early instability detection, in case a transition from a stable to a non-stabilizing controller is unknowingly carried out, due to modeling errors ect. The idea being that the stability margins would gradually deteriorate throughout the transition, until the system eventually becomes unstable. This is a very common situation during initial controller deployment, where it is not yet certain if the controller stabilizes the system in practice. Applying this technique, could make the initial deployment more secure, as it is not an all-in attempt.

Additionally, the transition parameter could be used as a tuning parameter. It might give skeptical technicians a reason to give a MIMO controller a first chance, as the system can be tuned through a single parameter. After all, SISO systems are favored because of their simplicity, and this would certainly simplify the required tuning efforts of MIMO controllers.

The YKP has previously been used in Plug-and-Play Control, where additional sensors or actuators are added to an existing control system during operation, and is described in [Bendtsen et al., 2013]. However, the concept of using it for controller switching has not yet been investigated in practice.

These are just some of the possible and still unexplored benefits of the YKP. And for these reasons, the YKP will be used for the controller switching over the conventional bumpless transfer.

1.4 Project Outline

In this section the outline of the project will be specified based on the results and decisions of the previous analysis.

The remaining part of the report is dedicated to answering the following problem statement:

> **Is it possible to perform a sequential MIMO controller activation of a MIMO system, from a SISO controlled system using the Youla-Kucera parameterization?**

To help answer this question, a "generic" industrial MIMO system will be used as a case study. The requirements for the case study are that it is a real and accessible system, which allows for both theoretical and practical evaluation. Furthermore, the dynamics of the case study has to be well established to alleviate the efforts of modeling the system as this is not the prime focus of this project.

This project is done in collaboration with Grundfos, which has kindly provided access to a steam boiler located at Danish Crown in Sønderborg. As a steam boiler is a MIMO system with known dynamics, it is an obvious candidate for the case study. To answer the problem statement, the following steps are carried out:

- Stepwise Commissioning design with the Youla-Kucera parameterization.
- A description of the steam boiler and the challenges in controlling and starting it, along with a model and a parameter identification.
- Stepwise Commissioning design for the steam boiler.
- Practical test on the real steam boiler at Danish Crown.

Chapter 2

Stepwise Commissioning Design

2.1 Stepwise Commissioning Introduction

In this chapter a stepwise commissioning strategy is developed. The main objective is to design a controller $K(\gamma)$, where the transition parameter $\gamma \in [0;1]$ controls the transition from an initial controller K_0 to the controller K_1 as illustrated on Figure 2.1. When $\gamma = 0$ the initial controller K_0 is active and when $\gamma = 1$ the controller K_1 is active. The intention is to gradually change the controller by increasing γ from 0 to 1. But how should one approach the remaining part of the transition, denoted by $\gamma \in]0;1[$, while still ensuring closed loop stability? One way this can be accomplished is through the Youla-Kucera parameterization (YKP), which will be investigated in this chapter.

To do this, the concept of the YKP and how double coprime factorizations (DCFs) are calculated are introduced in Section 2.2 and Section 2.3. These concepts are considered preliminaries, which is described and reflected upon to help the reader understand the proposed method. Based on these concepts, a stepwise commissioning strategy using the YKP will be developed in Section 2.4. In Section 2.5 this strategy will be expanded to a sequential stepwise commissioning strategy, of which some practical considerations are made in Section 2.6. Lastly, to give a notion of the dynamics of the proposed method, an example of a generic multiple input multiple output (MIMO) system is carried out in Section 2.7.

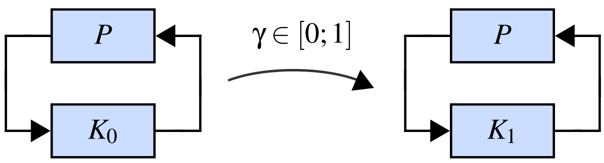

Figure 2.1: Controller changing through the transition parameter $\gamma \in [0;1]$.

2.2 Youla-Kucera parameterization

The main idea behind the YKP is to characterize all closed loop stabilizing controllers of a plant. This might appear as a difficult task, and for this reason Example 2.1 will give a notion as to how this can be done.

Example 2.1 (Motivational Example)
Lets try to define all the closed loop stabilizing controllers of the stable and proper single input single output (SISO) plant $P(s)$ using [Anderson, 1998, pp. 1485-1486]. The generic closed loop system $G(s)$ of the system depicted on Figure 2.2 is defined by

$$G(s) = \frac{y(s)}{r(s)} = \frac{C(s)P(s)}{1+C(s)P(s)} = \frac{C(s)}{1+C(s)P(s)}P(s) = Q(s)P(s). \tag{2.1}$$

As the product of any two stable and proper transfer functions are stable, the stabilization problem amounts to finding a controller $C(s)$ that stabilizes

$$Q(s) = \frac{u(s)}{r(s)} = \frac{C(s)}{1 + C(s)P(s)}. \tag{2.2}$$

Lets assume a stable and proper $Q(s)$ is known, which permits a stabilizing controller $C(s)$ to be obtained by solving for it from (2.2), which equals

$$C(s) = \frac{Q(s)}{1 - P(s)Q(s)}. \tag{2.3}$$

This transfer function can be shown to be proper and stabilizes the closed loop system $G(s)$ if $Q(s)$ is stable and proper. Hence, the set of all stabilizing controllers $C(s)$ of the plant $P(s)$ are characterized by the set of all the stable and proper transfer functions, which is the key principle of the YKP.

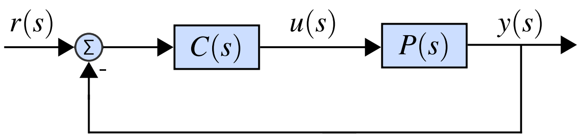

Figure 2.2: The closed loop system $G(s)$.

The application of Example 2.1 is limited to open loop stable SISO plants, which significantly limits the field of applications. The YKP explains how the ideas of Example 2.1 extends to stable and unstable MIMO systems. In Definition 2.1, the different classes of transfer function matrices are specified which are used throughout this chapter.

Definition 2.1 (The Transfer Function Matrix Classes $\mathbb{S}^-$ and $\mathbb{S}$)
Let $\mathbb{S}^-$ be the set of all real, rational, stable and proper transfer function matrices of appropriate dimensions in continuous or discrete time. Similarly, let $\mathbb{S}$ be the set of all real, rational and proper transfer function matrices of appropriate dimensions in continuous or discrete time. To be specific, stable does not include marginally stable, which is considered unstable in this context.

To properly understand the YKP, the concept of coprime factorizations is crucial, which will be defined in Definition 2.2.

Definition 2.2 (Left- and right-coprime factorizations over $\mathbb{S}^-$ [Anderson, 1998, sec. 3])
The transfer function matrix pair $\left(\tilde{N}_r, \tilde{D}_r\right)$ is right-coprime over $\mathbb{S}^-$ if $\tilde{N}_r, \tilde{D}_r \in \mathbb{S}^-$ and the transfer function matrices $X, Y \in \mathbb{S}^-$ exists such that

$$X\tilde{N}_r + Y\tilde{D}_r = I. \tag{2.4}$$

Similarly, the transfer function matrix pair $\left(\tilde{N}_l, \tilde{D}_l\right)$ is left-coprime over $\mathbb{S}^-$ if $\tilde{N}_l, \tilde{D}_l \in \mathbb{S}^-$ and the transfer function matrices $X, Y \in \mathbb{S}^-$ exists such that

$$\tilde{N}_l X + \tilde{D}_l Y = I. \tag{2.5}$$

Note that the right-coprime transfer function matrices over $\mathbb{S}^-$ are denoted by $\tilde{(\cdot)}_r$, while the left-coprime matrices over $\mathbb{S}^-$ are denoted by $\tilde{(\cdot)}_l$. The left- and right-coprime factorizations of the transfer function matrix $P \in \mathbb{S}$ over $\mathbb{S}^-$ are respectively defined by

$$P = \tilde{D}_l^{-1}\tilde{N}_l = \tilde{N}_r\tilde{D}_r^{-1}, \tag{2.6}$$

where the pair $\left(\tilde{N}_r, \tilde{D}_r\right)$ is right-coprime over $\mathbb{S}^-$ and the pair $\left(\tilde{N}_l, \tilde{D}_l\right)$ is left-coprime over $\mathbb{S}^-$.

The equations (2.5) and (2.4) are formally called the Bezout identity, and requires that the greatest common denominator of eg. $\tilde{N}_r$ and $\tilde{D}_r$ are 1. To be specific, the left- and-right coprime factorizations of P in (2.6) cannot have any pole-zero cancellations for them to be right- or left-coprime over $\mathbb{S}^-$ [Bendtsen et al., 2013, sec. II]. Furthermore, note that the left and right coprime factorizations are not necessarily equal.

The left- and right-coprime factorizations over $\mathbb{S}^-$ can be determined using known formulas for the purposes of this project, which will be introduced in the next section. For now, the following example aims to give a notion as to how these factorizations can be made.

Example 2.2 (Right-coprime facotrization over $\mathbb{S}^-$ of a transfer function)
A right-coprime factorization over $\mathbb{S}^-$ of the transfer function

$$P(s) = \frac{1}{(s-1)(s-2)} \tag{2.7}$$

can be determined according to Definition 2.2, which require $P(s)$ to be factorized according to $\tilde{N}_r\tilde{D}_r^{-1}$. Introducing the polynomial $a(s)$, allows $P(s)$ to be rewritten into

$$P(s) = \frac{1}{a(s)}\frac{a(s)}{(s-1)(s-2)} = \underbrace{\frac{1}{a(s)}}_{\tilde{N}_r}\underbrace{\left(\frac{(s-1)(s-2)}{a(s)}\right)}_{\tilde{D}_r}{}^{-1}. \tag{2.8}$$

For $\tilde{N}_r$ and $\tilde{D}_r$ to be in $\mathbb{S}^-$, the polynomial $a(s)$ must at least contain two stable zeros for $\tilde{D}_r$ to be proper and no unstable zeros to ensure stability. Selecting $a(n) = (s+1)^2$ results in the coprime factorizations over $\mathbb{S}^-$

$$\tilde{N}_r = \frac{1}{(s+1)^2} \text{ and } \tilde{D}_r = \frac{(s-1)(s-2)}{(s+1)^2}. \tag{2.9}$$

The pair $\left(\tilde{N}_r, \tilde{D}_r\right)$ is right-coprime over $\mathbb{S}^-$, as $\tilde{N}_r$ and $\tilde{D}_r$ does not share any common zeros. Notice that even though $P(s)$ is unstable and does not belong to $\mathbb{S}^-$, its coprime factorizations are still members of $\mathbb{S}^-$, which will be crucial later on. To give an example of how X and Y can be picked, consider the transfer functions

$$X = \frac{19s-11}{s+1} \text{ and } Y = \frac{s+6}{s+1}, \tag{2.10}$$

which can be shown to satisfy (2.4). Inserting X and Y results in

$$X\tilde{N}_r + Y\tilde{D}_r = \frac{19s-11}{s+1}\frac{1}{(s+1)^2} + \frac{s+6}{s+1}\frac{(s-1)(s-2)}{(s+1)^2} = \frac{19s-11}{(s+1)^3} + \frac{(s+6)(s-1)(s-2)}{(s+1)^3}$$
$$= \frac{(19s-11)+(s+6)(s-1)(s-2)}{(s+1)^3} = \frac{s^3+3s^2+3s+1}{s^3+3s^2+3s+1} = 1,$$

which yield the expected result.

As the notion of coprime factorizations has been described, the YKP will be defined in the following.

Definition 2.3 (Youla-Kucera parameterization [Anderson, 1998, sec. 3])
Let the plant $P \in \mathbb{S}$ and any stabilizing controller $K \in \mathbb{S}$ be described by the left- and right coprime factorizations over $\mathbb{S}^-$, as described by Definition 2.2, according to

$$P = \tilde{N}_r\tilde{D}_r^{-1} = \tilde{D}_l^{-1}\tilde{N}_l \text{ and} \tag{2.11a}$$
$$K = \tilde{X}_r\tilde{Y}_r^{-1} = \tilde{Y}_l^{-1}\tilde{X}_l. \tag{2.11b}$$

Then the set of all stabilizing controllers of the plant P can be described by the set of all $Q \in \mathbb{S}^-$ given by

$$K_r(Q) = \left(\tilde{X}_r + \tilde{D}_rQ\right)\left(\tilde{Y}_r - \tilde{N}_rQ\right)^{-1} \text{ and} \tag{2.12a}$$
$$K_l(Q) = \left(\tilde{Y}_l - Q\tilde{N}_l\right)^{-1}\left(\tilde{X}_l + Q\tilde{D}_l\right), \tag{2.12b}$$

in terms of the left and right coprime factorizations, respectively. These controllers are denoted the left- and right Youla-Kucera (YK) controllers, which are depicted on Figure 2.3.

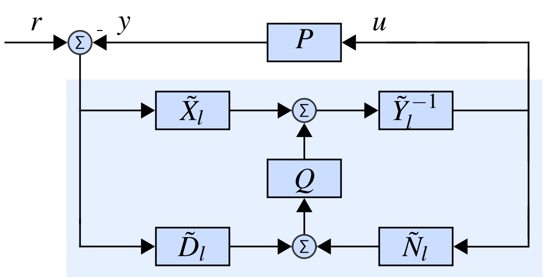

(a) The left coprime YK controller $K_l(Q)$.

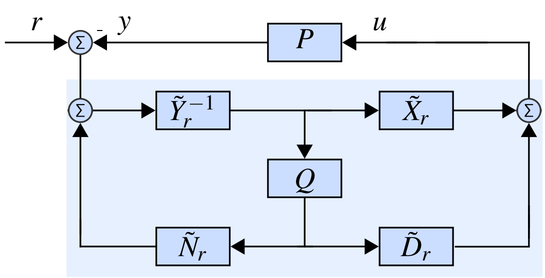

(b) The right coprime YK controller $K_r(Q)$.

Figure 2.3: The left and right coprime factorization YKP.

Notice that the key ideas of Example 2.1 are present in Definition 2.3. Namely that all stabilizing and proper controllers can be characterized in terms of all $Q \in \mathbb{S}^-$, which henceforth is denoted the YK parameter. Moreover, to include both stable and unstable plants an initial stabilizing controller is necessary, which can still be left out if the plant is open loop stable.

As the concept of the YKP and coprime factorizations has been introduced, a structured way of selecting them will be described in the following section.

2.3 Double Coprime Factorization

In this section, a description of how the left- and right-coprime factorization over $\mathbb{S}^-$ can be calculated, which are required by Definition 2.3. These factorizations are selected as a DCF over $\mathbb{S}^-$ according to Definition 2.4. Some benefits of this factorization will be explained followed by how they can be chosen.

Definition 2.4 (Double Coprime Factorization over $\mathbb{S}^-$ [Anderson, 1998, sec. 3])
Let the left- and right coprime factorizations over $\mathbb{S}^-$ of the plant $P \in \mathbb{S}$ and the controller $K \in \mathbb{S}$ be defined as in Definition 2.3, where

$$P = \tilde{N}_r \tilde{D}_r^{-1} = \tilde{D}_l^{-1} \tilde{N}_l \text{ and} \tag{2.13a}$$
$$K = \tilde{X}_r \tilde{Y}_r^{-1} = \tilde{Y}_l^{-1} \tilde{X}_l . \tag{2.13b}$$

If (2.14) holds, then the factorizations denoted by (2.13) are both left- and right-coprime over $\mathbb{S}^-$ and is said to be a double coprime factorization (DCF) over $\mathbb{S}^-$.

$$\begin{bmatrix} \tilde{Y}_l & \tilde{X}_l \\ -\tilde{N}_l & \tilde{D}_l \end{bmatrix} \begin{bmatrix} \tilde{D}_r & -\tilde{X}_r \\ \tilde{N}_r & \tilde{Y}_r \end{bmatrix} = \begin{bmatrix} I & 0 \\ 0 & I \end{bmatrix} \tag{2.14}$$

If (2.13) is a DCF over $\mathbb{S}^-$, then the left and right coprime YK controllers $K_l(Q)$ and $K_r(Q)$ are equal and is denoted $K_{lr}(Q)$ for clarity [Anderson, 1998, sec. 3]. Hence, (2.12) simplifies to

$$K_{lr}(Q) = K_l(Q) = K_r(Q) = \left(\tilde{X}_r + \tilde{D}_r Q\right)\left(\tilde{Y}_r - \tilde{N}_r Q\right)^{-1} = \left(\tilde{Y}_l - Q\tilde{N}_l\right)^{-1}\left(\tilde{X}_l + Q\tilde{D}_l\right). \tag{2.15}$$

Additionally, it is not obvious that the transfer functions of the closed loop system are affine in Q, which are depicted on Figure 2.4. If (2.13) is a DCF then the closed loop transfer function simplifies significantly from (2.16) to (2.17) [Anderson, 1998, sec. 3]. In particular, since $\tilde{N}_r$, $\tilde{X}_l$ and $\tilde{D}_l$ are required to be stable as they belong to $\mathbb{S}^-$, G_{DCF} too is stable.

$$G(Q) = PK_{lr}(Q)\left(I + PK_{lr}(Q)\right)^{-1} = \begin{bmatrix} \tilde{N}_r & 0 \end{bmatrix} \begin{bmatrix} I & Q \\ 0 & I \end{bmatrix} \begin{bmatrix} \tilde{D}_r & -\tilde{X}_r \\ \tilde{N}_r & \tilde{Y}_r \end{bmatrix}^{-1} \begin{bmatrix} 0 \\ I \end{bmatrix} \tag{2.16}$$

$$G_{\text{DCF}}(Q) = PK_{lr}(Q)\left(I + PK_{lr}(Q)\right)^{-1} = \tilde{N}_r\left(\tilde{X}_l + Q\tilde{D}_l\right) \tag{2.17}$$

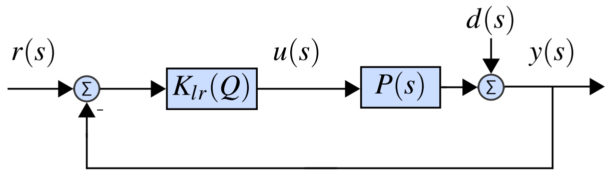

Figure 2.4: The closed loop system $G(s)$ of the DCF YK controller $K_{lr}(Q)$ and the plant $P(s)$, which has the reference $r(s)$ and the disturbance $d(s)$.

Similarly, the output sensitivity, which is the transfer function matrix linking the disturbance d to the output y is given by

$$S_{\mathrm{DCF}} = (I + PK_{lr}(Q))^{-1} = \left(\tilde{Y}_r - \tilde{N}_r Q\right)\tilde{D}_l. \tag{2.18}$$

The concept and some benefits of choosing the right- or left-coprime factorizations as a DCF has been described. However, the biggest benefit is by far that expressions exist to determine the DCF, which will be described in the following section.

2.3.1 Calculation of Double Coprime Factorizations over $\mathbb{S}^{-}$

Standard expressions exist to find the DCF of a plant P and controller K, of which it has been chosen to focus on the transfer function descriptions. This is due to the state space descriptions assume an observer based controller, which exclude the SISO-class controllers that is necessary for this project as described in Section 1.4 (Project Outline). That being said, the transfer function descriptions can still be used for state space controllers, which will be elaborated on in Section 2.6 (Practical Considerations).

The method adopted for the calculation of the DCF in this project is described in [Sugie and Ono, 1989, pp. 682-685]. For this method to work for the plant $P \in \mathbb{S}$ and the stabilizing controller $K \in \mathbb{S}$, any preliminary left- and right-coprime factorization of K over $\mathbb{S}^{-}$ is required, according to

$$K = \tilde{N}_{r,K}\tilde{D}_{r,K}^{-1} = \tilde{D}_{l,K}^{-1}\tilde{N}_{l,K}. \tag{2.19}$$

Then the DCF over $\mathbb{S}^{-}$ of P and K is given by:

$$\tilde{N}_r = P(I+KP)^{-1}\tilde{D}_{l,K}^{-1} \qquad \tilde{D}_r = (I+KP)^{-1}\tilde{D}_{l,K}^{-1} \qquad \tilde{X}_r = \tilde{N}_{r,K} \qquad \tilde{Y}_r = \tilde{D}_{r,K} \tag{2.20a}$$

$$\tilde{N}_l = \tilde{D}_{r,K}^{-1}(I+PK)^{-1}P \qquad \tilde{D}_l = \tilde{D}_{r,K}^{-1}(I+PK)^{-1} \qquad \tilde{X}_l = \tilde{N}_{l,K} \qquad \tilde{Y}_l = \tilde{D}_{l,K} \tag{2.20b}$$

However, the task of finding these matrices becomes significantly more straightforward if the initial stabilizing controller K is required to be stable ($K \in \mathbb{S}^{-}$), which permit (2.19) to be chosen according to

$$\tilde{N}_{r,K} = \tilde{N}_{l,K} = K \text{ and} \tag{2.21a}$$

$$\tilde{D}_{r,K} = \tilde{D}_{l,K} = I. \tag{2.21b}$$

Hence, the DCF of P and K is given in terms of P and K and equals:

$$\tilde{N}_r = P(I+KP)^{-1} \qquad \tilde{D}_r = (I+KP)^{-1} \qquad \tilde{X}_r = K \qquad \tilde{Y}_r = I \tag{2.22a}$$

$$\tilde{N}_l = (I+PK)^{-1}P \qquad \tilde{D}_l = (I+PK)^{-1} \qquad \tilde{X}_l = K \qquad \tilde{Y}_l = I \tag{2.22b}$$

This approach has the remarkable benefit of not requiring additional design choices, which might carry the potential of developing a low complexity stepwise commissioning strategy. Keep in mind that it does exclude the widely used PID class controller as an initial controller due to its integrator. Even though it constrains the choice of the initial controller K, then keep in mind that $Q \in \mathbb{S}^{-}$ describes all the stabilizing controllers for P, including the unstable ones which belong to $\mathbb{S}$. It is possible to work with this constraint and for this reason the initial controller K is assumed to be stable. A workaround for this this constraint will be found in Section 2.5 (Sequential Stepwise Commissioning Strategy), but for now some additional aspects of this particular choice of DCF over $\mathbb{S}^-$ is described.

The YKP given by (2.15) can be expressed in terms of the controller K and the plant P by inserting (2.22) into (2.15) and the following expression for $K_{lr}(Q)$ is obtained

$$\begin{aligned} K_{lr}(Q) &= \left(\tilde{X}_r + \tilde{D}_r Q\right)\left(\tilde{Y}_r - \tilde{N}_r Q\right)^{-1} \\ &= \left(K + (I+KP)^{-1} Q\right)\left(I + P(I+KP)^{-1} Q\right)^{-1}. \end{aligned} \tag{2.23}$$

According to [Sugie and Ono, 1989,pp. 694] it can be rewritten into

$$K(Q) = K + Q\left[I - P(I+KP)^{-1} Q\right]^{-1}. \tag{2.24}$$

To simplify these equations further, the feedback interconnection operator $\star$ is introduced in Definition 2.5, which results in

$$K(Q) = K + Q\left[I - (P \star K)\, Q\right]^{-1} = K + Q \star \left[-(P \star K)\right]. \tag{2.25}$$

Definition 2.5 (Negative Feedback Interconnection Operator)
The negative feedback interconnection of two systems P and K, as depicted on Figure 2.5, are denoted by the $\star$-operator according to

$$P \star K = P(I+KP)^{-1} = (I+PK)^{-1} P. \tag{2.26}$$

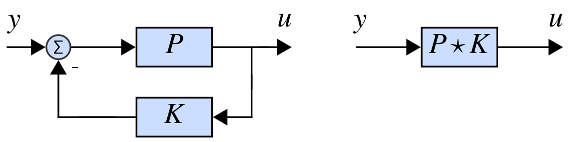

Figure 2.5: Negative feedback interconnection, which is simplified to $P \star K$.

This means that the YKP of the plant $P \in \mathbb{S}$ and the stabilizing controller $K \in \mathbb{S}^-$ is given in terms of a fixed reference structure, which is depicted on Figure 2.6(a) in a negative feedback configuration. This figure consists of three parts, which becomes clearer by neglecting the reference r, as it has no effect on the closed loop stability, which allows for the rewriting depicted on Figure 2.6(b). Two of the three parts are copies of the negative feedback loop $P \star K$, which is stable as K by definition stabilizes P. These two parts remove the effects of the controller K. Hence, the YK parameter Q is decoupled from the effects of the controller K. Consequently, this means that the last part, namely the YK parameter Q, only reacts on the error between the two system outputs e_{YK}, which originates from the reference r.

This concludes the preliminaries required for the proposed sequential stepwise commissioning method. A stepwise commissioning strategy will be formulated based on these results in Section 2.4, which will be expanded to a sequential stepwise commissioning strategy in Section 2.5.

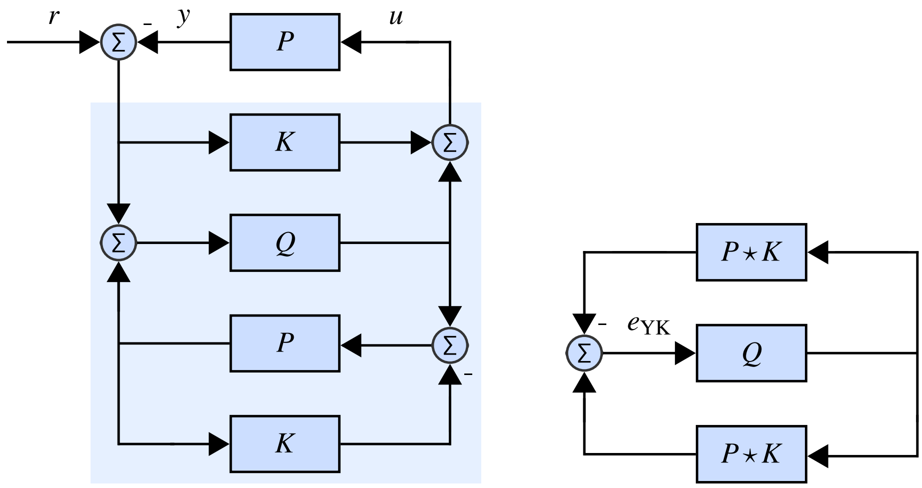

(a) The structure of the YKP of the plant $P \in \mathbb{S}$ and the stabilizing controller $K \in \mathbb{S}^-$ in a negative feedback configuration. The shaded area is the YK controller $K(Q)$.

(b) The simplified version of Figure 2.6(a) without the reference r.

Figure 2.6: Block diagrams of the YKP.

2.4 Stepwise Commissioning Strategy

In this section a stepwise commissioning strategy will be established. As described in Section 2.1 (Stepwise Commissioning Introduction), the goal is to develop a gradual controller transition from an initial controller K_0 to the controller K_1 through a transition parameter $\gamma \in [0;1]$, as illustrated on Figure 2.7. When $\gamma = 0$ the initial stabilizing controller K_0 is active, while $\gamma = 1$ makes the stabilizing controller K_1 active. The challenge was to ensure closed loop stability in the region $\gamma \in]0;1[$. This problem will be handled in this section by applying the YKP as explained in the previous section.

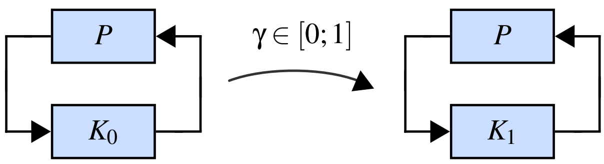

Figure 2.7: Controller changing through the transition parameter $\gamma \in [0;1]$.

Lets consider the YK controller given by (2.24), which is restated in (2.27) in the context of this section.

$$K_{0\to 1}(Q) = K_0 + Q\left[I - P\left(I + K_0 P\right)^{-1} Q\right]^{-1} \tag{2.27}$$

Where

$\mathbb{S}$ is the set of all real, rational and proper transfer function matrices of appropriate dimensions
$\mathbb{S}^-$ is the set of all real, rational, stable and proper transfer function matrices of appropriate dimensions
$Q \in \mathbb{S}^-$ is the the YK parameter
$K_{0\to1}(Q) \in \mathbb{S}^-$ is the DCF YK controller which transition between K_0 and K_1 as a function of Q
$P \in \mathbb{S}$ is the plant
$K_0 \in \mathbb{S}^-$ is the initial stabilizing controller

Notice that $K_{0\to1}(0) = K_0$, which suggest that a transition between the initial controller K_0 and K_1, can occur through the transition parameter $\gamma \in [0;1]$ and the YK parameter $Q_{0\to1}$ by defining

$$K_{0\to1}(\gamma\, Q_{0\to1}). \tag{2.28}$$

The key idea is to exploit that the closed loop system is stable when $\gamma\, Q_{0\to1} \in \mathbb{S}^-$, which is true when $Q_{0\to1} \in \mathbb{S}^-$, as multiplying by the factor $\gamma \in [0;1]$ has no impact on stability. As both K_0 and K_1 is known, the following can be defined:

$$K_{0\to1}(\gamma\, Q_{0\to1})|_{\gamma=0} = K_{0\to1}(0) = K_0 \tag{2.29a}$$
$$K_{0\to1}(\gamma\, Q_{0\to1})|_{\gamma=1} = K_{0\to1}(Q_{0\to1}) = K_1 \tag{2.29b}$$

This mean that only (2.29b) is depending on $Q_{0\to1}$. Hence, one reasonably straight forward way of obtaining a $Q_{0\to1}$ is to solve for it in (2.29b). It is given by

$$K_1 = K(Q_{0\to1}) = K_0 + Q_{0\to1}\left[I - P\,(I + K_0P)^{-1}\, Q_{0\to1}\right]^{-1}, \tag{2.30}$$

and solving for $Q_{0\to1}$ results in

$$Q_{0\to1} = \left[I + (K_1 - K_0)\, P\,(I + K_0P)^{-1}\right]^{-1}(K_1 - K_0)\,. \tag{2.31}$$

This expression can be simplified into (2.32) using Definition 2.5 , which is depicted on Figure 2.8(a).

$$Q_{0\to1} = [I + (K_1 - K_0)\,(P \star K_0)]^{-1}\,(K_1 - K_0) = (K_1 - K_0) \star [P \star K_0] \tag{2.32}$$

Inserting $Q_{0\to1}$ in (2.28) results in

$$K_{0\to1}(\gamma\, Q_{0\to1}) = K_0 + [\gamma(K_1 - K_0) \star (P \star K_0)] \star [-\,(P \star K_0)]\,, \tag{2.33}$$

which is depicted on Figure 2.8(b). This double coprime YK controller provides a way of gradually transitioning from the controller $K_0 \in \mathbb{S}^-$ to the stabilizing controller $K_1 \in \mathbb{S}$ through the transition parameter γ, while ensuring closed loop stability for all $\gamma \in [0;1]$. Moreover, it has a fixed reference structure, which is highly desirable. As a strategy for changing between two controllers now has been developed, this concept can be extended to a sequence of controllers.

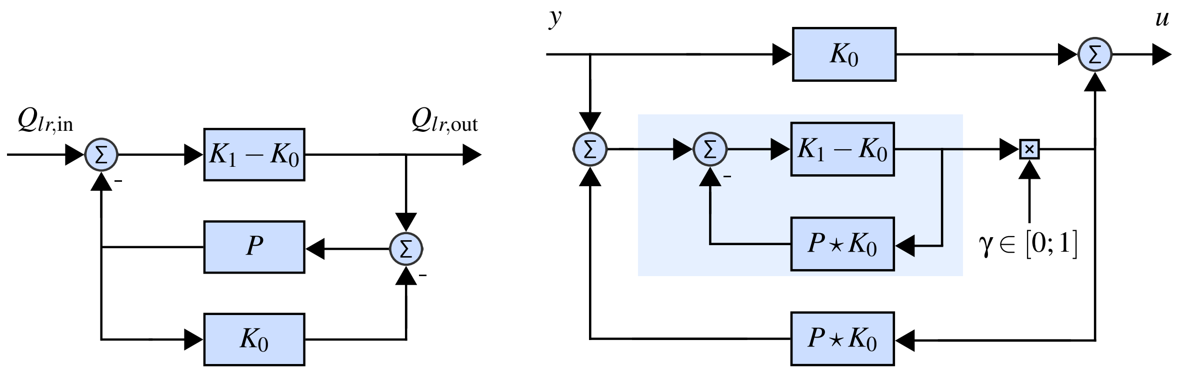

(a) The structure of the YK parameter $Q_{0\to 1}$.

(b) The YK controller $u = K_{0\to 1}(\gamma)\,y$. The shaded area is the YK parameter $Q_{0\to 1}$.

Figure 2.8: The final YK parameter and controller.

2.5 Sequential Stepwise Commissioning Strategy

In this section a strategy for sequential stepwise commissioning multiple controllers are developed. The goal will be to expand the already established stepwise commissioning strategy explained in Section 2.4 to sequentially activate a finite set of n stabilizing controllers denoted by $\mathcal{K} = \{K_1, ..., K_n\}$.

In the previous section a strategy for switching from an initial stabilizing controller $K_0 \in \mathbb{S}^-$ to one of the stabilizing controller in $\mathcal{K}$ is carried out. Additionally, it has been established that it is not desired that K_0 is restricted to $\mathbb{S}^-$. To avoid this problem, the initial controller K_0 is not required to be a part of $\mathcal{K}$, but simply be any stabilizing controller. Hence, $\mathcal{K} \in \mathbb{S}$ and $K_0 \in \mathbb{S}^-$.

The problem which needs to be solved is to design a YK parameter Q, which permits the sequential stepwise commissioning controller, $K_{\text{SSC}}(Q)$, to sequentially transition through the elements of $\mathcal{K}$. This means that Q must be designed to include the finite set of YK parameters $\mathcal{Q} = \{Q_1, Q_2, ..., Q_n\}$, which satisfies

$$K_{\text{SSC}}(Q_i) = K_i. \tag{2.34}$$

One reasonably straight forward way of solving this problem is to select the elements of $\mathcal{Q}$ to transition $K_{\text{SSC}}(Q)$ from the initial controller K_0 to K_i. This can be done using (2.32), which can be reformulated into

$$Q_i = (K_i - K_0) \star [P \star K_0]. \tag{2.35}$$

This means that the YK parameters are independent of each other. Hence, it is possible to ensure that $\mathcal{Q} \subset Q$ by making Q a linear combination of the elements in $\mathcal{Q}$ according to

$$Q = \sum_{i=1}^{n} \gamma_i \, Q_i, \tag{2.36}$$

where $\gamma_i \in [0;1]$. The controller which permit the gradual transition between the controllers in $\mathcal{K}$ is then given by (2.37).

$$
\begin{aligned}
K_{\text{SSC}}(\gamma_1, ..., \gamma_n) &= K_0 + \left(\sum_{i=1}^{n} [\gamma_i \; Q_i] \right) \star (-(P \star K_0)) \\
&= K_0 + \left(\sum_{i=1}^{n} [\gamma_i \; (K_i - K_0) \star (P \star K_0)] \right) \star [-(P \star K_0)]
\end{aligned} \tag{2.37}
$$

To transition between $K_j \in \mathcal{K}$ and $K_k \in \mathcal{K}$ with $j \neq k$ using the transition parameter $\gamma_{j \to k} \in [0;1]$, (2.38) can be used.

$$\gamma_j = 1 - \gamma_{j \to k} \tag{2.38a}$$

$$\gamma_k = \gamma_{j \to k} \tag{2.38b}$$

$$1 = \sum_{i=1}^{n} \gamma_i \tag{2.38c}$$

To elaborate, (2.38c) force all transition parameters except γ_j and γ_i to be 0 throughout the transition as the sum of (2.38a) and (2.38b) are 1. It allows the transition to take place as specified by Figure 2.9. The controllers spanned by (2.37) is depicted as the blue shaded area. By enforcing (2.38) this area is limited to the black edges. As this concludes the sequential stepwise commissioning strategy, some practical considerations will be elaborated upon.

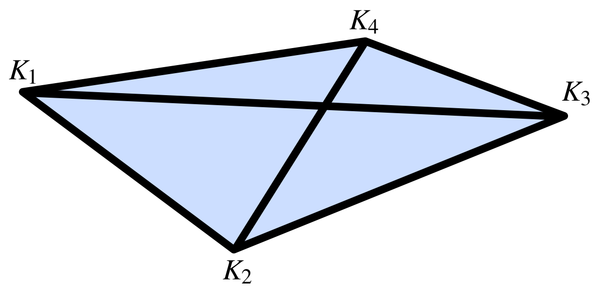

Figure 2.9: Four controllers depicted in a non-specific transfer function space.

2.6 Practical Considerations

A collection of practical considerations related to the proposed stepwise commissioning strategy is collected in this section.

2.6.1 State Space Interpretation

Throughout the development and discussion of the proposed sequential stepwise commissioning method, only transfer function matrices has been considered. Fortunately, all the operations performed on transfer function matrices can also be performed on state space systems, which are described in more detail in Section A.1 (State Space Algebra).

2.6.2 The Size of the Sequential Stepwise Commissioning Controller

One drawback of adapting the proposed sequential commissioning method is a dramatic increase in the number of the controller states. This subsection is dedicated on elaborating on this issue and suggest some guidelines as well as a possible solution to this problem.

To be specific, let s_p denote the number of internal states of the plant P, s_0 denote the number of internal states of the initial controller K_0 and s_i denote the number of internal states of the controller $K_i \in \mathcal{K}$. The total number of states then equals

$$s_0\,(2+2n)+s_p\,(1+n)+\sum_{i=1}^{n} s_i \tag{2.39}$$

This reveals that the states of the initial controller K_0 is desired to be selected as low as possible, as two copies goes into every additionally added controller. If possible it should be selected to have zero states, which is possible if P is open loop stable.

Another way to reduce the controller size is to remove the controllers which are not a part of the current transition, as they have no impact on the transition under any circumstances. Hence, the transition between K_j and K_k as in (2.38) and (2.37) can be simplified to

$$K_{\text{SSC},j\to k}(\gamma_{j\to k}) = K_0 + \left[Q_j\,(1-\gamma_{j\to k}) + Q_k\,\gamma_{j\to k}\right] \star \left[-\,(P\star K_0)\right], \tag{2.40}$$

with $\gamma_{j\to k} \in [0;1]$. Consequently, the states of this controller is reduced to

$$6\,s_0 + 3\,s_p + s_j + s_k, \tag{2.41}$$

which is considered the minimal number of states this type of controller can have. Furthermore, it might be beneficial to wait until Q_k has settled to proceed with the transition as it would introduce less transients.

2.6.3 Order of Operation of the Transition Parameter

A less obvious fact is that it does matter if the transition parameter γ_i is post- or pre-multiplied with the YK parameter Q_i. Consider the two systems

$$Q_i\,\gamma_i \text{ and } \gamma_i\,Q_i, \tag{2.42}$$

which in terms of its dynamical properties are equal for a static γ_i. However, please keep in mind that the internal states of these systems are not equal for $\gamma_i = 0$. If γ_i is post-multiplied, Q_i is uncontrollable as the input is simply zero. Consequently, if γ_i is pre-multiplied, Q_i is unobservable as the output is simply zero, but it does allow the states to settle while $\gamma_i = 0$. Hence, less transients are expected if γ_i is pre-multiplied, as Q_i has time to settle prior to the transition, which will be demonstrated in Section 2.7 (Stepwise Commissioning Example).

As this concludes the practical considerations related to the sequential stepwise commissioning controller, an example of the proposed method is carried out.

2.7 Stepwise Commissioning Example

This section will demonstrate the method developed in Section 2.5. The purpose is to show that the method works for MIMO systems, and for this reason the system is chosen to be rather simple. The plant has been chosen to be a two input two output system described by

$$\begin{bmatrix} y_1(s) \\ y_2(s) \end{bmatrix} = \underbrace{\begin{bmatrix} \frac{4}{(s+1)(s+2)} & -\frac{1}{s+1} \\ \frac{2}{s+1} & -\frac{1}{(s+1)(s+2)} \end{bmatrix}}_{P} \begin{bmatrix} u_1(s) \\ u_2(s) \end{bmatrix}. \tag{2.43a}$$

Two stabilizing MIMO controllers are designed for this system $\mathcal{K} = \{K_1,\ K_2\}$, which are

$$K_1 = \begin{bmatrix} 0.002 & 1.8 \\ -1.6 & -0.1 \end{bmatrix} \quad \text{and} \quad K_2 = \begin{bmatrix} \frac{0.002s+0.21}{s} & 1.8 \\ \frac{-1.6s-2.19}{s} & -0.1 \end{bmatrix}. \tag{2.44a}$$

The controller K_1 is a proportional controller, which is expected to give steady state errors. The controller K_2 extend K_1 with integral action, which ensure no steady state error on the reference of $y_1(s)$. Furthermore, as $P \in \mathbb{S}^-$, the initial stabilizing controller K_0 can be selected as $K_0 = 0$. As the developed method is generic and the sequential stepwise commissioning controller is given by (2.37), the focus will be on how the transition affects the system.

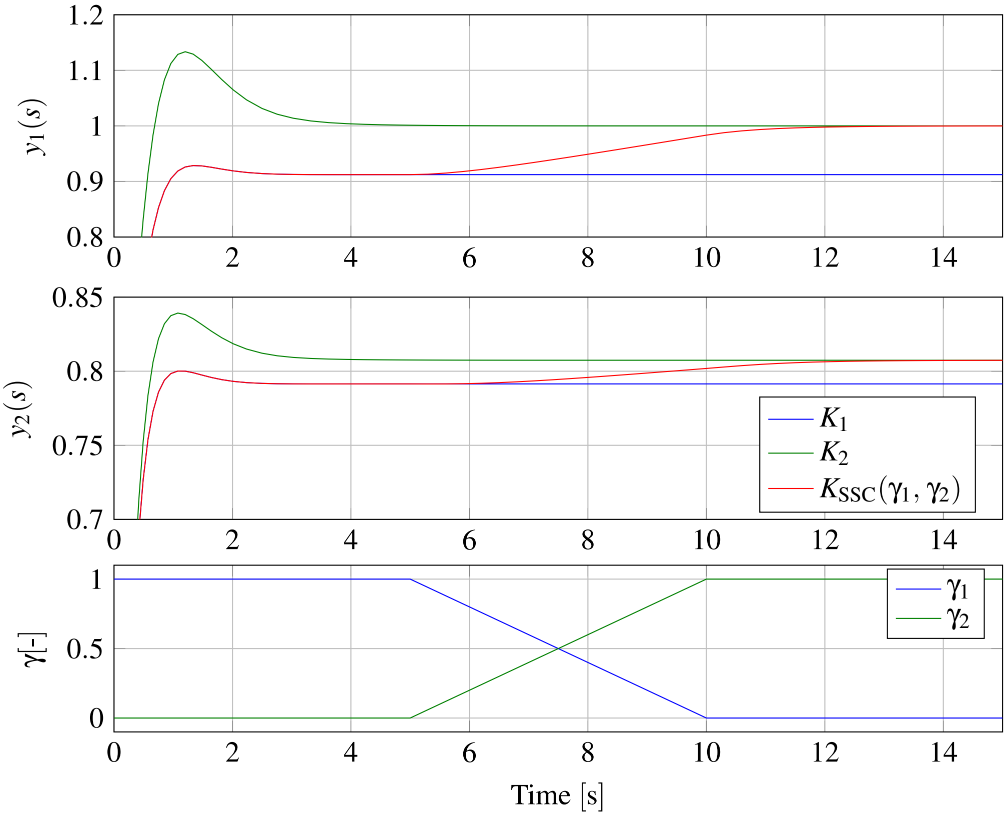

Figure 2.10: Closed loop step response with the controllers K_1, K_2 and $K_{SSC}(\gamma_1, \gamma_2)$. The reference for both outputs are 1.

First off, a step response of the closed loop system with the controllers K_1, K_2 and $K_{SSC}(\gamma_1, \gamma_2)$ are depicted on Figure 2.10. At $t = 5$s the transition parameter γ_2 increments from 0 to 1 and γ_1 from 1 to 0, which makes the controller $K_{SSC}(\gamma_1, \gamma_2)$ change behavior from K_1 to K_2. At $t = 10$s the transition is complete and the output $y_1(s)$ gradually move towards its reference in a controlled manner. Notice that even though the step response of both K_1 and K_2 has an overshoot, the transition between the controllers does not have any overshoot, which is the desired result. However, as suggested in Section 2.6 this most likely is due to Q_2 have had settled prior to the transition. To demonstrate that this is the case, Figure 2.11 shows the response of $y_1(s)$ with γ_1 and γ_2 both post- and pre-multiplied on Q_1 and Q_2, respectively. Notice that the difference between the two responses are significant, as the blue trace has no overshoot while the red one has a significant overshot.

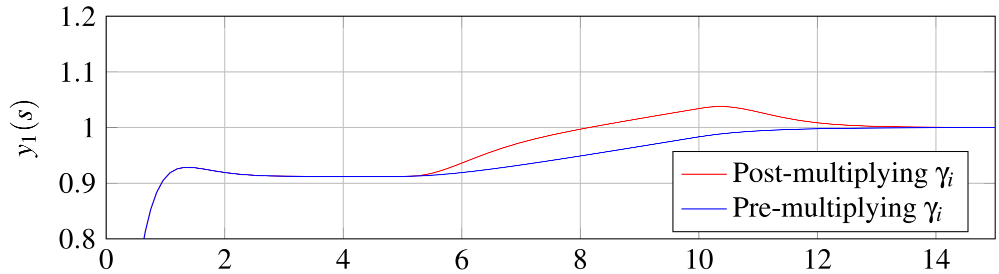

Figure 2.11: The difference between pre- and post-multiplying with γ_1 and γ_2 with Q_1 and Q_2, respectively.

The singular value response is the MIMO system equivalent of the magnitude response of a SISO system. It is insightful to investigate this for the transition, as it depicts very clearly that the transition happens gradually. On Figure 2.12 the singular value response of the open loop system $PK_{SSC}(1-\gamma, \gamma)$ is depicted with the transition parameter γ going from 0 to 1. Notice that the magnitude responses changes in a smooth fashion between the controllers, especially for the bottom most singular value. However, the transition to the integrator occurs less smooth, but it is expected as it has infinite DC-gain.

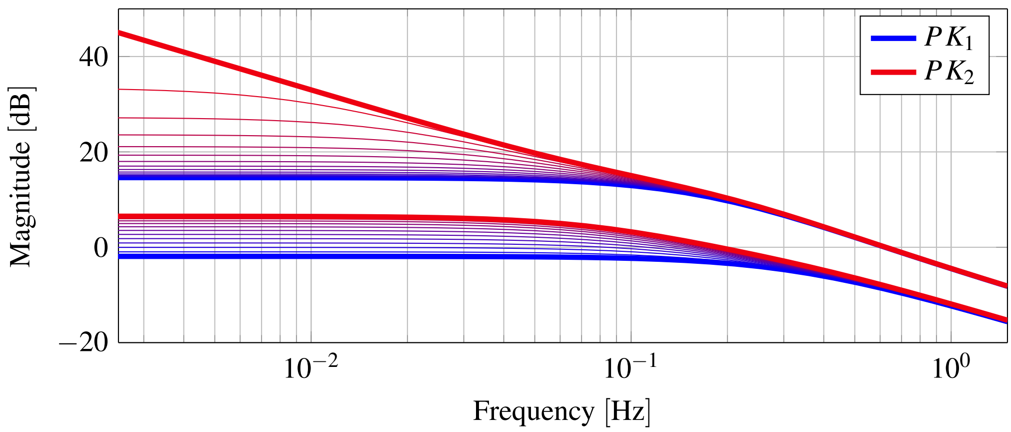

Figure 2.12: Singular values of the open loop system denoted by $PK_{SSC}(1-\gamma, \gamma)$ for $\gamma \in [0;1]$. The transition is color coded and move from blue to red as γ goes from 0 to 1.

Another way of displaying how the transition takes place is through how its poles and zeros move throughout the transition. The poles and zeros of $PK_{SSC}(1, 0)$ $[K_1]$ and $PK_{SSC}(0, 1)$ $[K_2]$ are depicted on Figure 2.13. Notice that there are quite a lot of canceled poles, which originate from the way the controller has been constructed. After all, the controller does contain multiple copies of the plant P. On the bottom plots of Figure 2.13 the pole movement of the transition between the two controllers is depicted. Notice that some of the pole-zero cancellations diverge at $0 < \gamma$ and converge again at $\gamma = 1$. This concludes the stepwise commissioning example and consequently the stepwise commissioning design.

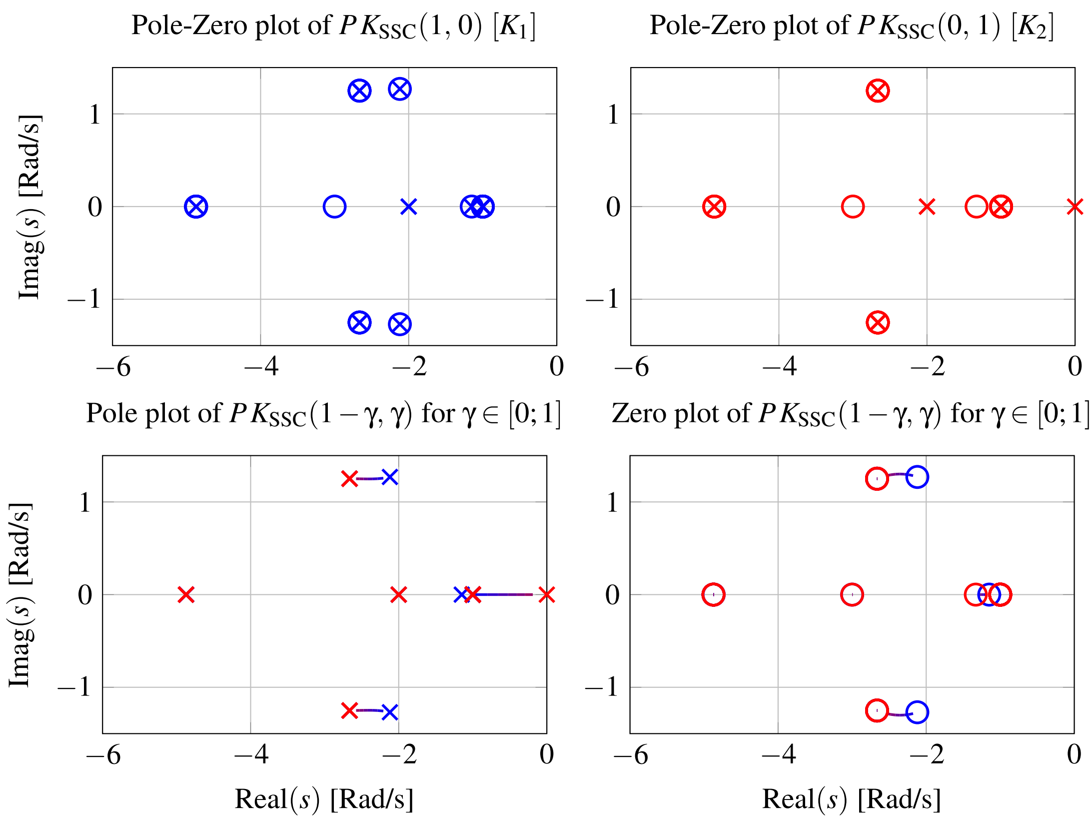

Figure 2.13: Top plots: The Pole-Zero plot of K_1, K_2. Bottom plots: The pole and zero movement of $PK_{SSC}(1-\gamma, \gamma)$ as γ goes from 0 to 1. Once again, K_1 is denoted by blue and K_2 by red.

Chapter 3

Interim Conclusion

In this part of the report the problems of introducing MIMO controllers in the industry was investigated. In Chapter 1 it has been determined that one of the reasons is that MIMO controllers are harder to commission, as the startup procedure of industrial MIMO systems are determined from empirically established guidelines and regulations specific to the individual system. To avoid this problem the MIMO system was assumed to be initialized and operating with a series of SISO controllers in Section 1.2. This requires the MIMO controller to be stepwise commissioned from a bank of SISO controllers, which was decided to be carried out using the YKP in Section 1.3.

In Chapter 2 a stepwise commissioning strategy was designed. First, the YKP and the principle behind it was introduced in Section 2.2 along with the concept of left- and right coprime factorizations. Then double coprime factorizations was introduced, which allowed the YKP to be described with a fixed reference structure in Section 2.3. Based on these concepts, a stepwise commissioning strategy was developed in Section 2.4, which allowed the transition between a stable and stabilizing controller to a stabilizing controller. This restriction was lifted in Section 2.5, where the previous stepwise commissioning strategy was generalized to permit the sequential stepwise commissioning of any number of stabilizing controllers. To demonstrate the developed stepwise commissioning method, an example of its application was carried out in Section 2.7, which aimed to illustrate the dynamics of the method.

PART II

CASE STUDY: STEAM BOILER

Chapter 4

Steam Boiler System

This chapter describes a general Steam Boiler setup as well as the Steam Boiler at Danish Crown located in Sønderborg. First a general Steam Boiler and its individual components is described.

4.1 Description of the Steam Boiler System

A steam boiler is used for industrial steam production, which is commonly used for decentralized heating and cleaning purposes. As steam can be used for sterilization, it is heavily used across many industries ranging from the food to the medical industry.

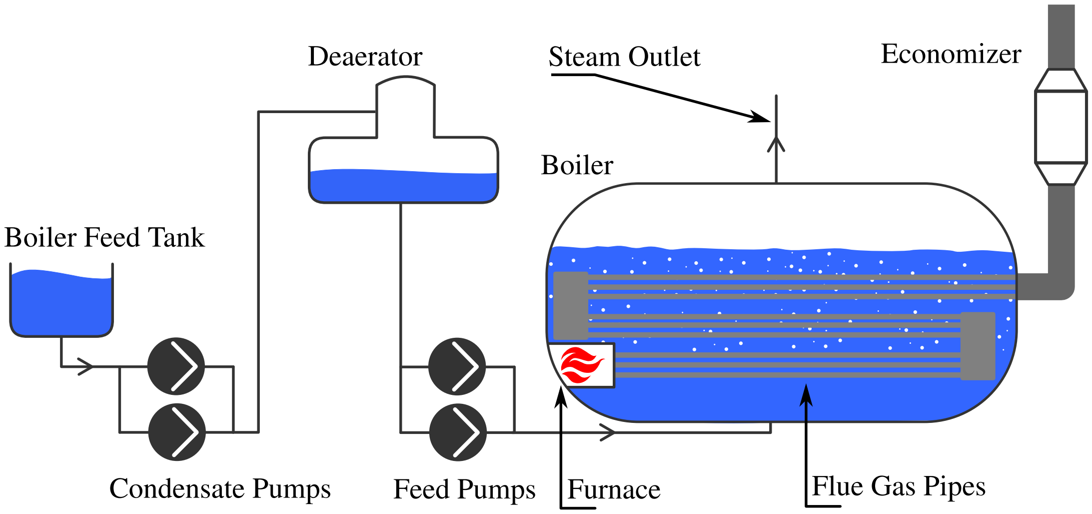

Figure 4.1: The main components of a basic fire tube steam boiler [Pétursson, 2015,pp. 6].

As the Danish Crown boiler is a fire tube steam boiler, this chapter will focus on this boiler type. The main components of a basic fire tube steam boiler system are depicted on Figure 4.1 and are explained using [Grundfos, 2012].

Boiler The boiler is the main component and produces steam from feed water. The feed water is heated by burning fuel, which produces flue gas that travels through flue gas pipes, hence the name fire tube. The flue gas pipes transfer heat from the flue gas to the water in the boiler.

Deaerator The deaerators' primary task is to reduce the level of diluted oxygen and carbonic acid levels in the feed water, to protect it against corrosion. For steam boilers, this is commonly done by heating the feed water to around 100-110 °C. By heating water, its solubility is decreased and some of its diluted content is released. To promote this effect, the boiling point is increased by increasing its pressure. This type of deaerator, has the added benefit of doubling as a preheater for the feed water and is usually powered by the generated steam.

Boiler Feed Tank The Boiler Feed Tank is used as a water buffer for the steam boiler feed water, which is provided by an external water source. In a closed steam boiler system, up to 80-90% of the produced steam can be recycled after it condensates[Vedsted, 2008,pp. 18]. It is collected and returned to the Boiler Feed Tank, which saves energy as it is hotter compared to the external water source.

Economizer To increase efficiency, the exhaust flue gas is used to preheat the feed water.

Pumps The condensate pump and feed pumps are used to keep a desired water level in both the deaerator and boiler.

4.1.1 Safety and Regulations

In this section a collection of safety and regulations relevant to fire tube boiler control is described using [Vedsted, 2008, pp. 373 - 381].

The boiler must be equipped with an automatic level control, if it is necessary for operation. It must keep the water level between the lowest permissible water level (LWL) and the highest permissible water level (HWL), which is specific to the individual boiler.

Equipment must be installed that prevents the water level to go above HWL. This equipment does not need to be contained in a dedicated device and can therefore be a part of the automatic level controller. If the water level gets too high, water can enter the steam outlet. If combined with a high steam flow it can break pipes, equipment and cause leakages.

The HWL must at least be 100 mm above the highest located heating surface, which include the furnace and flue gas pipes. In addition, if the flue gas temperature exceeds 400 °C and the furnace is slow to react, it must at least take 7 minutes for the water level to reach the heating surfaces from LWL, with maximum steam demand and the feed pumps turned off.

Two separate and dedicated dry-boiling protection devises must be installed, which disable the furnace if the water level reaches LWL. These devises must contain both an electrical and a mechanical dry-boiling protection device. If the water level reaches any heating surfaces, it will overheat and can cause leakages.

In addition, a dedicated over-pressure protection device must be installed, which disables the furnace if the pressure reaches its maximum allowed operating pressure. If any protection device that disables the furnace is triggered, it must be manually reactivated.

4.1.2 Steam Boiler Startup and operation

The steam boiler operation can be divided into three phases, namely preparation, startup and operation. Even though these phases are not equally important in terms of steam boiler control, it gives an indication of the practical limit for how automated a boiler can be. To give an understanding of this, these phases will be explained using [Vedsted, 2008,pp. 312-313]. The following is an overview of the recommended steps:

Preparation

1. The main stop valve and all blowdown valves are closed. The main stop valve allows steam from passing through the steam outlet if opened. Blowdown valves are used to blow sludge and other impurities out, which are naturally collected on the bottom of these containers. They can also be used to drain the containers of water, as it is located at the bottommost point of the boiler drum.
2. All insulation valves must be opened. These values include and are not limited to the feed water valve and the vent valve. The feed water valve is located between the feed water pump and the feed water inlet of the drum, which allows it to be filled with water using the feed pumps. The vent valve is located on the boiler drum and prevents pressure buildup inside the drum before operation.

Startup

3. The water level must be above LWL.
4. The flue gas pipes are carefully vented before the furnace is ignited to prevent explosion hazards, from leftover fuel.
5. The rate of water heating must not occur faster than the boiler manufacturer allows, which limits thermal stress on the boiler.
6. When dry steam escapes though the air vent, it is closed and the water level sensors are checked by draining some water from the boiler drums blowdown valve. It is very important to check this, as most boiler damages are caused by low water level or incorrect measurement of it.
7. All blowdown valves are checked for leakages and all connected steam powered equipment must be ready for operation.

Operation

8. When the drum pressure reaches its intended operating pressure, the main stop valve is gently opened. This slowly heats external steam powered equipment and prevents a buildup of condensed water. If the condensed water buildup is combined with a large steam flow, the condensed water can break pipes, equipment and cause leakages as it collides with objects.

It is suggested that the feed water controller can be activated after step 3 when the water level is close to its intended operating point. Likewise, the pressure controller can be turned on when the drum pressure is close to the boiler operating pressure at step 8.

Based on the recommended startup procedure, it can be concluded that it will not be practical to automate the startup completely. This is caused by the fact that it requires alot of human interaction, which is impractical to automate and unnecessary, which supports the claim made in Section 1.2 (Difficulties in introducing MIMO controllers in the industry).

4.1.3 The Danish Crown steam boiler

The Danish Crown steam boiler is similar to the general steam boiler. It operates around 8 Bar and does not have an economizer. It is depicted on Figure 4.2 with relevant components, sensors and controllers.

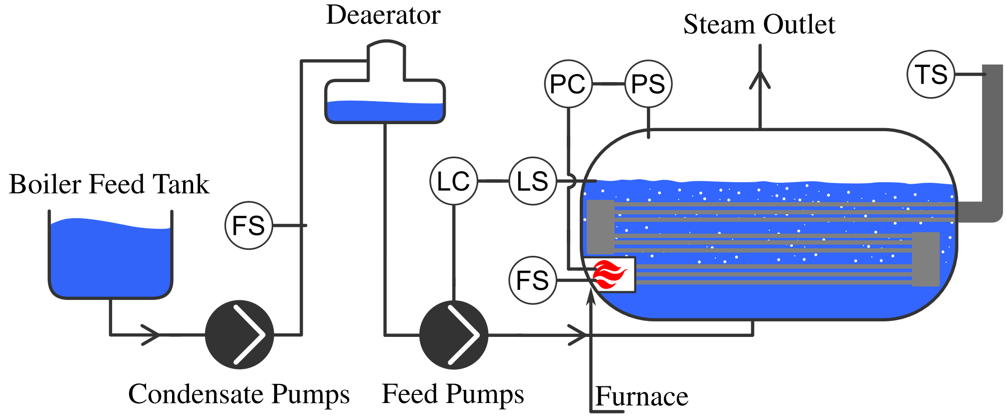

Figure 4.2: The Danish Crown steam boiler with relevant sensors, actuators and controllers. Modified from [Pétursson, 2015,pp. 14].

The relevant sensors and their functions are:

FS The flow sensors (FSs) measures the flow of feed water into the deaerator and fuel into the furnace.
PS The pressure sensor (PS) measures the pressure of the steam in the boiler.
LS The level sensor (LS) measures the water level in the boiler.
TS The temperature sensor (TS) measures the temperature of the exhaust flue gas.

The relevant actuators and controllers and their function are:

PC The pressure controller (PC) is used to maintain a fixed pressure in the boiler drum by controlling the fuel flow into the furnace. It is unknown which type of controller the PC is.
LC The level controller (LC), also known as boiler feed controller, is used to maintain a fixed water level in the boiler by controlling the feed pumps. This current controller is known to be an on/off type controller.

The agreement between Danish Crown and Grundfos does not permit any changes to the pressure controller, but does allow changes to the level controller. The collective controller structure is still a multiple input multiple output (MIMO) controller, but the design freedom is restricted to a multiple input single output (MISO) controller of the feed pump. This no longer allow for a complete sequential MIMO controller activation, which would be desired. However, it does permit a partial one, which is enough to verify if the proposed method works. That being said, as Grundfos is a pump manufacturer and is looking into new pump applications, this project is of great value to them.

For this reason, the related challenges of boiler feed control in a steam boiler system will be described in the following.

4.2 Steam Boiler Feed Control

In this section the difficulties in boiler feed control is explained, which include pump cavitation and the shrink and swell effect. Then the benefits of replacing the controller with a MISO control strategy are discussed.

4.2.1 Pumps and Cavitation

The Danish Crown steam boiler utilizes centrifugal pumps to move water, which will be explained using [Grundfos, 2006, pp. 30-41]. On Figure 4.3(a) an example of a pump performance curve is displayed. It displays a pumps water flow Q for a given pump head H and speed n. The pump head can be interpreted as the pumping resistance generated from counter pressure at the inlet compared to the outlet. It is determined from the pressure difference across the pump according to

$$H = \frac{p_{\text{outlet}} - p_{\text{inlet}}}{\rho g}. \tag{4.1}$$

Where

H is the pump head	[m]
p is the pressure	[Bar]
ρ is the density of the fluid	$\left[\text{kg/m}^3\right]$
g is the gravitational constant	$9.82 \left[\text{m/s}^2\right]$

To get a better understanding of this, Figure 4.3(b) depicts the pump head H made from a column of water after the outlet, which contribute with counter pressure and pump head. The start of the inlet is lowered into a tank of water, which does not provide any pressure at the inlet and does not contribute with any pump head.

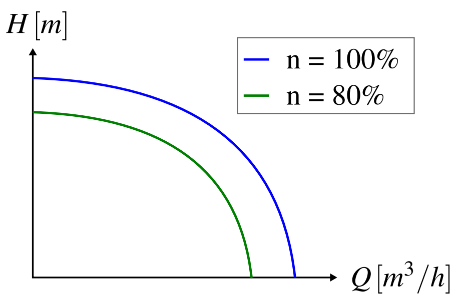

(a) Example of pump performance curve [Pétursson, 2015,pp. 14] and [Grundfos, 2006,pp. 34].

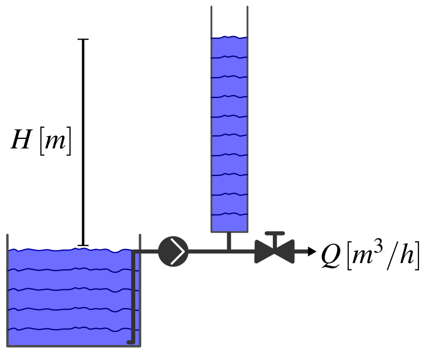

(b) How pump head is measured. [Pétursson, 2015,pp. 14] and [Grundfos, 2006,pp. 34].

Figure 4.3: Pump curve and pump head.

Centrifugal pumps work by rotating an impeller, which add kinetic energy to the fluid. This increases both the pressure and velocity of the fluid, as it is pushed from the impeller inlet to its edges. However, this also decrease the pressure of the fluid inside the pump compared to the inlet, which is called net positive suction head (NPSH) and is positive and stated in meters. As the name indicates, it is the suction and consequently vacuum or negative pressure relative to the inlet, which is generated inside the pump denoted in head. An example of NPSH is depicted on Figure 4.4(a) on the green trace in terms of pressure.

This vacuum is physically created on the backside of the impeller blades, as the fluid is pulled away from it as the impeller rotates. If this pressure drops below the boiling point of the fluid, the fluid boils and bubbles of vapor is formed, which eventually implode as the pressure increases above its boiling pressure p_{boil}. This is illustrated on the blue trace on Figure 4.4(b), where the vapor bubbles is formed at the first of the two intersections at p_{boil} and collapses at the second intersection. The collapse of the vapor bubbles emits shock waves throughout the fluid, which can damage the impeller in close proximity of the collapses and drastically decrease the lifespan of the pump. This is illustrated on Figure 4.4(a), where the collapsing vapor bubbles are damaging the backside of the impeller blades.

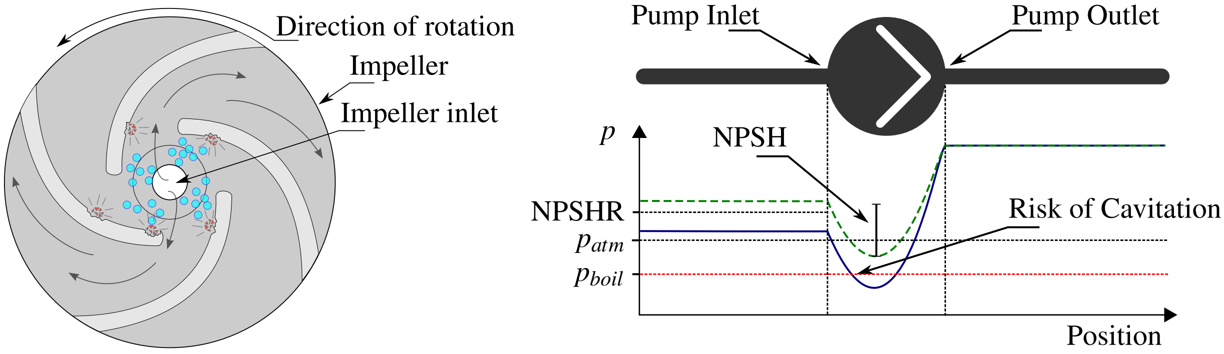

(a) Centrifugal pump impeller undergoing cavitation. [Pétursson, 2015,pp. 8] and [Grundfos, 2006,pp. 40].

(b) The pressure throughout the pump. The blue and green traces, show the pressure throughout the pump as a function of different inlet pressures with fixed outlet pressure [Pétursson, 2015,pp. 8].

Figure 4.4: Pumps and Cavitation.

To avoid this in steam boiler systems, the inlet pressure is increased above the net positive suction head required (NPSHR). It is the minimum required inlet pressure to avoid cavitation and depends on several factors, of which the pressure difference between the inlet and outlet is one of them. For steam boiler systems, the feed pumps usually have the highest risk of cavitation, as the water temperature from the deaerator is close to its boiling point at atmospheric pressure. This is illustrated on Figure 4.5, which shows how the boiling pressure increases with pressure. It increases the NPSHR significantly compared to room temperature and is generally compensated for by increasing the height of the deaerator. The intention is to increase the inlet pressure above NPSHR, which is depicted on Figure 4.5.

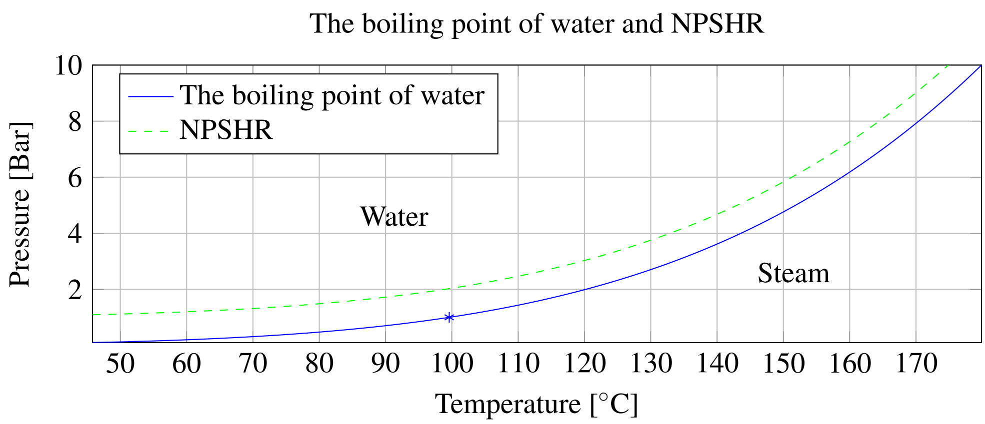

Figure 4.5: The boiling point of water in pressure as a function of temperature (blue) and the NPSHR with a NPSH of 100m (green). Water is liquid above the blue graph and steam below it. For reference, the marked blue dot is the boiling point at atmospheric pressure.

4.2.2 The Shrink and Swell Effect

In steam boiler systems, the steam production occurs throughout the water in the boiler. Consequently, the water level sensor measures both the water and steam vapor under the water surface. Unlike water, steam density is heavily influenced by pressure changes as depicted on Figure 4.6, which makes the measured water level dependent on the boiler pressure. For instance, a change of ± 0.5 Bar from 8 Bar leads to a change of steam density of at least 5.6%.

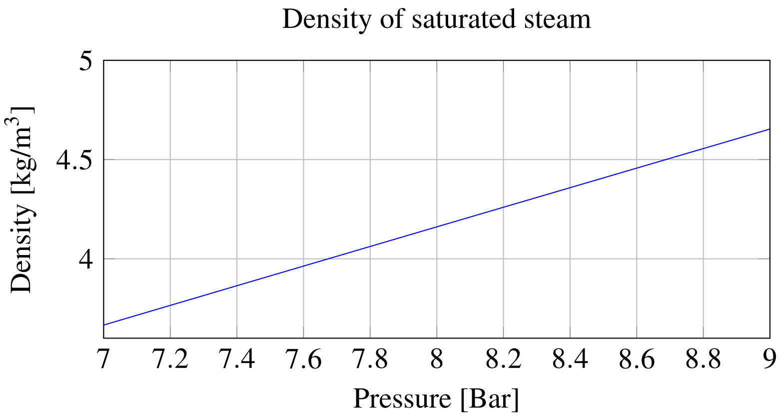

Figure 4.6: Density of steam as a function of pressure in the vicinity of 8 Bar. Generated using XSteam [Holmgren, 2007], which is a steam property lookup table for Matlab.

This effect is called the shrink and swell effect, and introduces non-minimum phase dynamics to the water level sensor. It manifests itself when the pressure in the boiler or the feed water temperature or flow changes.

Swelling is best illustrated from a scenario when the steam demand is increased, which makes the boiler pressure drop. This increases the steam vapor volume and makes the steam swell and increase the water surface level. Hence, the water level sensor measures an increase in water level, while in reality it is falling due to the increased steam demand. Shrinking is the reverse effect of swelling, which makes the water level appear to be falling while it is rising due to a pressure rise in the boiler [Åström and Bell, 1999,pp. 367].

Shrinking also occurs when the feed water flow is increased or its temperature is decreased. In both cases, the energy required to maintain the boiler pressure is increased, which if not compensated for by the burner, will decrease the boiler pressure and cause shrinking. Swelling occurs when the feed water flow is decreased or its temperature is increased.

To get a better understanding of the challenges this phenomenon introduces, it is useful to understand how the water level is measured. The Danish Crown steam boiler has a glass water level gauge for water level measurements, as depicted to the left side of the steam boiler on Figure 4.7.a. It is connected to both the steam and the water part of the boiler, and the water surface level should be the same as in the boiler as depicted on Figure 4.7.a. This is due to the fact that the pressure from the two water columns must be equal on either side of the bottommost horizontal pipe.

When the steam boiler is operating and steam bubbles exists under the water surface, the water level rises as depicted on Figure 4.7.b. Additionally, the water surface level in the gauge is lower than that of the boiler drum. This is caused by the average density of the combined water and steam in the boiler is less than the water in the gauge, and requires more water height to produce the same pressure. Please note that the gauge is indifferent to whatever is below the bottommost pipe, as it provide no pressure at the pipe. Lastly, swelling is depicted on Figure 4.7.c as a result of a pressure drop, which increases the steam bubble size.

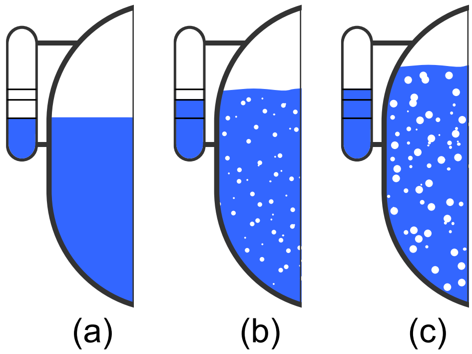

Figure 4.7: The level gauge and water and steam behavior in different situations with fixed amount of water. In (a), the steam boiler is turned off. In (b), the steam boiler is turned on and working under normal conditions. In (c), the steam pressure is lower than in (b) and the steam is swelling.

4.2.3 Benefits of adopting a MISO boiler feed control strategy

The current boiler feed strategy at Danish Crown uses a variable speed pump, but apply on/off control. It is a hysteresis like strategy, which turns the pump completely on when the water level reaches a lower bound and turns off when it reaches an upper bound. It has the benefit of being inexpensive as it require little tuning and is simple to install. However, it imposes thermal stress on the steam boiler due to larger temperature variations of the water in the boiler drum. This is caused by a relatively large quantity of water being added to the boiler in a short period. It cools down the water inside the boiler, which impairs the steam production capacity until normal operation conditions have been restored. It also require a large amount of start and stop cycles of the pumps, which makes the pumps liable to cavitation as the NPSH is at its highest, when it is operating at full speed.

Adopting a boiler feed strategy based on a variable speed pump, can lower the internal temperature fluctuations and can therefore maintain a more consistent steam production. In addition, as the feed water demand is more consistent, the deaerator demand will also be consistent. This can result in less variations of the feed water temperature during high steam demands, which lowers the amount of oxygen in the water and decrease the risk of corrosion. Using a MISO feed water controller, the pressure and temperature fluctuations in the boiler drum is expected to be further decreased. Hence, the expected lifetime of the boiler will be increased.

An insight into fire tube steam boilers and the difficulties of feed water control have now been introduced. The following will introduce a dynamic model, which will be the basis for the control development, testing and verification.

Chapter 5

Steam Boiler Model

This chapter describes the steam boiler model used for the control design. The model is taken from [Pétursson, 2015], which is a previous student project made in collaboration with Grundfos. It focuses on steam boiler modeling and boiler feed control of the Danish Crown steam boiler, and have data available for parameter identification. The model is intended to be used for future steam boiler control projects, such as this one. Unfortunately, the parameter identification was not carried out, which will be a task for this project.

First, an overview of the model will be made, which include the underlying model assumptions. Then the parameter identification of the non-linear model will be carried out. Lastly, the dynamic model will be stated, its operating point determined and its system dynamics linearized.

On Figure 5.1 the steam boiler system is depicted. The steam boiler has two actuators, namely the feed water pumps and the furnace. It has two disturbance inputs, which is the feed water temperature and the steam demand. It has two outputs, which are the water level and steam pressure sensor. As it is only possible to control the feed water flow, as the furnace is controlled by an existing pressure controller. For this reason, the pressure controller will be included as a part of the model.

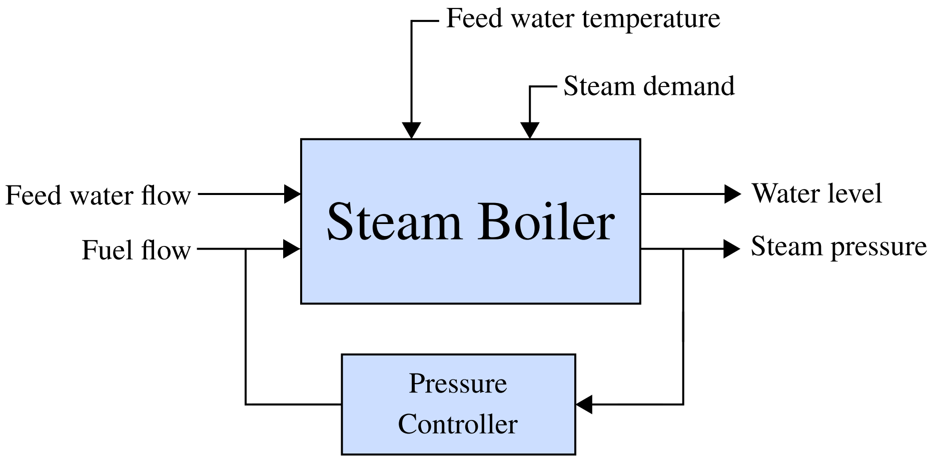

Figure 5.1: Steam boiler inputs and outputs.

5.1 Steam Boiler Model Overview

On Figure 5.2 a detailed overview of the steam boiler model is depicted. It aims to give an overview of the input and output flows, but also to give an insight to the model structure. The core concept behind the model is to keep track of the masses and energies, as they both progress throughout the system. The specific enthalpy h is used to keep track of the energy, as it is an energy measure per unit mass.

The Furnace burns the fuel flow $\dot{m}_{fu}$ and transfers the heat flow $Q_{m,f\rightarrow w}$ to the water in the boiler drum through the flue gas pipes. As burning fuel requires air, both the airflow $\dot{m}_a$ and specific enthalpy h_a is required. In return, the exhaust flue gas leaves the flue gas pipes with mass flow $\dot{m}_{fg}$ and specific enthalpy h_{fg}.

The boiler drum is considered a two-part system separated by the water surface. The part above the water surface is steam of which $\dot{m}_s$ leaves the system through the steam outlet with specific enthalpy h_s. The part below the water surface includes both water and steam as described in Subsection 4.2.2. As the steam evaporates from the heat flow $Q_{m,f\rightarrow w}$, it transitions to the steam part through $\dot{m}_{b\rightarrow s}$. The feed water flow $\dot{m}_{fw}$ adds water with specific enthalpy h_{fw} to the boiler drum. The level sensor measures the water surface height L_w, and the pressure sensor measures the steam pressure p_s.

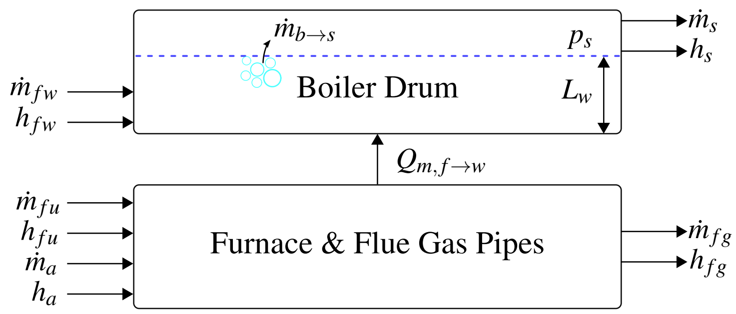

Where

p is the pressure	[Bar]
$\dot{m}$ is the mass flow	[kg/s]
h is the specific enthalpy	[J/kg]
L is the level	[m]
Q is the heat flow	[J/s]

With subscript

s for steam
a for air
$m,f\rightarrow w$ for flue gas pipes and furnace to water
fw for feed water
fg for flue gas
fu for fuel

Figure 5.2: Detailed overview of the inputs and outputs of the steam boiler model, and intermediate flow variables [Pétursson, 2015,pp. 17].

5.1.1 Steam Boiler Model Assumptions

This section describes the assumptions behind the derived steam boiler using [Pétursson, 2015,pp. 18-19, 25].

No feed water pump dynamics The feed water pumps are assumed to be flow controlled and contain no dynamics.

Water and steam is in saturation within the steam boiler Both the steam and water in the boiler is assumed to be saturated. This mean that the specific enthalpy h, density ρ and specific heat capacity c is no longer a function of its temperature T, and only depends on its pressure p.

Boiler volume It is assumed that the total internal steam boiler volume V_t is only composed of saturated steam V_s and saturated water V_w.

Steam bubbles under the water surface The shrink and swell effect was described in Subsection 4.2.2, which describe the existence of steam bubbles under the water surface. To track this behavior, the steam bubble volume is modeled according to (5.1). It describes the transition of steam between the water and steam region in terms of the average time constant τ_b. The steam bubble mass is expressed in terms of its density and volume.

$$\dot{m}_{b\rightarrow s} = \frac{1}{\tau_b}\rho_s V_b \tag{5.1}$$

Where

$\dot{m}_{b\rightarrow s}$ is the steam bubbles to steam mass flow	[kg/s]
τ_b is the steam bubble time constant	[s]
ρ_s is the steam density	$\left[\mathrm{kg/m^3}\right]$
V_b is the steam bubble volume	$\left[\mathrm{m^3}\right]$

Furnace and flue gas pipes dynamics As the closed loop steam boiler time constant is at minimum 200 times slower than the inherent dynamics of the furnace and flue gas pipes, they are neglected.

Furnace and flue gas pipes temperature assumptions The specific enthalpy h can be expressed in terms of the specific heat capacity c and temperature T according to

$$h = cT. \tag{5.2}$$

Where

h is the specific enthalpy	[J/kg]
c_p is the specific heat capacity	[J/(kg °C)]
T is the temperature	[°C]

The metal pipe jacket temperature is assumed to be equal to the steam temperature, $T_m \approx T_s$. In addition, the temperature of the input air T_a and fuel T_{fu}, and the output flue gas temperature T_{fg} is constant.

No energy loss to the surroundings The steam boiler is assumed perfectly thermodynamically isolated. This is a fair assumption, as this type of energy loss is neglectable compared to losses through the flue gas pipes and the steam outlet.

5.1.2 Steam Boiler Model Principle

Due to the saturation assumptions made in Subsection 5.1.1, all specific enthalpies and densities are a function of the pressure and is known for both steam and water. This allows the system to be described in terms of two states, namely the volume V to keeping track of internal mass, and the pressure p to keep track of energies. To give an insight into the underlying model and its structure, an example will be made based on a mass and enthalpy equation for a generic system described by (5.3). (5.3a) is the mass of the system, which is rewritten in terms of the volume V and the density $\rho(p)$. (5.3b) is the enthalpy of the system, which is rewritten in terms of its specific enthalpy $h(p)$, density $\rho(p)$ and volume V. To ease the notation, only V and p is a function of time in these equations.

$$m = \rho(p)V \tag{5.3a}$$

$$\mathcal{H} = h(p)m = h(p)\rho(p)V = U + pV \tag{5.3b}$$

Where

m is the mass	[m]
$\rho(p)$ is the density	$\left[\text{kg/m}^3\right]$
V is the volume	$\left[\text{m}^3\right]$
$\mathcal{H}$ is the enthalpy	[J]
$h(p)$ is specific enthalpy	[J/kg]
p is the pressure	[Bar]
U is the internal energy	[J]

The internal energy U is used for the energy balance and is isolated in (5.3b) and equals

$$U = h(p)\rho(p)V - pV. \tag{5.4}$$

Taking the time derivative of u and m equals (5.5a) and (5.5b).

$$\dot{m} = \dot{p}\rho(p)V + \dot{V}\rho(p) \tag{5.5a}$$

$$\begin{aligned} \dot{U} &= D_t\left[h(p)\rho(p)V\right] - D_t\left[pV\right] \\ &= \dot{p}D_p h(p)\rho(p)V + \dot{p}h(p)D_p\rho(p)V + h(p)\rho(p)\dot{V} - \dot{p}V - p\dot{V} \\ &= \dot{p}\left[D_p h(p)\rho(p)V + h(p)D_p\rho(p)V - V\right] + \dot{V}\left[h(p)\rho(p) - p\right] \end{aligned} \tag{5.5b}$$

Recall that the model keeps track of what enters and leaves the system through the mass flows $\dot{m}$ and specific enthalpies h or heat flow Q. This allow the pressure p and volume V of a system to be tracked by defining what enters and leaves the system according to

$$\dot{m} = m_{in} - m_{out} \text{ and} \tag{5.6}$$

$$\dot{U} = h_{in}\dot{m}_{in} - h_{out}\dot{m}_{out} + Q_{in} - Q_{out}. \tag{5.7}$$

The model structure of the generic system can then be determined according to

$$\begin{bmatrix} \rho(p)V & \rho(p) \\ D_p h(p)\rho(p)V + h(p)D_p\rho(p)V - V & h(p)\rho(p) - p \end{bmatrix} \begin{bmatrix} \dot{p} \\ \dot{V} \end{bmatrix} = \begin{bmatrix} \dot{m}_{in} - \dot{m}_{out} \\ \dot{m}_{in}h_{in} - \dot{m}_{out}h_{out} + Q_{in} - Q_{out} \end{bmatrix}, \tag{5.8}$$

where the states can be solved for by inverting the first matrix.

5.2 Steam Boiler Model

5.2.1 System Dynamic

The non-linear steam boiler model has the form:

$$\underbrace{\begin{bmatrix} J_{sb,11}(p_s,V_w) & J_{sb,12}(p_s) & 0 \\ J_{sb,21}(p_s,V_w) & J_{sb,22}(p_s) & 0 \\ J_{sb,31}(p_s,V_w,V_b) & J_{sb,32}(p_s) & J_{sb,33}(p_s) \end{bmatrix}}_{J_{sb}(x_{sb})} \underbrace{\begin{bmatrix} \dot{p}_s \\ \dot{V}_w \\ \dot{V}_b \end{bmatrix}}_{\dot{x}_{sb}} = \underbrace{\begin{bmatrix} H_{sb,1}(p_s,\dot{m}_{fw},\dot{m}_s) \\ H_{sb,2}(p_s,\dot{m}_{fw},\dot{m}_{fu},\dot{m}_s,T_{fw}) \\ H_{sb,3}(p_s,V_b,\dot{m}_{fw}) \end{bmatrix}}_{H_{sb}(x_{sb},\ u_{sb},\ d_{sb})} \tag{5.9}$$

Where

$x_{sb} = [p_s \quad V_w \quad V_b]^T$ is the steam boiler states.
$u_{sb} = [\dot{m}_{fw} \quad \dot{m}_{fu}]^T$ is the steam boiler inputs.
$d_{sb} = [\dot{m}_s \quad T_{fw}]^T$ is the steam boiler disturbances.

The elements in $J_{sb}(x)$ are given by:

$$J_{sb,11}(p_s,V_w) = \frac{d\rho_w(p_s)}{dp_s}V_w + \frac{d\rho_s(p_s)}{dp_s}(V_t - V_w) \tag{5.10a}$$

$$J_{sb,12}(p_s) = \rho_w(p_s) - \rho_s(p_s) \tag{5.10b}$$

$$J_{sb,21}(p_s,V_w) = \begin{pmatrix} \frac{dh_w(p_s)}{dp_s}\rho_w(p_s)V_w + \frac{d\rho_w(p_s)}{dp_s}h_w(p_s)V_w + \frac{dh_s(p_s)}{dp_s}\rho_s(p_s)(V_t - V_w) + \ \dots \\ \frac{d\rho_s(p_s)}{dp_s}h_s(p_s)(V_t - V_w) - V_t + \frac{dT_s(p_s)}{dp_s}c_{p,m}\rho_{m,b}V_{m,b} \end{pmatrix} \tag{5.10c}$$

$$J_{sb,22}(p_s) = h_w(p_s)\rho_w(p_s) - h_s(p_s)\rho_s(p_s) \tag{5.10d}$$

$$J_{sb,31}(p_s,V_w,V_b) = \frac{d\rho_w(p_s)}{dp_s}V_w + \frac{d\rho_s(p_s)}{dp_s}V_b \tag{5.10e}$$

$$J_{sb,32}(p_s) = \rho_w(p_s) \tag{5.10f}$$

$$J_{sb,33}(p_s) = \rho_s(p_s) \tag{5.10g}$$

The elements in $H_{sb}(x_{sb},u_{sb},d_{sb})$ are given by:

$$H_{sb,1}(p_s,\dot{m}_{fw},\dot{m}_s) = \dot{m}_{fw} - \dot{m}_s \tag{5.11a}$$

$$H_{sb,2}(p_s,\dot{m}_{fw},\dot{m}_{fu},\dot{m}_s,T_{fw}) = \begin{pmatrix} \dot{m}_{fw}h_{fw}(T_{fw}) + \dot{m}_{fu}(H_{fu} + c_{p,fu}T_{fu} - c_{p,fg}T_{fg}) + \ \dots \\ \dot{m}_a(\dot{m}_{fu})(c_{p,a}T_a - c_{p,fg}T_{fg}) - \dot{m}_s h_s(p_s) \end{pmatrix} \tag{5.11b}$$

$$H_{sb,3}(p_s,V_b,m_{fw}) = \dot{m}_{fw} - V_b\frac{1}{\tau_b}\rho_s(p_s) \tag{5.11c}$$

Where		With subscript
p is the pressure	[Bar]	s for steam
ρ is the specific density	$\left[\mathrm{kg/m^3}\right]$	a for air
V is the volume	$\left[\mathrm{m^3}\right]$	atm for atmospheric
m is the mass	[kg]	fw for feed water
$\dot{m}$ is the mass flow	[kg/s]	b for steam bubbles
T is the temperature	[°C]	w for water
h is the specific enthalpy	[J/kg]	fg for flue gas
c_p is the specific heat capacity	[J/(kg °C)]	

The fuel to air ratio The air mass flow $\dot{m}_a$ into the furnace is a function of the fuel mass flow $\dot{m}_{fu}$ according to

$$\dot{m}_a(\dot{m}_{fu}) = a\dot{m}_{fu}. \tag{5.12}$$

Where

a is the air to fuel ratio parameter [-]

Steam outlet model The steam outlet is determined by a simple valve model according to (5.13), which will be used to create a realistic steam outlet behavior. This model explains a relationship between the steam pressure and the valve position.

$$\dot{m}_s = k\sqrt{p_s - p_{atm}}. \tag{5.13}$$

Where

$\dot{m}_s$ is the steam mass flow	$[\mathrm{kg/s}]$
k is the opening degree	$\left[\mathrm{kg}/\left(\mathrm{s}\sqrt{\mathrm{Bar}}\right)\right]$
p_s is the steam pressure	$[\mathrm{Bar}]$
p_{atm} is the atmospheric pressure	$[\mathrm{Bar}]$

5.2.2 Measurement Model

The Danish Crown steam boiler has two sensors, namely a pressure sensor and level sensor. The pressure sensor measures the steam pressure p_s directly. The level sensor measures the water surface level L_{w+b} in the boiler drum as depicted on Figure 5.3.

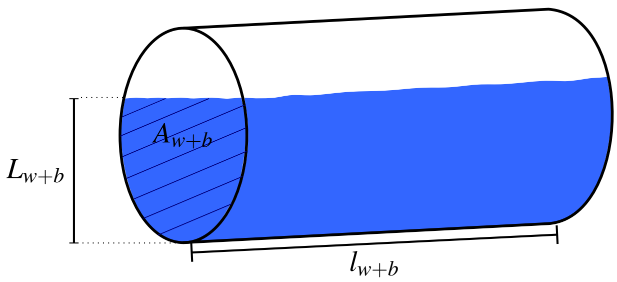

Figure 5.3: Geometric illustration of the boiler drum, where the water surface level L_{w+b} is measured. [Pétursson, 2015,pp. 35]

The measured water level is a function of three volumes, which are the water volume V_w, the steam bubble volume V_s and the furnace and flue gas pipes volume $V_{m,f}$. The relationship between the measured water surface level and the water surface volume is described by

$$V_w + V_b + V_{m,f} = l_{w+b}A_{w+b} = l_{w+b}\left[\pi r^2 - r^2\cos^{-1}\left(\frac{L_w - r}{r}\right) + (L_w - r)\sqrt{r^2 - (L_w - r)^2}\right]. \tag{5.14}$$

Where

V_w is the water volume	$\left[\mathrm{m}^3\right]$
V_b is the steam bubble volume	$\left[\mathrm{m}^3\right]$
$V_{m,f}$ is the furnace and flue gas pipes volume	$\left[\mathrm{m}^3\right]$
A_{w+b} is the water and steam bubble area	$\left[\mathrm{m}^2\right]$
l_{w+b} is the water and steam bubble length	$[\mathrm{m}]$
r is the steam boiler drum radius	$[\mathrm{m}]$

As it is not practical to solve analytically for L_w in (5.14), for now it will be denoted by $L_w\left(V_w+V_b+V_{m,f}\right)$. In practice, a lookup table will be used to determine L_w from V_{w+b}. This concludes the measurement model, which equals

$$y_{sb} = h_{sb}(x) = \begin{bmatrix} p_s \\ L_w\left(V_w+V_b+V_{m,f}\right) \end{bmatrix}. \tag{5.15}$$

Where

y is the measurement vector
$h_{sb}(x)$ is a vector with measurement equations
x is the states

5.3 System Identification

In this section the steam boiler model described in Subsection 5.2.1 will be modified to fit the Danish Crown Steam boiler based on data gathered by a previous project conducted in collaboration with Grundfos. The identification itself was not carried out, which will be one of the tasks for this project and is described in this section.

In Subsection 4.1.3 the sensors installed was stated but not described. Additional sensors was installed to measure all the inputs and outputs of the steam boiler model stated in Subsection 5.2.1 for the identification. On Figure 5.4, the Danish Crown steam boiler with the sensors used for the system identification is depicted. On Table 5.1, an overview of the sensors and their functions are stated. On Figure 5.5 a 3000 second preview of the measured data is depicted of the almost 16 hour long measurement log.

Notice that FS1 is a trip meter, which means that no continuous readings are available from this sensor. This means that the burner controller settings needs to be identified through other means, which will be described in Subsection 5.3.5. Furthermore, the feed water flow $\dot{m}_{fw}$ need to be recovered from the differential pressure sensor dPS, which is carried out in Subsection 5.3.4.

Before these issues are handled, the importance of different parts of the model will be investigated through the measurements series. These parts are the steam outlet valve model in Subsection 5.3.2, the existence of the steam bubbles are investigated in Subsection 5.3.3 and lastly the relevance of the flue gas pipes are considered in Subsection 5.3.6.

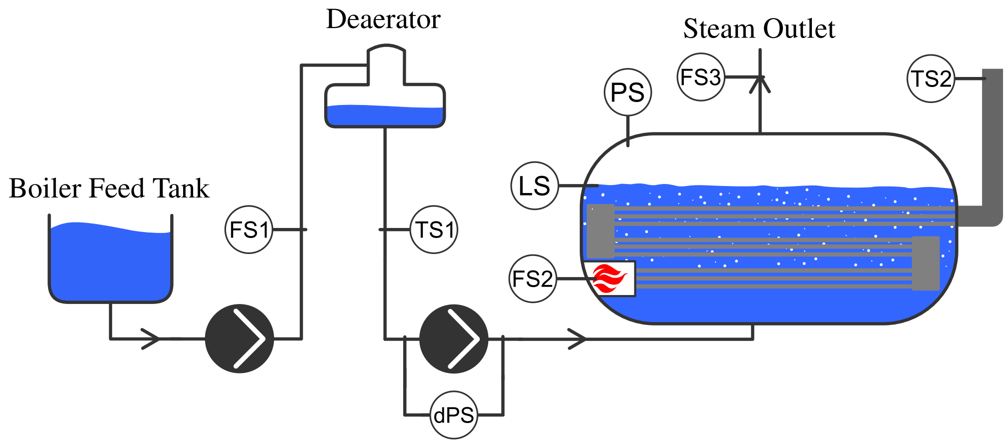

Figure 5.4: The sensors at the Danish Crown steam boiler for the system identification. Modified from [Pétursson, 2015,pp. 14].

Installed Sensors	
Sensor	**Description**
FS1	This sensor is a trip meter, which keeps track of the total used feed water in volume $[m^3]$. It must be manually read and cannot be used for control.
LS	Measures the water level in percentage between the LWL and HWL, which can be used for control.
PS	Measures the pressure of the boiler, which can be used for control.
TS2	Measures the temperature of the exhaust flue gas pipe, which can be used for control.
FS2	This sensor measures the fuel consumption of the burner. However, this sensor is a trip meter, and cannot be used for control.

Added sensors for the identification	
Sensor	**Description**
TS1	Measures the temperature of the feed water pipe.
dPS	Measures the pressure difference over the pump, which can be used to calculate the feed water flow $\dot{m}_{fw}$.
FS3	Measures the steam outlet mass flow $[kg/s]$.

Table 5.1: Detailed description of the sensors used for the system identification.

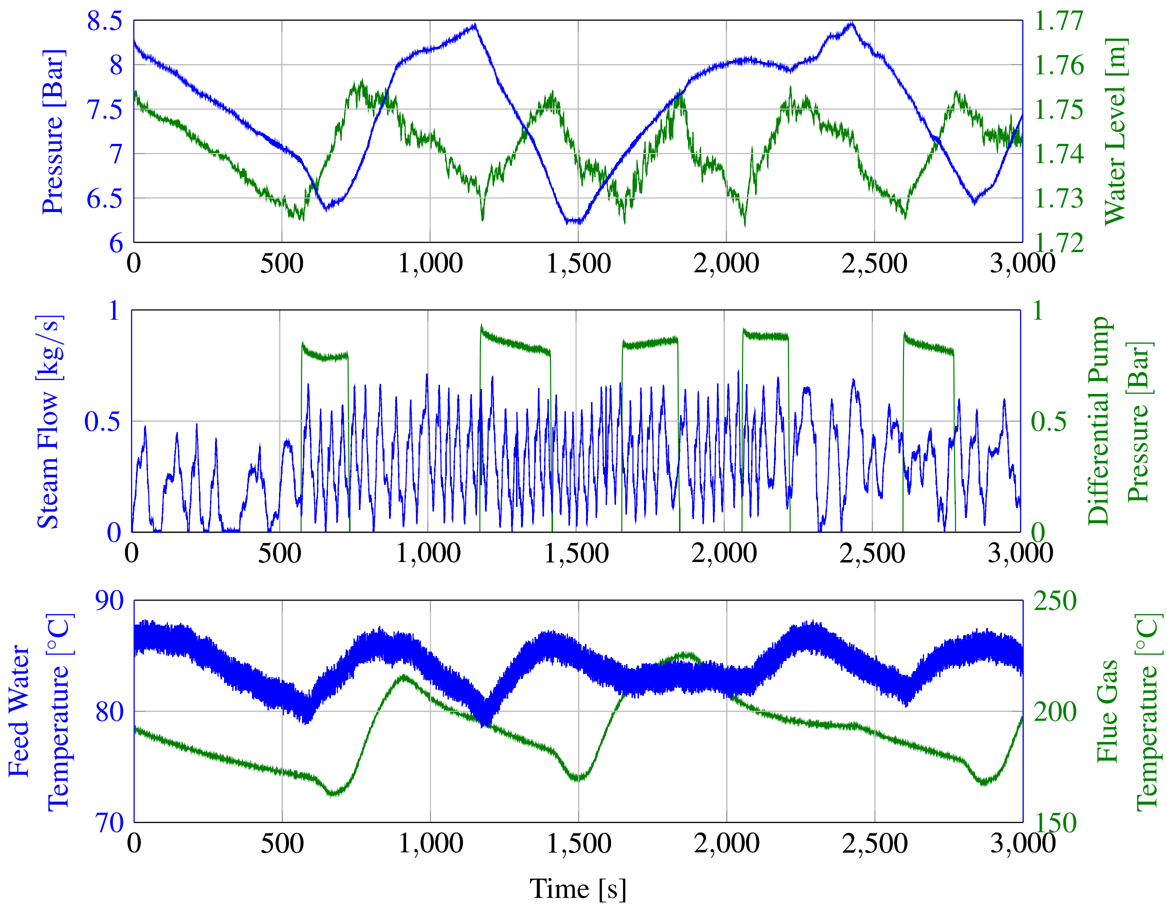

Figure 5.5: A 3000 second preview of the steam boiler readings.

5.3.1 Preliminary Parameters

In this subsection the preliminary parameters are stated. These include directly measured parameters, which are stated in Table 5.2. They where carried out at the same time as the measurements, hence, not by the author.

Parameter	Description	Source	Value
l_{w+b}	Length of the boiler	measuring tape	3.79 [m]
r	Radius of the boiler drum	measuring tape	1.04 [m]
V_t	The total water volume of the boiler drum	data sheet	7.8 [m^3]
$V_{m,f}$	The volume of the furnace and flue gas pipes	$V_{m,f} = l_{w+b}\pi r^2 - V_t$	5.2 [m^3]

Table 5.2: Directly measured parameters.

The Matlab steam and water property table `XSteam` [Holmgren, 2007] is used to find the specific enthalpy $h(p)$, density $\rho(p)$ and temperature $T(p)$ of saturated water and steam. However, it does not compute the pressure derivative of these properties, which are approximated through numerical differentiation. For instance,

$$\frac{dh(p)}{dp} = \frac{h(p+\Delta p) - h(p)}{\Delta p}, \tag{5.16}$$

approximates the pressure derivative of $h(p)$ at the pressure p. Δp is selected to equal 0.1 Bar as it has found to produce good results.

5.3.2 Steam outlet valve model

In this subsection the validity of the outlet steam valve model governed by (5.13) is questioned, which is restated in (5.17).

$$\dot{m}_s = k\sqrt{p_s - p_{atm}}. \tag{5.17}$$

This model is used to explain a relationship between the steam outlet mass flow $\dot{m}_s$ and the steam pressure p_s, which is not the case for the danish crown steam boiler. This can be demonstrated on the middle plot of Figure 5.5, where the amplitude of the steam outlet is consistent despite large changes in pressure. Specifically, the steam outlet flow at $t = 600$s and $t = 1200$s are the same in terms of magnitude, despite a large pressure difference between the two. If the model was correct, the amplitude of $\dot{m}_s$ should be consistently larger for higher steam pressure p_s. To be fair, this model might be valid to model the steam outlet behavior of other steam boiler systems, so the correctness of this model is not questioned. But as the data does not support the use of this model, it is not used.

5.3.3 Existence of Steam Bubbles

This section investigates the existence of the steam bubbles under the water surface, which is represented as the steam bubble volume V_b in the system model. The preliminary information necessary to investigate this phenomenon is described in Subsection 4.2.2 (The Shrink and Swell Effect).

The steam bubble volume V_b is caused by the steam outtake $\dot{m}_s$ and steam bubbles are largest at lower pressure. Hence, to investigate the impact of the largest occurring steam bubble volume, a combination of low pressure and high steam demand is preferred.

These conditions are fulfilled in Figure 5.6 marked with the red box, where an above average steam flow is observed at a low boiler pressure, with $\dot{m}_s = 0.59$ kg/s and $\dot{p}_s = 6.8$ Bar. For reference, the average output flow for the entire measurement series is 0.29 kg/s and the lowest observed boiler pressure is 6.12 Bar. This results in a 4 mm rise in the water level L_w, which is present for a total of 5 s. It is considered insignificant compared to a 14 cm span between LWL and HWL, while considering both the length and magnitude. For this reason, the steam bubble volume is assumed to be zero at all times.

That being said, the effects of the steam bubbles appear to have a phase shift. This fits well with the steam bubble model, at it assumed a first order model relationship between the steam bubble volume and the steam flow.

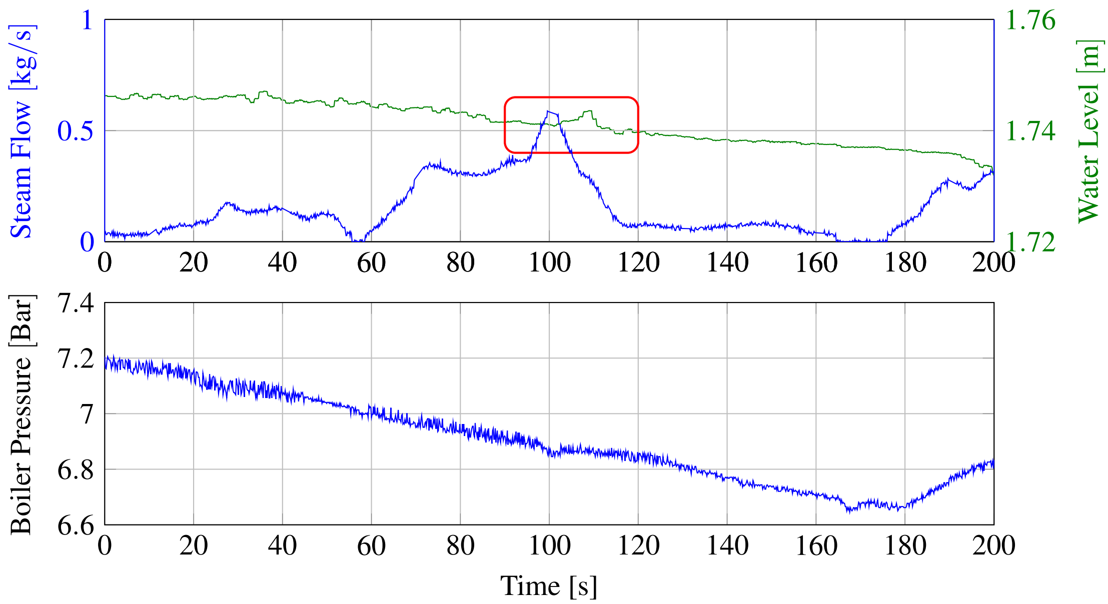

Figure 5.6: Steam bubble impact on the level measurements.

5.3.4 Feed Water flow measurement from the Differential Pressure Sensor

By knowing the percentile angular velocity of the pump n and the pressure difference Δp over the pump, the mass flow through it can be calculated using its pump curve. The pump head H can be expressed in terms of the differential pressure Δp across it, as described by (4.1). Hence, the feed water flow can be stated as a function of the shape $\dot{m}_{fw}(H(\Delta p), n)$. The pump is assumed to run at full speed, given that the pump is on/off controlled. However, this assumption is proven to be faulty in Section B.1.

This requires the feed water flow to be found through different means, of which the water level sensor and steam outlet flow will be utilized in conjunction with the mass balance equation introduced in Subsection 5.1.2. This is considered valid, as the integrated steam outlet mass flow is 16.5 m^3 and the total feed water is 16.8 m^3. Both for the entire measurement series. Using this equation change of water mass in the boiler denoted by $\dot{m}_w$ can be written as

$$\dot{m}_w = \dot{m}_{fw} - \dot{m}_s, \tag{5.18}$$

which has two unknown terms, of which only the steam outlet flow $\dot{m}_s$ is known. This require $\dot{m}_w$ to be determined. As the level controller is known to be a hysteresis like controller, it is considered sufficient to look at the start and stop point of its on cycle. By integrating (5.18) over the pumps on cycle, the change of water equals (5.19). The water mass can be found through the level measurements, which for convenience is denoted $V_w(L_w)$, and the water density $\rho_w(p_s)$ as stated in (5.20).

$$\int_{t_{\text{start}}}^{t_{\text{stop}}} \dot{m}_{fw}\, dt - \int_{t_{\text{start}}}^{t_{\text{stop}}} \dot{m}_s\, dt = \int_{t_{\text{start}}}^{t_{\text{stop}}} \dot{m}_w\, dt = m_w(t_{\text{stop}}) - m_w(t_{\text{start}}) \tag{5.19}$$

$$= \rho_w(p_s(t_{\text{stop}}))\, V_w(L_w(t_{\text{stop}})) - \rho_w(p_s(t_{\text{start}}))\, V_w(L_w(t_{\text{start}})) \tag{5.20}$$

The average feed water flow $\dot{m}_{fw,avg}$ for the start/stop period can then be approximated through

$$\dot{m}_{fw,avg} = \frac{\Delta m_{fw}}{\Delta t} = \frac{\int_{t_{\text{start}}}^{t_{\text{stop}}} \dot{m}_{fw}\, dt}{t_{\text{stop}} - t_{\text{start}}} \tag{5.21}$$

$$= \frac{\int_{t_{\text{start}}}^{t_{\text{stop}}} \dot{m}_s\, dt + \rho_w(p_s(t_{\text{stop}}))\, V_w(L_w(t_{\text{stop}})) - \rho_w(p_s(t_{\text{start}}))\, V_w(L_w(t_{\text{start}}))}{t_{\text{stop}} - t_{\text{start}}}. \tag{5.22}$$

On Figure 5.7 a series of 4 feed water refill cycles is depicted. The approximated feed water flow appear to be quite inconsistent in terms of magnitude, but will later on be shown to be quite accurate. The exact reason for the inconsistency is not known for certain by the author, however the mean value for 25 feed water cycles are 1.06 [kg/s], which all of the presented cycles are relatively close to.

5.3.5 Burner Controller Identification

In this subsection, the burner controller is identified. For clarity, the settings which are related to the burner from the steam boiler model through the fuel flow $\dot{m}_{fu}$ and flue gas temperature T_{fg} are

$$\dot{U}_{fu} = \dot{m}_{fu}\,(H_{fu} + c_{p,fu}\,T_{fu} - c_{p,fg}\,T_{fg}) + \dot{m}_a(\dot{m}_{fu})\,(c_{p,a}\,T_a - c_{p,fg}\,T_{fg}), \tag{5.23}$$

where $\dot{U}_{fu}$ is denoted the burner energy contribution. Unfortunately, no output signal was available on the fuel flow sensor, which makes it harder to determine the type and settings of the unknown pressure controller. To solve this problem, the burner model denoted by (5.23) is abandoned, which require an alternative method of identifying the pressure controller.

The initial hypothesis is that the burner controller operates in a hysteresis like fashion, similar to the level controller. However, it appears to have two stages during its on cycle, which can be illustrated from the steam pressure behavior, which is depicted on the middle plot of Figure 5.7. The first stage appear to be active for $t = 678$s (1) to 913s (2) where a large amount of energy is added by the burner. The second stage is active for $t = 913$ (2) to 1181s (3) where significantly less energy is added by the burner. The burner becomes active when the steam pressure drops below 6.4 Bar and inactive when it reaches around

8.375 Bar, of which energy is added according to

$$\dot{U}_{fu}(\text{burner state}, p_s) = \begin{cases} \dot{U}_{\text{BS }1} & \text{burner state} = \text{"Burner Active"} \ \wedge p_s < 8 \text{ Bar} \\ \dot{U}_{\text{BS }2} & \text{burner state} = \text{"Burner Active"} \ \wedge 8 \text{ Bar} \leq p_s \\ 0 & \text{burner state} = \text{"Burner Inactive"} \end{cases} . \tag{5.24}$$

Where $\dot{U}_{\text{BS }1}$ and $\dot{U}_{\text{BS }2}$ is the burner energy contribution settings, which will be identified in this section.

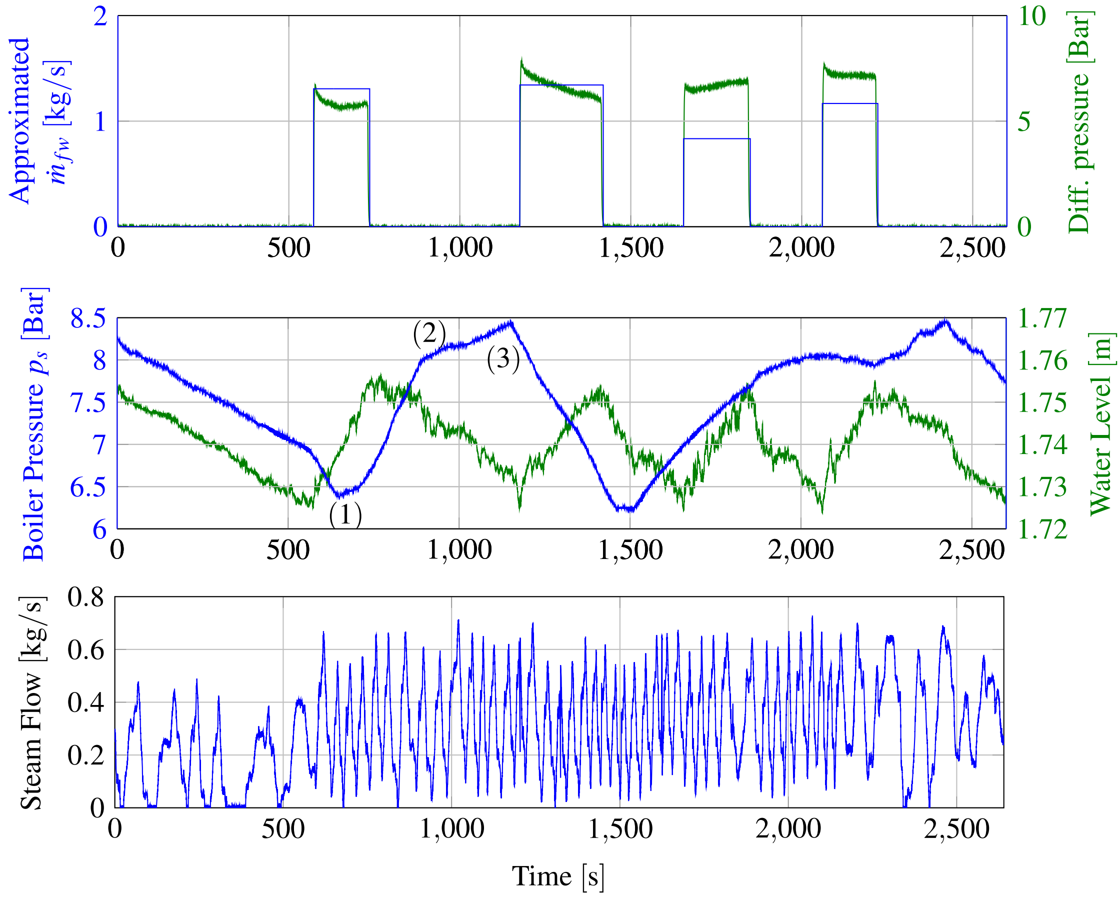

Figure 5.7: Pressure difference over the pump and the estimated water flow.

To determine these settings, it is crucial to keep track of the total internal energy in the boiler, of which the ideas of Subsection 5.1.2 is used. Two equations from this section is used, which are the enthalpy equation as restated in (5.25) and its derivative as a function of its inputs and outputs, which is restated in (5.26). The first equation will be used to determine the internal energy in the steam boiler, while the second one is used to keep track of the steam output $\dot{m}_s$ and the feed water input $\dot{m}_{fw}$. This approach is closely related to the recovery of the feed water measurements in Subsection 5.3.4, but uses energy balances instead of mass balances.

$$U = [h(p)\rho(p) - p]\,V \tag{5.25}$$

$$\dot{U} = h_{in}(p)\,\dot{m}_{in} - h_{out}(p)\,\dot{m}_{out} \tag{5.26}$$

Where

m is the mass	[m]
$\rho(p)$ is the density	$\left[\mathrm{kg/m^3}\right]$
V is the volume	$\left[\mathrm{m^3}\right]$
$h(p)$ is specific enthalpy	[J/kg]
p is the pressure	[Bar]
U is the internal energy	[J]

The internal energy in the steam boiler U_{sys} is a product of the internal energy of the steam U_s and the water U_w according to

$$U_w = [h_w(p_s)\,\rho_w(p_s) - p_s]\,V_w = [h_w(p_s)\,\rho_w(p_s) - p_s]\,V_w(L_w) \text{ and} \tag{5.27}$$

$$U_s = [h_s(p_s)\,\rho_s(p_s) - p_s]\,V_s = [h_s(p_s)\,\rho_s(p_s) - p_s]\,[V_t - V_w(L_w)]\,. \tag{5.28}$$

The volume of the water V_w can be found through the water level measurements L_w and its measurement model, which is stated in Subsection 5.2.2. For convenience, it is simply referenced to as $V_w(L_w)$. The steam volume V_s is the remaining steam boiler volume, which can be found through the total steam boiler volume V_t as $V_s = V_t - V_w(L_w)$. Hence, the total internal energy in the steam boiler can be determined through

$$U_{sys} = [h_w(p_s)\,\rho_w(p_s) - p_s]\,V_w(L_w) + [h_s(p_s)\,\rho_s(p_s) - p_s]\,[V_t - V_w(L_w)]\,, \tag{5.29}$$

which is depicted on the top plot of Figure 5.8 as the blue trace for a single burner cycle. On this plot it is possible to anticipate the two burner stages, which are denoted by BS 1 and 2. For comparison the energy contribution of the steam and feed water is depicted on the red trace.

To calculate the energy added by the burner to the water $\dot{U}_{fu}$, the internal energy change caused by the feed water $\dot{U}_{fw}$ or steam outlet $\dot{U}_s$ must be accounted for. For convenience, the sum of these are denoted $\dot{U}_{fw,s}$. Hence, the change of internal energy of the boiler U_{sys} can be stated according to

$$\dot{U}_{sys} = \dot{U}_{fw} + \dot{U}_s + \dot{U}_{fu} = \dot{U}_{fu} + \dot{U}_{fw,s}. \tag{5.30}$$

Using (5.26), $\dot{U}_{fw,s}$ can be determined according to

$$\dot{U}_{fw,s} = h_{fw}(p_s)\,\dot{m}_{fw} - h_s(p_s)\,\dot{m}_s. \tag{5.31}$$

Integrating (5.30) results in (5.32), which gives an expression that can be used in conjunction with (5.29) to calculate the energy added from the burner, which is obtained by solving for it and equals (5.33).

$$\begin{aligned} U_{sys}(t) - U_{sys}(0) &= \int_0^t \dot{U}_{fu}\,dt + \int_0^t \dot{U}_{fw,s}\,dt \\ &= \int_0^t \dot{U}_{fu}\,dt + \int_0^t h_{fw}(p_s)\dot{m}_{fw} - h_s(p_s)\,\dot{m}_s\,dt \end{aligned} \tag{5.32}$$

$$\int_0^t \dot{U}_{fu}\,dt = U_{sys} - U_{sys}(0) - \int_0^t h_{fw}(p_s)\dot{m}_{fw} - h_s(p_s)\,\dot{m}_s\,dt \tag{5.33}$$

A plot of (5.33) is depicted on the bottom plot of Figure 5.8 as the blue trace. This plot is the difference between the energy in the system (blue trace of the top plot of Figure 5.8) and the energy added by the feed water and energy leaving from the steam outlet (red trace of the top plot of Figure 5.8).

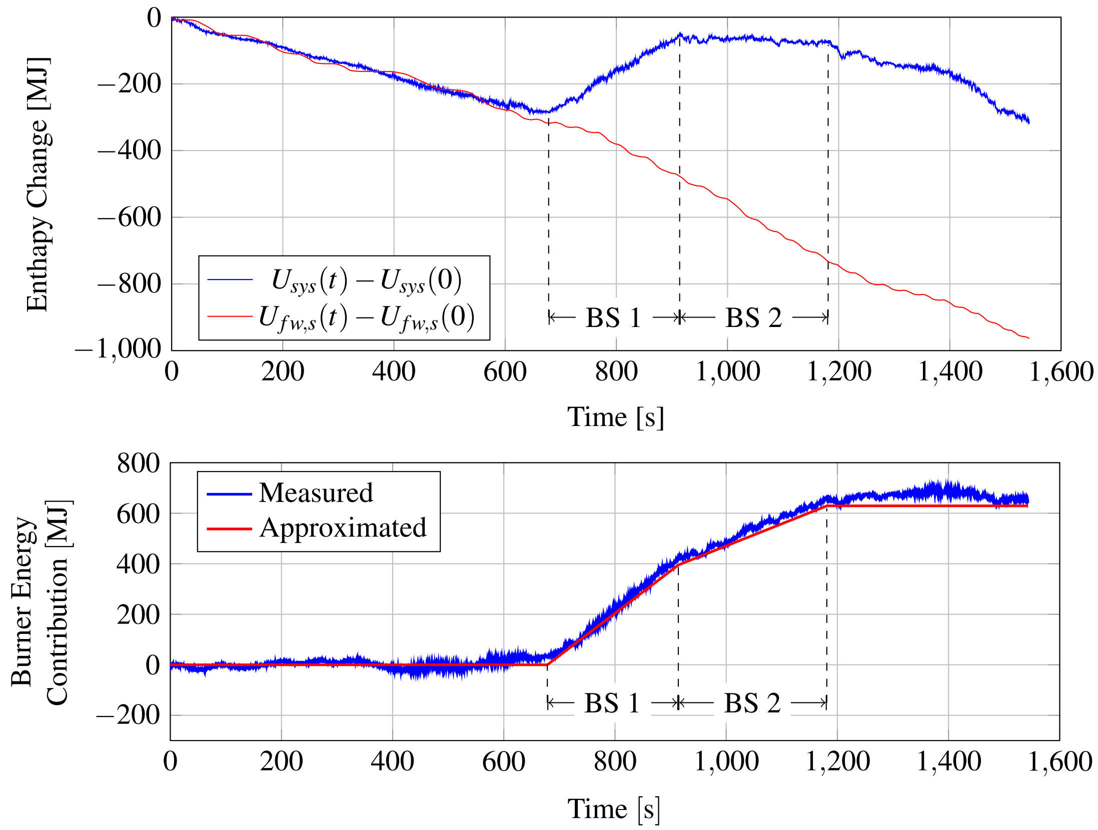

Figure 5.8: Top plot: Enthalpy change of the system $U_{sys}(t)$ and the enthalpy change caused by the feed water and steam outlet $U_{fw,s}(t)$. Bottom plot: The energy contribution from the burner and its approximated contribution. BS 1 and 2 refer to burner stage 1 and 2.

The rate of added energy is calculated by taking the average energy added in this period, which are found to equal

$$\dot{U}_{\text{BS 1}} = 1.68 \text{ MJ/s and } \dot{U}_{\text{BS 2}} = 0.87 \text{ MJ/s}. \tag{5.34}$$

On a side note, it appear very likely that burner stage 1 is full burner capacity, while stage 2 is half capacity.

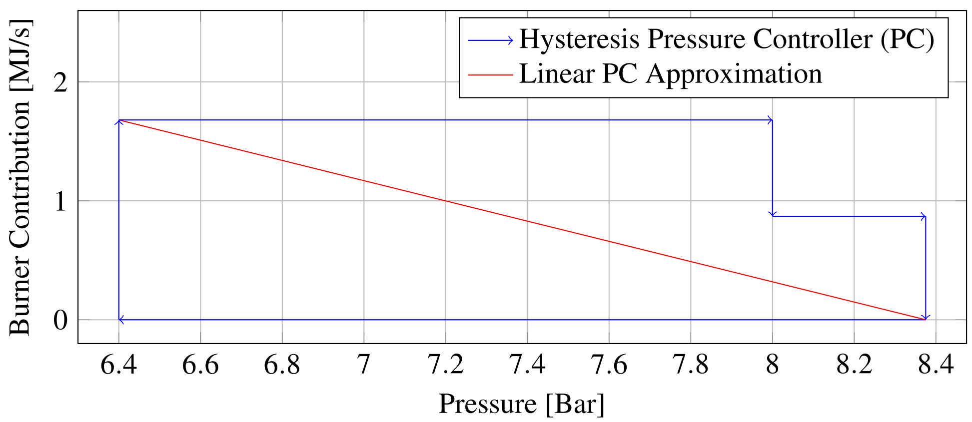

Figure 5.9: The identified hysteresis pressure controller and its linear approximation.

The identified hysteresis pressure controller behavior is depicted on Figure 5.9 as the blue curve. As the intention is to get a linear model of the plant, a linear model of the pressure controller is necessary as well. For this purpose, the linear approximation depicted as the red curve will be used. As this approximation is inherently linear, it can be found in terms of the pressure operating point $p_{s,o}$, according to

$$\delta \dot{U}_{fu} = \mathcal{F}_{fu}\left(p_s - p_{s,o}\right) = -0.81\ \frac{\text{MJ/s}}{\text{Bar}}\ \left(p_s - p_{s,o}\right). \tag{5.35}$$

It has to be said that the linear model is far from ideal, but it is considered the best possible option. This model will be revisited in Subsection 5.4.2 (Linearization).

5.3.6 The burner and flue gas pipe metal

This essentially only leaves out the parameters related to the flue gas pipes, which are found in $J_{sb,21}(p_s, V_w)$ in the steam boiler model, which is restated and equals:

$$\begin{aligned} J_{sb,21}(p_s,V_w) = {} & \frac{dh_w(p_s)}{dp_s}\rho_w(p_s)V_w + \frac{d\rho_w(p_s)}{dp_s}h_w(p_s)V_w + \frac{dh_s(p_s)}{dp_s}\rho_s(p_s)(V_t - V_w) + \\ & \frac{d\rho_s(p_s)}{dp_s}h_s(p_s)(V_t - V_w) - V_t + \frac{dT_s(p_s)}{dp_s}c_{p,m}\,\underbrace{\rho_{m,b}V_{m,b}}_{P_1}, \end{aligned} \tag{5.36}$$

The relevant part is denoted by P_1, which will be determined using a parameter estimation algorithm. This is carried out using the Matlab toolbox called Sensetool, which is described in the following paragraph. Using this algorithm, the result depicted in (5.37) is found. To elaborate on the importance of this parameter, a comparison using the found parameter and assuming it is zero is depicted on Figure 5.10. This illustrates that the impact of P_1 parameter is rather low, which implies that this parameter could be neglected from the model. This makes sense, considering that the terms related to the water volume V_w is expected to be dominant in $J_{sb,21}(p_s, V_w)$ due to the magnitude of V_w.

$$P_1 = c_{p,m}\,\rho_{m,b}V_{m,b} = 0.966\ \frac{\text{MJ}}{^\circ\text{C}} \tag{5.37}$$

Senstool

Senstool is a Matlab toolbox used for parameter estimation of linear and nonlinear models with known structure. This section serves to give an overview of the principle using [Knudsen, 2004, chap. 3], which is available on the CD at `[Sources/Expermental modelling of dynamic systems.pdf]`.

One strong reason for using Senstool is that it can handle parameter identification of user-defined nonlinear models. This is especially useful if hysteresis dynamics is included in the model, such as the burner controller. Senstool require the user-defined model to be on the form of (5.38). Please notice that this gives a high degree of freedom, as the model execution is carried out by the user for all N samples.

$$y_m(\Theta) = \text{model}(t,\, u,\, \Theta) \tag{5.38}$$

Where

N is the number of samples
$y_m(\Theta) \in \mathbb{R}^N \times \mathbb{R}^m$ is a matrix containing the N estimated outputs
$t \in \mathbb{R}^N$ is a vector of the sampling times
$u \in \mathbb{R}^N \times \mathbb{R}^n$ is a matrix containing the N sampled model inputs
$\Theta \in \mathbb{R}^p$ is a vector with the model parameters

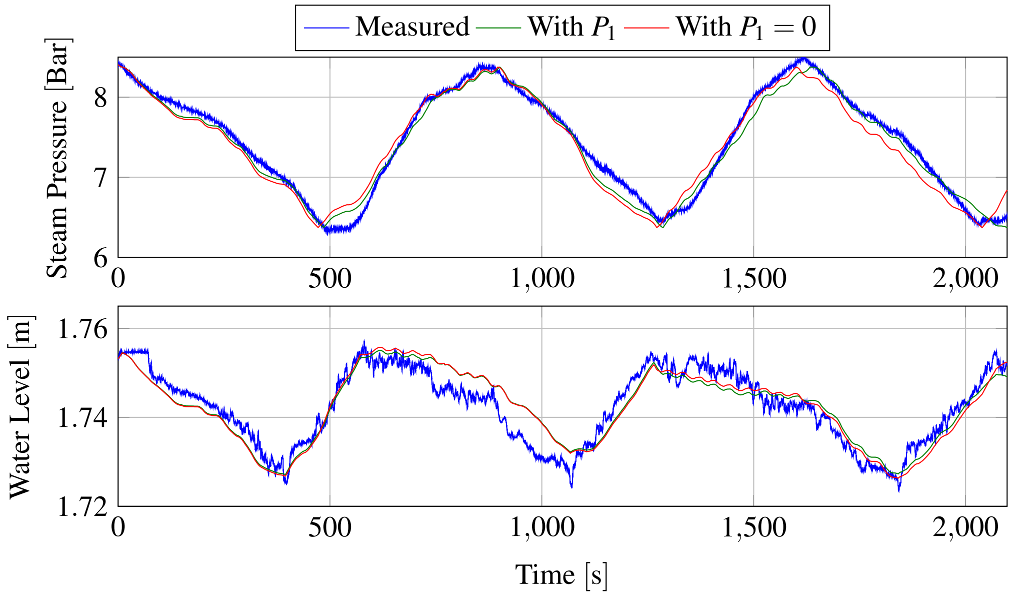

Figure 5.10: A comparison between the nonlinear model and the measured data with P_l =(5.37) and $P_l = 0$.

Senstool tries to change the parameters of Θ to minimize the predicted model error given by (5.39), by minimizing the cost function (5.40). To do this, Sensetool implements the Gauss-Newton Algorithm to carry out the minimization of the performance function. It is an iterative algorithm, which means that convergence is not guaranteed and a non-global minimum can be found. For more information about the Gauss-Newton Algorithm [Antoniou and Lu, 2007, pp. 138-140] provides a walkthrough of the underlying principles.

$$\varepsilon(k,\Theta) = y(k) - y_m(k,\Theta) \tag{5.39}$$

$$\mathcal{J}(\Theta) = \frac{1}{2N}\sum_{k=1}^{N} \varepsilon(k,\Theta)^T \varepsilon(k,\Theta) \tag{5.40}$$

Where

The use of k as an argument denoted the k'th sample of the variable
$y \in \mathbb{R}^N \times \mathbb{R}^l$ is a matrix containing the N measured outputs
$\mathcal{J}(\Theta) \in \mathbb{R}$ is the total cost as a function of the model parameters Θ

As this concludes the system identification, a summary of the identified model and the found parameters will be stated.

5.3.7 The System Identification Results

In this section, the results of the system identification is presented. The steam bubble volume state V_s has been removed in Subsection 5.3.3. The burner controller has been proven to be a hysteresis-like controller in Subsection 5.3.5, which are found to be governed by

$$\dot{U}_{fu}(\text{burner state}, p_s) = \begin{cases} \dot{U}_{\text{BS }1} & \text{burner state} = \text{"Burner Active"} \ \wedge p_s < 8 \text{ Bar} \\ \dot{U}_{\text{BS }2} & \text{burner state} = \text{"Burner Active"} \ \wedge 8 \text{ Bar} \leq p_s \\ 0 & \text{burner state} = \text{"Burner Inactive"} \end{cases}, \tag{5.41}$$

where, burner state, is the burner hysteresis state. This simplified the model significantly to

$$\underbrace{\begin{bmatrix} j_{11}(p_s,V_w) & j_{12}(p_s) \\ j_{21}(p_s,V_w) & j_{22}(p_s) \end{bmatrix}}_{J(x)} \underbrace{\begin{bmatrix} \dot{p}_s \\ \dot{V}_w \end{bmatrix}}_{\dot{x}} = \underbrace{\begin{bmatrix} H_1(p_s,\dot{m}_{fw},\dot{m}_s) \\ H_2(p_s,\dot{m}_{fw},\dot{U}_{fu},\dot{m}_s,T_{fw}) \end{bmatrix}}_{H(x,\ u,\ d)} \tag{5.42a}$$

$$y = h(x) = \begin{bmatrix} p_s \\ L_w\left(V_w + V_{m,f}\right) \end{bmatrix}. \tag{5.42b}$$

Where

$x = [p_s \quad V_w]^T$ is the Danish Crown steam boiler states.
$u = [\dot{m}_{fw}]^T$ is the Danish Crown steam boiler inputs.
$d = [\dot{m}_s \quad \dot{U}_{fu} \quad T_{fw}]^T$ is Danish Crown the steam boiler disturbances.

The elements in $J(x)$ are given by:

$$J_{11}(p_s,V_w) = \frac{d\rho_w(p_s)}{dp_s} V_w + \frac{d\rho_s(p_s)}{dp_s}(V_t - V_w) \tag{5.43a}$$

$$J_{12}(p_s) = \rho_w(p_s) - \rho_s(p_s) \tag{5.43b}$$

$$J_{21}(p_s,V_w) = \left(\begin{array}{l} \frac{dh_w(p_s)}{dp_s}\rho_w(p_s)V_w + \frac{d\rho_w(p_s)}{dp_s}h_w(p_s)V_w + \frac{dh_s(p_s)}{dp_s}\rho_s(p_s)(V_t - V_w) + \ \dots \\ \frac{d\rho_s(p_s)}{dp_s}h_s(p_s)(V_t - V_w) - V_t + \frac{dT_s(p_s)}{dp_s}c_{p,m}\,\rho_{m,b}V_{m,b} \end{array} \right) \tag{5.43c}$$

$$J_{22}(p_s) = h_w(p_s)\,\rho_w(p_s) - h_s(p_s)\,\rho_s(p_s) \tag{5.43d}$$

The elements in $H(x,u,d)$ are given by:

$$H_1(p_s,\dot{m}_{fw},\dot{m}_s) = \dot{m}_{fw} - \dot{m}_s \tag{5.44a}$$

$$H_2(p_s,\dot{m}_{fw},\dot{U}_{fu},\dot{m}_s,T_{fw}) = \dot{m}_{fw}\,h_{fw}(T_{fw}) + \dot{U}_{fu} - \dot{m}_s\,h_s(p_s) \tag{5.44b}$$

Figure 5.11 shows a comparison between the output of the above model as a function of the measured inputs and disturbances. It cannot be stressed enough that this plot is generated with another data-series than the one used for identification. The steam pressure appears to be a good fit, while the feed water at times deviate. This cannot be helped, as the approximation of this input was rather crude.

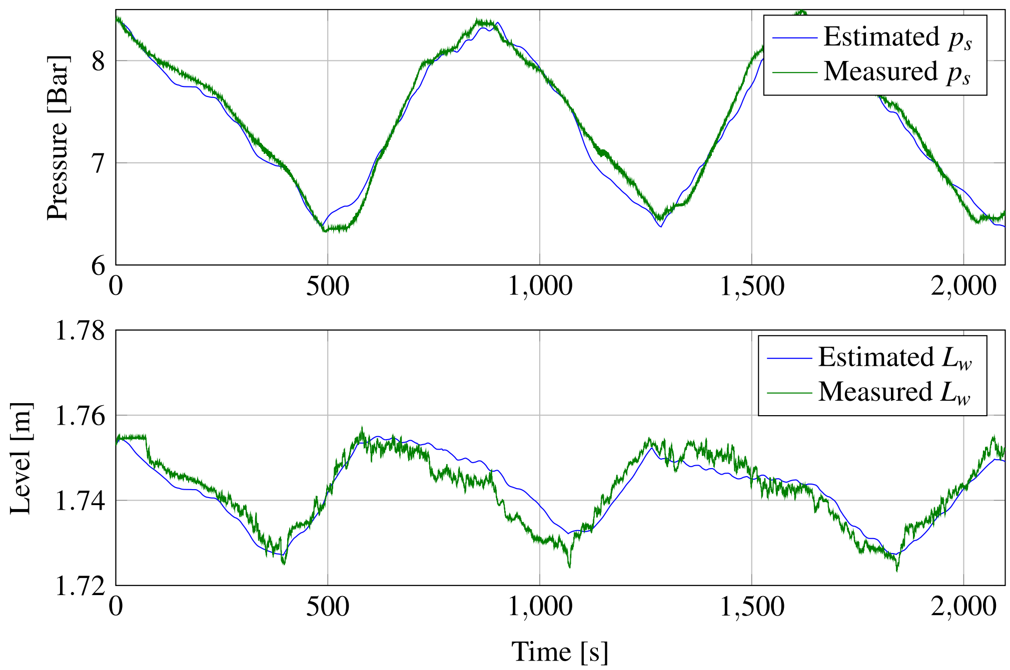

Figure 5.11: Comparison between the steam boiler model and the measured data with the same inputs in open loop.

Parameter	Description	Source	Value
l_{w+b}	Length of the boiler	measuring tape	3.79 [m]
r	Radius of the boiler drum	measuring tape	1.04 [m]
V_t	The total water volume of the boiler drum	data sheet	7.8 [m^3]
$V_{m,f}$	The volume of the furnace and flue gas pipes	$V_{m,f} = l_{w+b}\pi r^2 - V_t$	5.2 [m^3]
$\dot{U}_{\mathrm{BS}\,1}$	The burner contribution at stage 1	(5.34)	1.68 [MJ/s]
$\dot{U}_{\mathrm{BS}\,2}$	The burner contribution at stage 2	(5.34)	0.87 [MJ/s]
$c_{p,m}\rho_{m,b}V_{m,b}$	Flue gas pipe metal contribution	(5.37)	0.966 [$\frac{\mathrm{MJ}}{^\circ\mathrm{C}}$]

Table 5.3: Parameter identification results.

5.4 Linearization

In this section, the system equations described by (5.42) is linearized. First, the operating point will be determined, which is necessary for the linearization.

5.4.1 Operating Point

Definition 5.1 (Operating Point [Khalil, 2002, pp. 3])
For the states $x_o = x$ and external inputs $u_o = u$ to be an operating point for the non-autonomous system $\dot{x} = f(x,u)$,

$$\dot{x} = f(x_o, u_o) = 0 \tag{5.45}$$

must be satisfied. Where the subscript o indicate an operating point.

Applying Definition 5.1 to (5.42a) results in

$$H(x_o,u_o,d_o) = J(x_o)\dot{x} = J(x_o)0 = 0. \tag{5.46}$$

From the Danish Crown steam boiler measurements, the operating points of the pressure p_s, water level L_w, feed water temperature T_{fw} and the steam outlet flow $\dot{m}_s$ are determined. The operating points left to determine are the feed water flow $\dot{m}_{fw}$, the burner contribution $\dot{U}_{fu}$ and the water volume V_w. The operating points are determined from (5.46) and the output equation $y = h(x)$, which equals

$$0 = \dot{m}_{fw,o} - \dot{m}_{s,o} \text{ and} \tag{5.47a}$$
$$0 = \dot{m}_{fw,o} h_{fw}(T_{fw}) + \dot{U}_{fu,o} - \dot{m}_s h_s(p_{s,o}). \tag{5.47b}$$

From (5.47a) and (5.47b), the following can be stated:

$$\dot{m}_{s,o} = \dot{m}_{fw,o} \tag{5.48}$$
$$\dot{U}_{fu}(p_s) = \dot{m}_s h_s(p_{s,o}) - \dot{m}_{fw,o} h_{fw}(T_{fw}) = \dot{m}_{s,o}\left(h_s(p_{s,o}) - h_{fw}(T_{fw})\right) \tag{5.49}$$

The last operating point to determine is the water volume $V_{w,o}$, which is determined from the water surface level equation (5.14), which has the shape of

$$V_{w,o} + V_{m,f} = f(L_{w,o}), \tag{5.50}$$

where $f(L_w)$ is a function of L_w. Solving for the water volume operating point gives

$$V_{w,o} = f(L_{w,o}) - V_{m,f}. \tag{5.51}$$

Using these expressions all the operating points of the system can be calculated, which is depicted on Table 5.4. As the operating point for the system is determined, the system is now linearized.

Operating Point	**Source**	**Value**
Steam pressure $p_{s,o}$	Mean of the measurements	7.64 [Bar]
Water level $L_{w,o}$	Mean of the measurements	1.74 [m]
Steam outlet mass flow $\dot{m}_{s,o}$	Mean of the measurements	0.289 [kg/s]
Feed water temperature $T_{fw,o}$	Mean of the measurements	87.6[kg/s]
Feed water flow $\dot{m}_{fw,o}$	(5.48)	0.289 [kg/s]
Burner contribution $\dot{U}_{fu,o}$	(5.49)	0.6174 [MJ/s]
Water volume $V_{w,o}$	(5.51)	6.2 [m^3]

Table 5.4: Operating points of the Danish Crown steam boiler model given by (5.42a).

5.4.2 Linearization

In Section B.2 and Section B.3, a strategy for linearizing the system dynamics and measurement equation described by

$$J(x)\,\dot{x} = H_{sb}(x,u,d) \;\text{ and} \tag{5.52a}$$
$$y = h(x). \tag{5.52b}$$

For simplicity, the following definition is used.

Definition 5.2 (Expanded Eulers notation of differentiation)
Eulers notation for differentiation is adopted, and for simplicity the operating points is written into it, such that

$$D_a f(a_o,\, b_o) = \left.\frac{d\,f(a,b)}{d\,a}\right|_{a_o,b_o}. \tag{5.53}$$

The corresponding linearized system is given by:

$$\delta\dot{x} = \underbrace{J^{-1}(x_o)D_x H(x_o,\, u_o,\, d_o)}_{\mathcal{A}_c(x_o,\, u_o,\, d_o)}\delta x + \underbrace{J^{-1}(x_o)D_u H(x_o,\, u_o,\, d_o)}_{\mathcal{B}_{c,u}(x_o,\, u_o,\, d_o)}\delta u + \underbrace{J^{-1}(x_o)D_d H(x_o,\, u_o,\, d_o)}_{\mathcal{B}_{c,d}(x_o,\, u_o,\, d_o)}\delta d \tag{5.54a}$$
$$\delta y = \underbrace{D_x h(x_o)}_{\mathcal{C}_c(x_o)}\delta x \tag{5.54b}$$

With the coordinate change according to

$$\delta\dot{x} = \dot{x},\; \delta x = x - x_o,\; \delta u = u - u_o,\; \delta d = d - d_o \text{ and } \delta y = y - h(x_o).$$

Where

δ is the small signal value
The subscript o indicate an operating point
$x = [p_s \quad V_w]^T$ is the steam boiler states.
$u = [\dot{m}_{fw}]^T$ is the steam boiler inputs.
$d = [\dot{m}_s \quad \dot{U} \quad T_{fw}]^T$ is the steam boiler disturbances.
$\mathcal{A}_c(x_o,\, u_o,\, d_o) \in \mathbb{R}^{n\times n}$ is the continuous time state transition matrix
$\mathcal{B}_{c,u}(x_o,\, u_o,\, d_o) \in \mathbb{R}^{n\times m}$ is the continuous time input matrix
$\mathcal{B}_{c,d}(x_o,\, u_o,\, d_o) \in \mathbb{R}^{n\times k}$ is the continuous time disturbance input matrix
$\mathcal{C}_c(x_o) \in \mathbb{R}^{n\times l}$ is the continuous time output matrix

For clarity, the linearized system is governed by

$$\begin{bmatrix}\delta\dot{x}\\ \delta y\end{bmatrix} = \begin{bmatrix}\mathcal{A}_c(x_o,\, u_o,\, d_o) & \mathcal{B}_{c,d}(x_o,\, u_o,\, d_o) & \mathcal{B}_{c,u}(x_o,\, u_o,\, d_o)\\ \mathcal{C}_c(x_o) & 0 & 0\end{bmatrix}\begin{bmatrix}\delta x\\ \delta d\\ \delta u\end{bmatrix}. \tag{5.55}$$

Calculating the linear continuous time system with the operating points in Table 5.4 equals

$$\left[\begin{array}{c}\delta\dot{x}\\ \hline \delta y\end{array}\right] = \left[\begin{array}{cc|ccc|c} -10.3\,\text{e-6} & 0 & -14.9\,\text{e-3} & 6.74\,\text{e-9} & 7\,\text{e-6} & -2.67\,\text{e-3} \\ -0.4\,\text{e-6} & 0 & -1.66\,\text{e-3} & 263\,\text{e-12} & 275\,\text{e-9} & 1\,\text{e-3} \\ \hline 1 & 0 & 0 & 0 & 0 & 0 \\ 0 & 173\,\text{e-3} & 0 & 0 & 0 & 0 \end{array}\right] \left[\begin{array}{c}\delta x\\ \hline \delta d\\ \hline \delta u\end{array}\right]. \tag{5.56}$$

Adding the burner controller, which is governed by

$$\delta\dot{U}_{fu} = \mathcal{F}_{fu}\,\delta p_s = -0.81\,\frac{\text{MJ/s}}{\text{Bar}}\,\delta p_s, \tag{5.57}$$

which results in

$$\left[\begin{array}{c}\delta\dot{x}\\ \hline \delta y\end{array}\right] = \left[\begin{array}{cc|cc|c} -5.856\,\text{e-3} & 0 & -14.9\,\text{e-3} & 7\,\text{e-6} & -2.67\,\text{e-3} \\ -217.6\,\text{e-6} & 0 & -1.66\,\text{e-3} & 275\,\text{e-9} & 1\,\text{e-3} \\ \hline 1 & 0 & 0 & 0 & 0 \\ 0 & 173\,\text{e-3} & 0 & 0 & 0 \end{array}\right] \left[\begin{array}{c}\delta x\\ \hline \delta d\\ \hline \delta u\end{array}\right] \tag{5.58}$$

with $d = [\dot{m}_s \quad T_{fw}]$. This system has eigenvalues at 0 and -5.86e-3, which correspond to the water volume and steam pressure respectively. This concludes the modeling, parameter identification and linearization of the Danish Crown steam boiler, which leads to the stepwise commissioning design.

Chapter 6

Stepwise Commissioning Design

6.1 Introduction

In this chapter the stepwise commissioning design described in Chapter 2 (Stepwise Commissioning Design) is carried out for the Danish Crown steam boiler. For this purpose, a multiple input single output (MISO) and single input single output (SISO) class feed water controller must be designed as the current feed water controller is a hysteresis-like type, which cannot be used with the proposed stepwise commissioning method. This is due to the fact that linear controllers are required.

Keep in mind that the goal of this project is to make the startup of industrial MIMO controllers more straight forward, by exploiting the flexibility of the SISO class controllers for the startup phase. After the startup phase, the proposed sequential stepwise commissioning method explained in Chapter 2 (Stepwise Commissioning Design) will be used to transition from the SISO controllers to the MIMO controller, as described in Section 1.2 (Difficulties in introducing MIMO controllers in the industry).

For this reason, the SISO class feed water controller is designed as a PID-class controller, as it is considered the industrial SISO controller standard. The MISO feed water controller will be designed as an optimal observer based controller, as it is an established and well documented theory. The MISO feed water controller is designed in Section 6.2 and the SISO feed water controller is designed in Section 6.3. In addition, to make the two controllers comparable the SISO controller will be based on the MISO controller. These controllers will be used in a stepwise commissioning design in Section 6.5. Lastly, the controller sampling frequency has been selected to be 8 Hz, which is significantly faster than the dynamics of the steam boiler system.

However, before the controllers are designed, some guidelines regarding the controller performance will be established, which will be applied to the controllers in Section 6.4 (Controller Evaluation).

Steadiness As described in Subsection 4.2.3 (Benefits of adopting a MISO boiler feed control strategy), it is desired to achieve a steady water flow through the steam boiler system. To objectively evaluate the controllers ability to a maintain a steady control signal, henceforth denoted "steadiness", an additional cost function is established, which equals

$$\mathcal{J}_{u,\,\text{steadiness}} = \frac{1}{N-N_s}\sum_{n=N_s}^{N-1}\left(\dot{m}_{fw}(n) - \dot{m}_{s,\text{mean},N_s}(n)\right)^2 \text{ with} \tag{6.1a}$$

$$\dot{m}_{s,\text{mean},N_s}(n) = \frac{1}{N_s}\sum_{k=0}^{N_s-1}\dot{m}_s(n-k). \tag{6.1b}$$

Where $\dot{m}_{s,\text{mean},N_s}(n)$ is the mean steam outlet flow $\dot{m}_s$ over the last N_s samples. This cost function require the parameter N_s to be selected large enough to not be influenced by fast changes in the steam outlet flow. On Figure 6.1 a section of the steam outlet flow $\dot{m}_s$ is depicted. A N_s of 1600, which is equivalent to 200s, has been found to give a good representation of a steady flow, which is depicted on Figure 6.1.

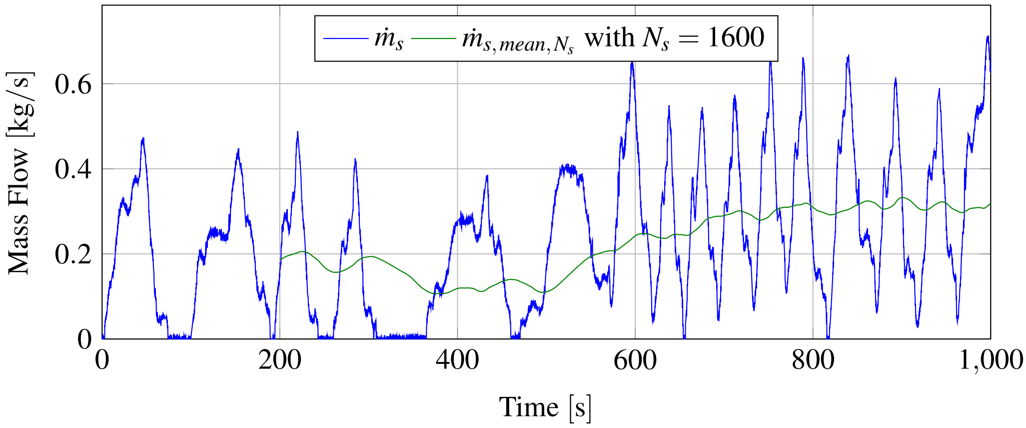

Figure 6.1: Measured Steam demand.

Min/Max Level The water level must be kept between the previous hysteresis controllers upper and lower water level bound, which will be referenced as the "Min/Max Level". As these limits are regarded as quite conservative in the first place, they will primarily serve as guidelines.

6.2 MISO Feed Water Controller

The MISO feed water controller is designed as a linear optimal controller. The primary reason for choosing this particular control design method is that it is possible to quantify control objectives through a cost function. The cost function assigns a cost to both the states $x(n)$ and the applied actuation $u(n)$ as described by (6.2a). It allows an optimal control law to be synthesized, which minimizes the total cost denoted by (6.2b) for a time frame of N samples [Sørensen and Andersen, 2010,pp. 1].

$$I(n) = x^T(n)\,\mathbf{Q}\,x(n) + u^T(n)\,\mathbf{R}\,u(n) \tag{6.2a}$$

$$\mathcal{J} = \sum_{n=0}^{N} I(n) \tag{6.2b}$$

Where

I is the cost
n is the sample number
x is the state vector
u is the input vector
$\mathbf{Q}$ is the state cost matrix
$\mathbf{R}$ is the input cost matrix
$\mathcal{J}$ is the total cost
N is the time frame

To put this into perspective, a typical control goal could be to keep the system states or outputs close to a reference, using as little actuation as possible. By using a cost function, it is possible to objectively specify "as close to" and "as little as", for the particular system through the weighting matrices $\mathbf{Q}$ and $\mathbf{R}$.

Even though all the states essentially are measured, the observer will be designed to estimate the steam outlet flow $\dot{m}_s$ as it is the primary disturbance. Additionally, the possibility of having access to such a sensor on a steam boiler is really low, considering that it is not widely used for feed water control and is expensive. For reference, the steam outlet flow sensor used for the identification has a price in the vicinity of 30000 DKK. However, having access to the steam outlet flow could indirectly lead to better controller steadiness, as it could dynamically track the operating point.

The remaining disturbance, which is the feed water temperature T_{fw}, will be assumed constant as the feed water controller does not benefit from it. Conversely, if the objective was to design a pressure controller it would be useful, as it requires more energy to maintain the pressure when colder than expected feed water is introduced into the boiler drum. This would presumably allow for less pressure variations, and therefore a better pressure controller.

This makes the controller an optimal linear observer based controller, which has two degrees of freedom, namely the feedback law matrix $\mathcal{F}$ and the observer gain matrix $\mathcal{O}$. The design of $\mathcal{F}$ and $\mathcal{O}$ are independent of each other due to the separation principle [Sørensen and Andersen, 2010,pp. 56].

In Subsection 6.2.1, an overview of the linear quadratic regulator (LQR) design technique is described, which will synthesize an optimal control law $\mathcal{F}$. In Subsection 6.2.2, an overview of the linear quadratic observer (LQO) design technique is described, which will synthesize an optimal observer gain $\mathcal{O}$. In addition, desirable features are added to the system model, such as integral action and disturbance model inclusion, which is described in Subsection 6.2.3.

6.2.1 Linear Quadratic Regulator

In this section, an overview of the infinite horizon LQR control design technique is granted based on [Sørensen and Andersen, 2010,chap. 2-3]. The infinite horizon optimal LQR problem is to

$$\underset{u(0),u(1),\ldots}{\text{minimize}} \quad \mathcal{J} = \sum_{n=0}^{\infty} I(n) = \sum_{n=0}^{\infty} \left[x^T(n)\,\mathbf{Q}\,x(n) + u^T(n)\,\mathbf{R}\,u(n)\right] \tag{6.3a}$$

subject to the dynamic system

$$x(n+1) = \mathcal{A}x(n) + \mathcal{B}u(n). \tag{6.3b}$$

Where

$\mathcal{A} \in \mathbb{R}^{n\times n}$ is the discrete time state transition matrix
$\mathcal{B} \in \mathbb{R}^{n\times m}$ is the discrete time input matrix
$\mathbf{Q} \in \mathbb{R}^{n\times n}$ is the positive definite state cost matrix
$\mathbf{R} \in \mathbb{R}^{m\times m}$ is the positive definite input cost matrix
$x(n) \in \mathbb{R}^{n}$ is the state vector

The LQR problem has the static solution

$$u^*(n) = -\mathcal{F}\,x(n), \tag{6.4}$$

where $u^*(n)$ is the optimal input and $\mathcal{F}$ is the optimal feedback law.

An infinite horizon LQR will find a control law, which is optimal for current and all future time. Hence, the cost function $I(n)$ is summed for infinite samples. It differs from a finite horizon LQR, which will only make it optimal for a specific future time. As the steam boiler is made for continuous operation without a known time frame, the infinite horizon LQR is adopted.

Matlab has implemented a function that solves (6.3), which is called through $\mathcal{F} = \texttt{dlqr}(\mathcal{A}, \mathcal{B}, \mathbf{Q}, \mathbf{R})$. For this reason, the details of how a LQR is solved, is not discussed any further. For more information, [Sørensen and Andersen, 2010,chap. 3.1] described how a finite horizon solution can be obtained and expands it to infinite horizon in [Sørensen and Andersen, 2010,chap. 4.1]. One practical detail is that both the execution and design of the controller can be implemented using standard linear algebra with a relative small memory footprint. This makes the method platform independent and allows for local feedback law design on the controller.

If the open loop system is known well enough to specify maximal values of each state and input, the weighting matrices can be selected according to Bryson's rule. These maximal values might originate from physical limitations or from practical assessments.

Definition 6.1 (Bryson's rule)
A reasonable choice of the weighting matrices **Q** and **R** is given by Bryson's rule. The weighting matrices are selected to be diagonal with

$$\mathbf{Q}_{i,i} = \frac{1}{x_{i,\max}^2} \text{ and} \tag{6.5a}$$

$$\mathbf{R}_{j,j} = \sigma \frac{1}{u_{j,\max}^2}. \tag{6.5b}$$

Where

$\mathbf{Q}_{i,i}$ is the i'th diagonal entry of $\mathbf{Q}$
$\mathbf{R}_{j,j}$ is the j'th diagonal entry of $\mathbf{R}$
$x_{i,\max}$ is the maximum acceptable value of the state x_i
$u_{j,\max}$ is the maximum acceptable value of the input u_j
$\sigma \in \mathbb{R}^+$ is the state-input cost ratio

The intuition behind Bryson's rule is that the states and inputs are normalized, such that the maximum acceptable value of every state and input is 1. This is very useful when the states have different units and magnitudes, which are not easy to compare. The state-input cost ratio σ is a scalar tuning parameter, which allow for a simple way of balancing between state deviation and input cost.

6.2.2 Linear Quadratic Observer

In this section, an overview of the infinite horizon LQO design is granted based on [Sørensen and Andersen, 2010, sec. 10.4-10.5].

The purpose of a LQO is to estimate the actual system states $x(n)$ from the measurements $y(n)$ of the system:

$$x(n+1) = \mathcal{A}x(n) + \mathcal{B}u(n) + w_x(n) \tag{6.6a}$$
$$y(n) = \mathcal{C}x(n) + w_y(n) \tag{6.6b}$$

Where
$w_x(n) \sim \mathcal{N}(0, \Sigma_x)$ is the state noise
Σ_x is the state noise covariance matrix
$w_y(n) \sim \mathcal{N}(0, \Sigma_y)$ is the measurement noise
Σ_y is the measurement noise covariance matrix

The LQO follows the structure of a normal observer, which according to [Franklin et al., 2010,pp. 484] is governed by (6.7). The intention is to correct the estimated state deviations, $\hat{x}(n) - x(n)$, through the estimated error correction term $O\hat{e}(n)$, of which the LQO will design an optimal observer gain O.

$$\hat{x}(n+1) = \mathcal{A}\hat{x}(n) + \mathcal{B}u(n) + O\hat{e}(n), \tag{6.7a}$$
$$\hat{e}(n) = y(n) - \hat{y}(n), \tag{6.7b}$$
$$\hat{y}(n) = \mathcal{C}\hat{x}(n) \text{ and} \tag{6.7c}$$
$$u(n) = \mathcal{F}\hat{x}(n). \tag{6.7d}$$

Where
$\hat{x}$ is the estimated state vector
$\hat{e}$ is the estimation error
$\hat{y}$ is the estimated output
$\mathcal{F}$ is the discrete time feedback law
O is the discrete time observer gain

As a perfect sensor does not exist, the zero mean measurement noise $w_y(n)$ is added to explain deviations. The state noise $w_x(n)$ is a stochastic representation of the unmodelled or the unmeasurable state disturbances with zero mean. A distinction between the two noise terms should be made, as the effects of the state noise $w_x(n)$ is desired to be tracked through the measurements, while the measurement noise $w_y(n)$ introduces uncertainty to the correctness of the measurements. Hence, the measurements contains both true and false information. As the true information is correlated with the deterministic dynamics of the system model, it is possible to produce a more precise estimate over time, compared to that of a single measurement. The infinite horizon LQO do this by minimizing the estimated state error over infinite time, given both the measurement noise covariance matrix Σ_y and the state noise covariance matrix Σ_x.

It is the relationship between the two noise covariance matrices, which determine how confident the observer is of the measurement. If the estimation errors are most likely to be caused by the measurement noise, the observer gain is selected low, which results in a slow observer. Hence, the estimated states will converge to the real states slower, as the error has less confidence. Conversely, if an estimation error is most likely to be caused by the state noise, the observer is faster as the observer gain is selected high.

A duality between the LQR and LQO exists, and the observer gain can be calculated using the same function as the LQR. It is found using the covariance matrices as cost matrices, and is found through

$$O = \texttt{dlqr}\left(\mathcal{A}^T, \mathcal{C}^T, \Sigma_x, \Sigma_y\right)^T. \tag{6.8}$$

As both the LQR and LQO have been introduced, the augmented systems used for observer and control design are described.

6.2.3 Augmented System Model

In this subsection, the models used for both the design of the control law and observer gain are augmented to implement additional features. These features include disturbance model inclusion and integral action. The equation system which allows these features to be included is stated, then the underlying reason for them is described. Then the augmented systems used for both control and observer design are described.

The system equations that allows the mentioned features to be included is depicted on Figure 6.2 and are

$$
\begin{aligned}
x_{\text{sys}}(n+1) &= \mathcal{A}_{\text{sys}}\, x_{\text{sys}}(n) + \mathcal{B}_{\text{sys}}\, u(n) + d(n) + w_{x,sys}(n), && \text{[System State]} \quad (6.9a)\\
y_{\text{sys}}(n) &= \mathcal{C}_{\text{sys}} x_{\text{sys}} + w_{y,sys}(n), && \text{[System Output]} \quad (6.9b)\\
x_d(n+1) &= x_d(n) + w_{d,sys}(n), && \text{[Disturbance Random Walk State]} \quad (6.9c)\\
d(n) &= \mathcal{B}_d\, x_d(n), && \text{[Disturbance]} \quad (6.9d)\\
e_i(n) &= \mathcal{B}_i\, y_{\text{sys}}(n) \text{ and} && \text{[Integral Error]} \quad (6.9e)\\
x_i(n+1) &= x_i(n) + e_i(n). && \text{[Integral Error State]} \quad (6.9f)
\end{aligned}
$$

The vectors are defined as

$$x_{\text{sys}}(n) = \begin{bmatrix} \delta p_s(n) & \delta V_w(n) \end{bmatrix}^T, \qquad x_d(n) = \delta \dot{m}_s(n) \text{ and} \qquad x_i(n) = \mathcal{B}_i x_e(n) = \delta L_{w,e}(n). \tag{6.10a}$$

Where

δp_s	is the small signal steam pressure	[Bar]
δV_w	is the small signal water volume	$[\text{m}^3]$
$\delta \dot{m}_s$	is the small signal steam outlet flow	[kg/s]
$\delta L_{w,e}$	is the integrated small signal water level	$[\text{m}^3]$

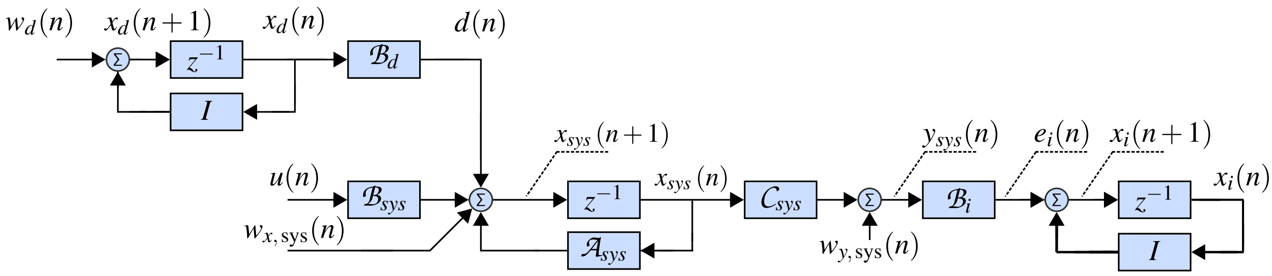

Figure 6.2: Block diagram of (6.9).

The system equations are governed by (6.9a) and (6.9b), which has two inputs, namely the control input $u(n)$ and the disturbance input $d(n)$. To understand the origin of the remaining equations, it is necessary to introduce the concept of a random walk model, which is governed by the two equations,

$$x_{rw}(n+1) = x_{rw}(n) + w_{x,rw}(n) \text{ and} \tag{6.11a}$$

$$u_{rw}(n) = \mathcal{B}_{rw} x_{rw}(n). \tag{6.11b}$$

Where

x_{rw} is the random walk state vector
u_{rw} is the random walk output vector
$\mathcal{B}_{rw}$ is the random walk output matrix
$w_{x,rw}(n) \sim \mathcal{N}(0, \Sigma_{x,rw})$ is the random walk state noise

The state noise $w_{x,rw}(n)$ allows the observer to track this state, as the state is assumed to change with state covariance matrix $\Sigma_{x,rw}$.

The random walk model is used to represent the disturbance state model given by (6.9c) and (6.9d). The intention is to estimate the steam outlet flow $\dot{m}_s$, as it is not measured and is the primary disturbance for the feed water controller. Recall that the matrix $\mathcal{B}_d$ is given by the system model, but only the part related to $\dot{m}_s$ will be used. Hence, the other disturbances are ignored.

Lastly, the integral action is added by also integrating the reference error $e(n)$, as described by (6.9f). It is constructed as a discrete integrator, which keep track of the integrated error by adding it at every iteration. As the control law is designed to bring all the system states to zero, the integral reference error state is no exception. Hence, it is the state space equivalent of integral action in PID based controllers. Integral action will only be employed on the water level error $L_{w,e}$.

However, the systems used for control law and observer gain design is different, as they serve different purposes. They will be described and designed separately, starting with the Observer Design followed by the control law design.

6.2.4 Observer Design

In this section the observer is designed based on Subsection 6.2.2 (Linear Quadratic Observer). The augmented system model is first established based on Subsection 6.2.3, then the specifics of the observer design are described.

The Augmented System Used for the Observer Design

The augmented system used for observer design, has the state vector

$$x_o(n) = [x_{\text{sys}}(n) \quad x_d(n)]^T, \tag{6.12}$$

which results in the augmented system:

$$x_o(n+1) = \overbrace{\begin{bmatrix} \mathcal{A}_{\text{sys}} & \mathcal{B}_d \\ 0 & I \end{bmatrix}}^{\mathcal{A}_o} x_o(n) + \overbrace{\begin{bmatrix} \mathcal{B}_{\text{sys}} \\ 0 \end{bmatrix}}^{\mathcal{B}_o} u(n) + w_x(n) \tag{6.13a}$$

$$y(n) = \underbrace{\begin{bmatrix} \mathcal{C}_{\text{sys}} & 0 \end{bmatrix}}_{\mathcal{C}_o} x(n) + w_y(n) \tag{6.13b}$$

Where

$w_x(n) \sim \mathcal{N}(0, \Sigma_x)$ is the state noise
Σ_x is the state noise covariance matrix
$w_y(n) \sim \mathcal{N}(0, \Sigma_y)$ is the measurement noise
Σ_y is the measurement noise covariance matrix

Notice that the matrix $\mathcal{B}_d$ is the disturbance model. The observer gain is designed according to Subsection 6.2.2, which gives the observer gain

$$O = \begin{bmatrix} O_{\text{sys}} \\ O_d \end{bmatrix}. \tag{6.14}$$

Observer Design

The design freedom in the observer design are the state covariance noise matrix Σ_x and the measurement noise covariance matrix Σ_y, which will be determined in this subsection based on the available measurement series.

The measurement noise covariance matrix Σ_y can quite accurately be determined by calculating the covariance of a measurement series where the system states are constant. However, the measurements available has no such data, which is compensated for by calculating the noise covariance matrix of a data-segment which is perceived as having constant states as a best guess. The measurements are considered uncorrelated due to the measurement-equation. As a result, the variance is used to calculate the diagonal elements of the state covariance matrix, which results in

$$\Sigma_y = \begin{bmatrix} 0.263\text{e-}6 & 0 \\ 0 & 1.04\text{e-}6 \end{bmatrix}, \tag{6.15}$$

where 0.263e-6 and 1.04e-6 are the variance of measurement noise of the pressure sensor and level sensor, respectively.

The state noise covariance matrix is determined by calculating the covariance of w_x for a time series, which is determined by solving for it in (6.13a), which results in (6.16a). Ideally this require the states of the system process x_o to be known, which will be generated using the nonlinear model which has the shape of (6.16b). This approach will only find the deviations caused by the linearization of the system model, which consequently means that deviations caused by unmodelled dynamics are considered. However, it will at least give an initial guess of the noise. Using this approach, the deviations depicted on the blue and red trace of Figure 6.3 is obtained. This reveal that the state noise is correlated with the burner input, which is depicted on the bottom plot of Figure 6.3. Burner stage 0 result in over-estimation and burner stage 1 and 2 results in under-estimation. To investigate if having access to the burner input decrease the state noise it has been added to the green plot, which results in significantly less state noise for the steam pressure p_s and the water volume V_w.

$$w_x(n) = x_o(n+1) - \mathcal{A}_o x_o(n) - \mathcal{B}_o u(n) \tag{6.16a}$$

$$x_o(n) = \begin{bmatrix} x_{sys}(n+1) \\ x_d(n+1) \end{bmatrix} = \begin{bmatrix} f_{sys}(x_{sys}(n), d(n), u(n)) \\ \dot{m}_s(n+1) \end{bmatrix} \tag{6.16b}$$

Where

$f_{sys}(x_{sys}(n), d(n), u(n))$ is the discrete time nonlinear steam boiler dynamics.
$d_m(n) = [\dot{m}_s(n) \quad T_{fw}(n)]^T$ is the measured disturbances.
$u_m(n) = \dot{m}_{fw}$ is the measured input

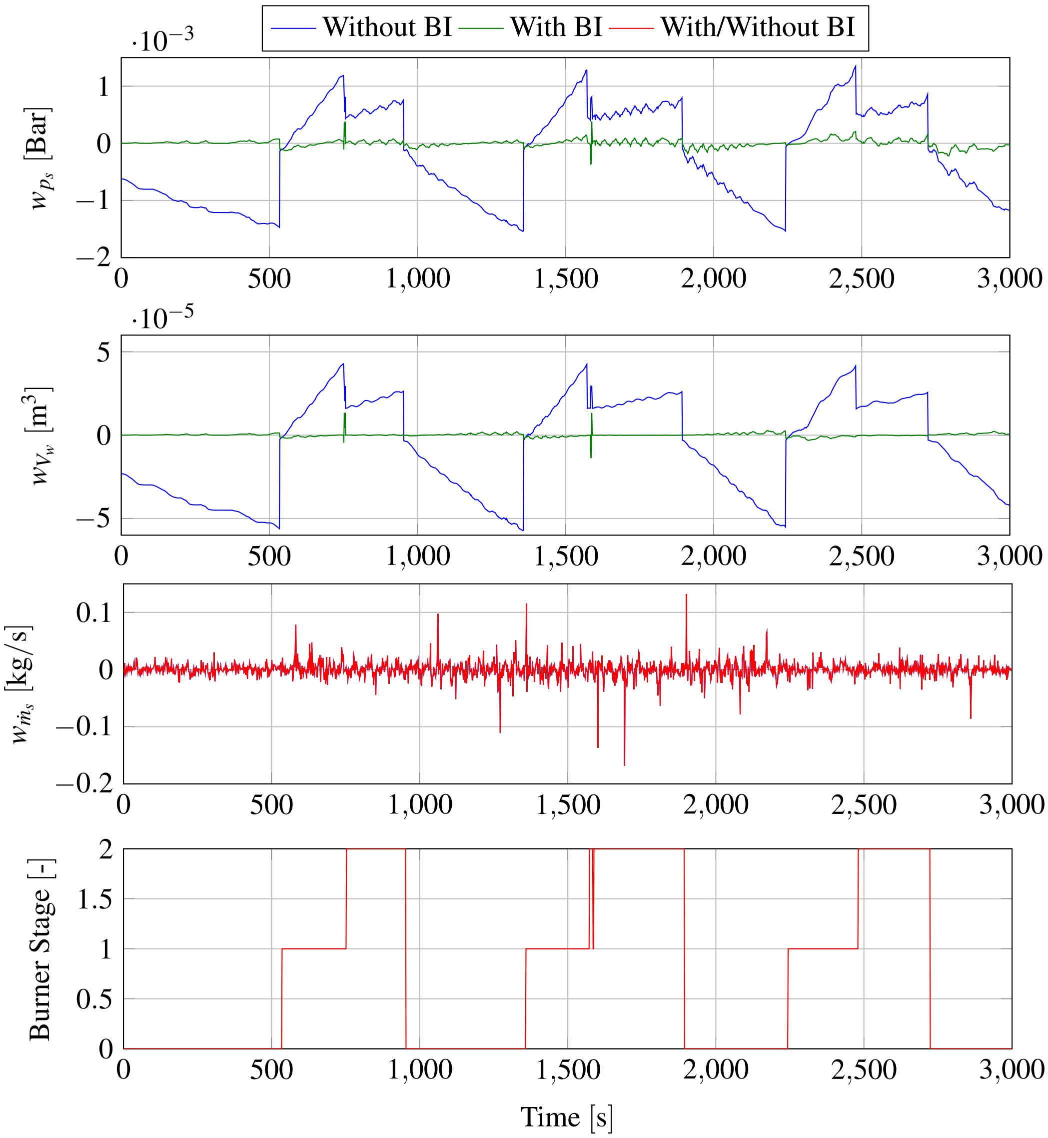

Figure 6.3: The state noise $w_x(n)$ generated using (6.16). BI is short for burner input.

The state covariance matrices obtained by calculating the covariance of the state noise presented on Figure 6.3 results in

$$\Sigma_x = \begin{bmatrix} 663.7\text{e-}9 & 23.6\text{e-}9 & 13.0\text{e-}9 \\ 23.6\text{e-}9 & 847.1\text{e-}12 & 346.6\text{e-}12 \\ 13.0\text{e-}9 & 346.6\text{e-}12 & 107.1\text{e-}6 \end{bmatrix} \text{ and} \tag{6.17}$$

$$\Sigma_{x,\text{with burner}} = \begin{bmatrix} 3.8\text{e-}9 & 3.3\text{e-}12 & -52.6\text{e-}12 \\ 3.3\text{e-}12 & 1.2\text{e-}12 & -138.7\text{e-}12 \\ -52.6\text{e-}12 & -138.7\text{e-}12 & 107.1\text{e-}6 \end{bmatrix}. \tag{6.18}$$

From this it can be concluded that the largest and therefore dominant source of state noise is the steam outlet flow, which also makes sense as it is the primary disturbance. Furthermore, the state covariance matrix with the burner input $\Sigma_{x,\text{with burner}}$ has significantly less state noise related to the steam pressure p_s and the water volume V_w, as suspected. Using Σ_x and Σ_y generates the observer gain O stated in (6.19a).

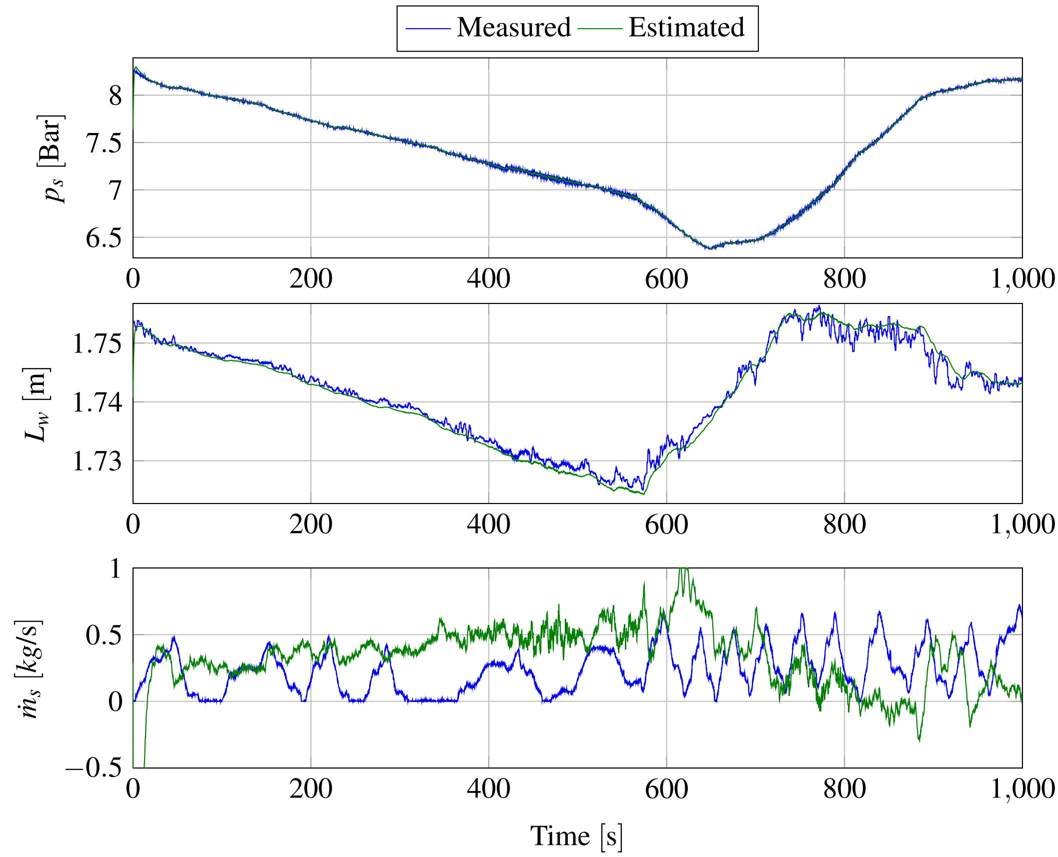

Figure 6.4: Estimated and measured outputs and steam outlet flow.

Using this observer gain for the linear observer generates the simulation results depicted on Figure 6.4. First off, the estimates of the of the steam pressure p_s and water volume V_w are good, as they has less noise. However, the steam outlet flow estimate appear to grow as the steam pressure declines, which is expected to be caused by the burner input. To elaborate on this, the steam outlet flow estimation error $\hat{\dot{m}}_s - \dot{m}_s$ is depicted on Figure 6.5, which depends on the steam pressure due to the pressure controller linearization. By adding the burner input, which results in the observer gain (6.19b), gives the steam outlet estimation results depicted on the top plot of Figure 6.6. The estimation offsets caused by the pressure controller linearization has been removed, which results in a significantly better estimation. The estimation error is now close to zero mean, which is considered an acceptable estimation.

$$O = \begin{bmatrix} 0.166 & 0.068 \\ 0.014 & 0.064 \\ -1.703 & -3.788 \end{bmatrix} \tag{6.19a}$$

$$O_{\text{with burner}} = \begin{bmatrix} 0.086 & 0.042 \\ 0.010 & 0.011 \\ -1.92 & -0.980 \end{bmatrix} \tag{6.19b}$$

$$O_{\text{sys}} = \begin{bmatrix} 0.166 & 0.068 \\ 0.014 & 0.064 \end{bmatrix} \tag{6.19c}$$

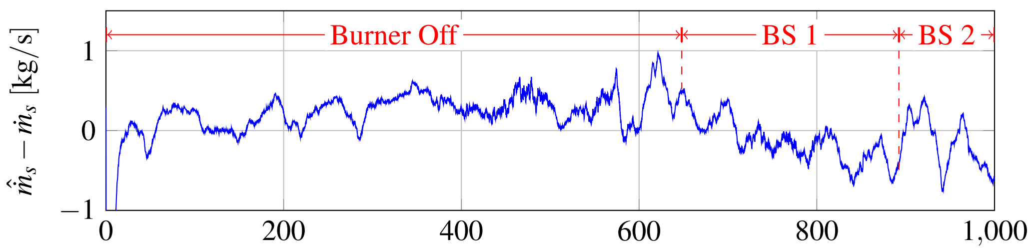

Figure 6.5: Steam outlet flow estimation error. BS is short for burner stage.

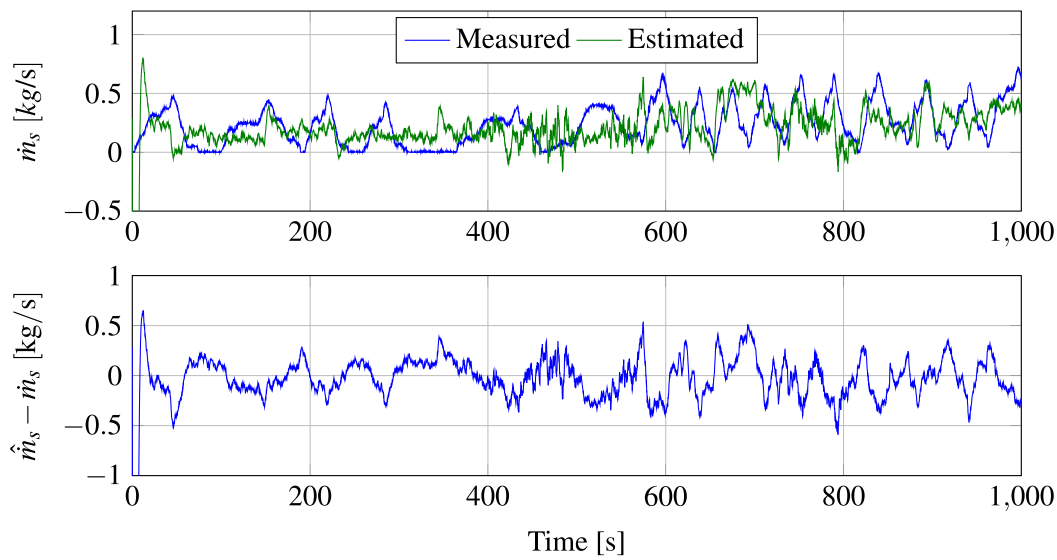

Figure 6.6: Top plot: Estimated and measured steam outlet flow with burner input. Bottom Plot: Steam outlet flow estimation error with burner input.

Even though the steam outlet estimation is acceptable with the burner signal, it does not change the fact that without it the estimation is less than acceptable. For this reason, the idea of estimation the steam outlet flow is abandoned and this state is removed from the observer. This means that the observer gain (6.19c) is used instead. Consequently, this means that the feedback law cannot take this state into consideration as well.

6.2.5 Control Law Design

In this section the control law is designed based on Subsection 6.2.1 (Linear Quadratic Regulator). First the control goal is discussed, then the augmented system model is established based on Subsection 6.2.3 (Augmented System Model), lastly the specifics of the control law design is described.

The Augmented System and Cost Function Used for Control Law Design

In Subsection 6.2.4 it was decided to abandon the idea of estimating the steam outlet flow due to poor estimation performance without the burner signal. Hence, this state is no longer a part of the control strategy. The augmented system for the control law design has the state vector

$$x_c(n) = [x_{\text{sys}}(n) \quad x_i(n)]^T. \tag{6.20}$$

The term $x_{\text{sys}}(n)$ is the system states while the integral reference error state $x_i(n)$ is added by the controller, which is established based on the discussion in Section 6.2 (MISO Feed Water Controller). Based on (6.9), the augmented system used for the control law design equals

$$x_c(n+1) = \begin{bmatrix} \mathcal{A}_{\text{sys}} & 0 \\ \mathcal{B}_i \mathcal{C}_{\text{sys}} & I \end{bmatrix} x_c(n) + \begin{bmatrix} \mathcal{B}_{\text{sys}} \\ 0 \end{bmatrix} u(n). \tag{6.21}$$

The control law is designed such that it will minimize the measurements $y_{\text{sys}}(n)$, the integral error state $x_i(n)$ and the control action $u(n)$. The cost function is selected as (6.22).

$$\begin{aligned} I_c(n) &= y_{\text{sys}}^T(n)\,\mathbf{Q}_e\,y_{\text{sys}}(n) + x_i^T(n)\,\mathbf{Q}_i\,x_i(n) + u^T(n)\,\mathbf{R}\,u(n) && (6.22a) \\ &= x_c^T(n) \underbrace{\begin{bmatrix} \mathcal{C}_{\text{sys}}^T \mathbf{Q}_e \mathcal{C}_{\text{sys}} & 0 \\ 0 & \mathbf{Q}_i \end{bmatrix}}_{\mathbf{Q}} x_c(n) + u^T(n)\,\mathbf{R}\,u(n). && (6.22b) \end{aligned}$$

The weighting matrices $\mathbf{Q}_e$, $\mathbf{Q}_i$ and $\mathbf{R}$ are found by employing Bryson's rule (Definition 6.1), which results in

$$\mathbf{Q}_e = \begin{bmatrix} \frac{1}{\delta p_{s,\max}^2} & 0 \\ 0 & \frac{1}{\delta L_{w,\max}^2} \end{bmatrix}, \qquad \mathbf{Q}_i = \begin{bmatrix} \frac{1}{\delta L_{w,e,\max}^2} \end{bmatrix} \text{ and } \qquad \mathbf{R} = \sigma \begin{bmatrix} \frac{1}{\delta \dot{m}_{fw,\max}^2} \end{bmatrix}. \tag{6.22c}$$

The LQR design explained in Subsection 6.2.1 with the cost function (6.22) will synthesize the control law with the structure

$$u(n) = -\left[\begin{array}{c|c} \mathcal{F}_{\text{sys}} & \mathcal{F}_i \end{array}\right] x_c(n). \tag{6.23}$$

Controller Design

The design freedom in the LQR controller design is the state cost matrix **Q** and the input cost matrix **R**, which will be determined in this section based on the measurement series and the controller requirements.

First off, δL_w is found from the smallest distance from the water level operating point to the "Min/Max Level" requirement, which results in $\delta L_{w,\max} = 0.0132$. The largest steam pressure cost is found by finding the largest deviation from the steam pressure operating point in the data set, which result in $\delta p_{s,\max} = 1.41$ Bar. Likewise, the largest occurring feed water input is expected to be equal to the largest occurring steam outlet flow relative to its operating point, which equals $\delta \dot{m}_{fw,\max} = \dot{m}_{s,\max} = 0.438$ kg/s.

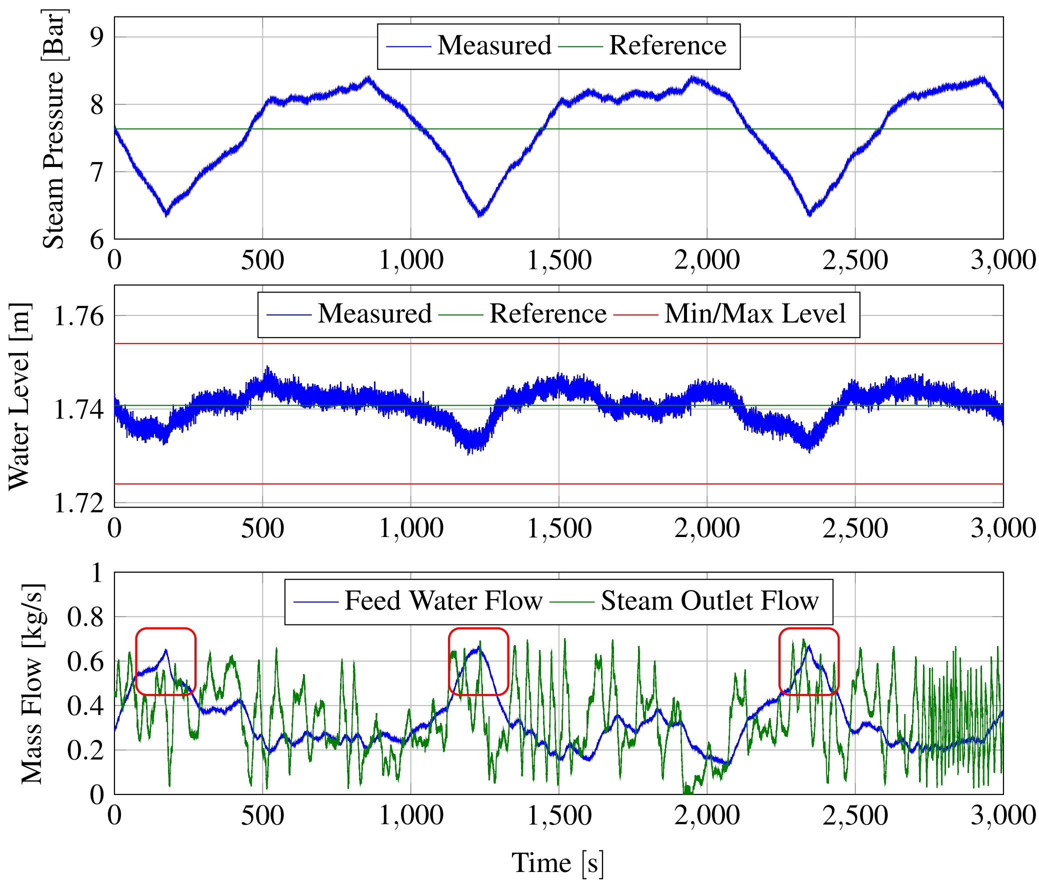

Figure 6.7: The simulated MISO feed water controller.

This only leaves out the maximum integral error feed water level $\delta L_{w,e,\max}$, which has to be selected high to improve the controllers steadiness. Through tuning, a value of $\delta L_{w,e,\max} = 5$ m has been found to produce good results, which might appear as a very high value compared to the other states. However, please keep in mind that the integral action has a supporting role in the controller, as its main purpose is to remove steady state errors, which suggest that a high value is not necessarily desired. The cost function then equals

$$I(n) = x_c^T(n) \begin{bmatrix} 0.503 \text{ Bar}^{-2} & 0 & 0 \\ 0 & 3.03 \text{ m}^{-2} & 0 \\ 0 & 0 & 0.01 \text{ m}^{-2} \end{bmatrix} x_c(n) + \sigma u^T(n) \left[52.2 \text{ (kg/s)}^{-2}\right] u(n),$$

of which the state-input cost ratio σ is the last free variable. Through tuning, good results have been found with a σ in the vicinity of $\sigma = 10$. In general, the controllers steadiness improves with higher σ at the operating steam demand level, which makes sense. However, for larger σ it also tend to decrease the controllers steadiness when the steam outlet demand level changes, of which $\sigma = 10$ appear as a good trade off between the two. This will be further investigated in Section 6.4 (Controller Evaluation). Based on this, the feed back law according to

$$\mathcal{F} = \begin{bmatrix} -0.15 & 8.74 & 0.028 \end{bmatrix} \tag{6.24}$$

is found.

The result of using these parameters is depicted on Figure 6.7, which is generated using the nonlinear system model with steam outlet flow from the measurement series. First off, the feed water controller keeps the water level between the "Min/Max Level" as intended. Please keep in mind that the water level itself has very little effect on the system, which means that the presented reference error is acceptable. Secondly, the control signal appear to be rather steady, but does seem to have periodic spikes which is correlated with the rise and fall of the steam pressure, which is marked with the red squares. To suppress this phenomenon it is further investigated and a pressure feed forward controller is designed in Subsection 6.2.6.

6.2.6 Pressure Feed Forward Design

In this subsection, the correlation between the steam pressure p_s and the water level L_w will be investigated. For this purpose, an expression for the water level L_w as a function of the steam pressure p_s with fixed water mass m_w is found based on Subsection 5.1.2 (Steam Boiler Model Principle) and Subsection 5.2.2 (Measurement Model).

As the water mass m_w is saturated, its relationship with the water volume V_w equals

$$m_w = \rho_w(p_s)V_w, \tag{6.25}$$

which combined with the measurement model results in

$$L_w(V_w + V_{m,f}) = L_w\left(\frac{m_w}{\rho_w(p_s)} + V_{m,f}\right), \tag{6.26}$$

where $V_{m,f}$ is the constant furnace and flue gas pipes volume. This expression will explain the relationship between the steam pressure p_s and the water level L_w, as desired. In addition, the water mass is selected to be in the operating point, which is satisfied by using (6.27) that results in (6.28).

$$m_w = \rho_w(p_{s,o})V_{w,o} \tag{6.27}$$

$$L_w(V_w + V_{m,f}) = L_w\left(\frac{\rho_w(p_{s,o})}{\rho_w(p_s)}V_{w,o} + V_{m,f}\right) \tag{6.28}$$

Using (6.28), the water level L_w as a function of the steam pressure p_s is depicted on Figure 6.8 for the steam pressure range observed in the Danish Crown steam boiler. This reveal that the steam pressure has a large influence on the water level, as it is responsible for a 16 mm level rise for a steam pressure change from 6 to 8.4 Bar. To put this into perspective, it is 53% of the "Min/Max Level"-range, which is significant. It should be noted that water in general is considered almost incompressible, but given the pressure range and water height, a 16 mm water level change is considered reasonable.

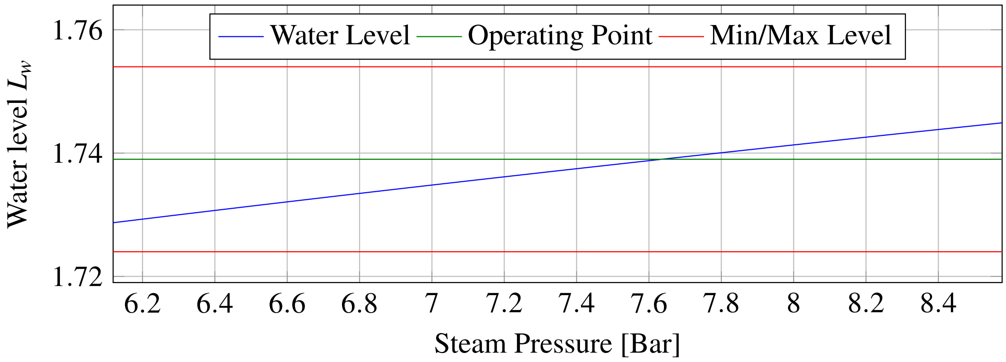

Figure 6.8: The water level as a function of the steam pressure with fixed water volume.

A first order least square fit of the water level in Figure 6.8 approximates the steam pressure contribution to the water level in terms of the small signal steam pressure δp_s as

$$L_{w,p_s}(\delta p_s) = \mathcal{F}_{\mathrm{FF},p_s}\,\delta p_s = 6.6\text{e-}3\,\frac{\mathrm{m}}{\mathrm{Bar}}\,\delta p_s. \tag{6.29}$$

The steam water level contribution $L_{w,p_s}(\delta p_s)$ is introduced through the reference $r(n)$ in the reference model depicted on Figure 6.9, which is governed by

$$y_e(n) = y_{\mathrm{sys}}(n) - r(n). \tag{6.30}$$

According to [Franklin et al., 2010,pp. 511], this is a common way of introducing the reference, when the reference objectives are directly measured.

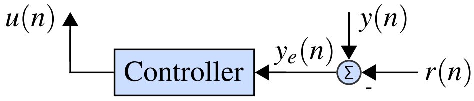

Figure 6.9: How the reference is introduced for state space controllers.

The reference to the controller is altered according to (6.31). Using this feed forward network, the controller input is pre-multiplied with $\mathcal{F}_{\mathrm{FF}}$ as shown in (6.32).

$$r(n) = \begin{bmatrix} 0 \\ \mathcal{F}_{\mathrm{FF},p_s}\delta p_s(n) \end{bmatrix} \tag{6.31}$$

$$y_e(n) = y_{\mathrm{sys}}(n) - r(n) = \begin{bmatrix} \delta p_s(n) \\ L_w(n) \end{bmatrix} - \begin{bmatrix} 0 \\ \mathcal{F}_{\mathrm{FF},p_s}\delta p_s(n) \end{bmatrix} = \underbrace{\begin{bmatrix} 1 & 0 \\ -\mathcal{F}_{\mathrm{FF},p_s} & 1 \end{bmatrix}}_{\mathcal{F}_{\mathrm{FF}}} \underbrace{\begin{bmatrix} \delta p_s(n) \\ L_w(n) \end{bmatrix}}_{y_{\mathrm{sys}}(n)} \tag{6.32}$$

By applying (6.32), the simulation result as depicted on Figure 6.11 is obtained. It has the same disturbances as the one without the pressure feed forward, which makes them comparable. The effect of the pressure feed forward reference is quite profound, as the steam pressure has significantly less impact on the feed water flow. Please notice how the feed water flow tracks the trend of the steam outlet flow on the bottom plot, which is the desired result. However, as the trend is tracked slowly, it also causes under- and over-shoots, which are visible at $t = 1250$s and $t = 2000$s, which are considered acceptable.

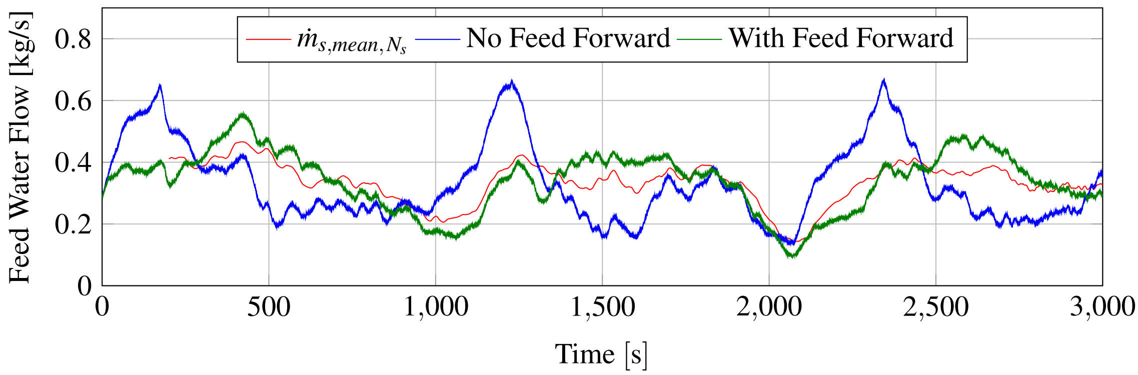

Figure 6.10: Comparison between the feed water flow with and without pressure feed forward.

On Figure 6.10 the feed water flow of the controller with and without the pressure feed forward is depicted. From this it is clear that the controller with pressure feed forward stays closer to the mean steam outlet flow, which is supported by calculating the steadiness of the controllers. The steadiness with pressure feed forward equals 6.4e-3 and 16.1e-3 without, which is a clear improvement. As this completes the MISO feed water controller design, the complete MISO feed water controller will be described.

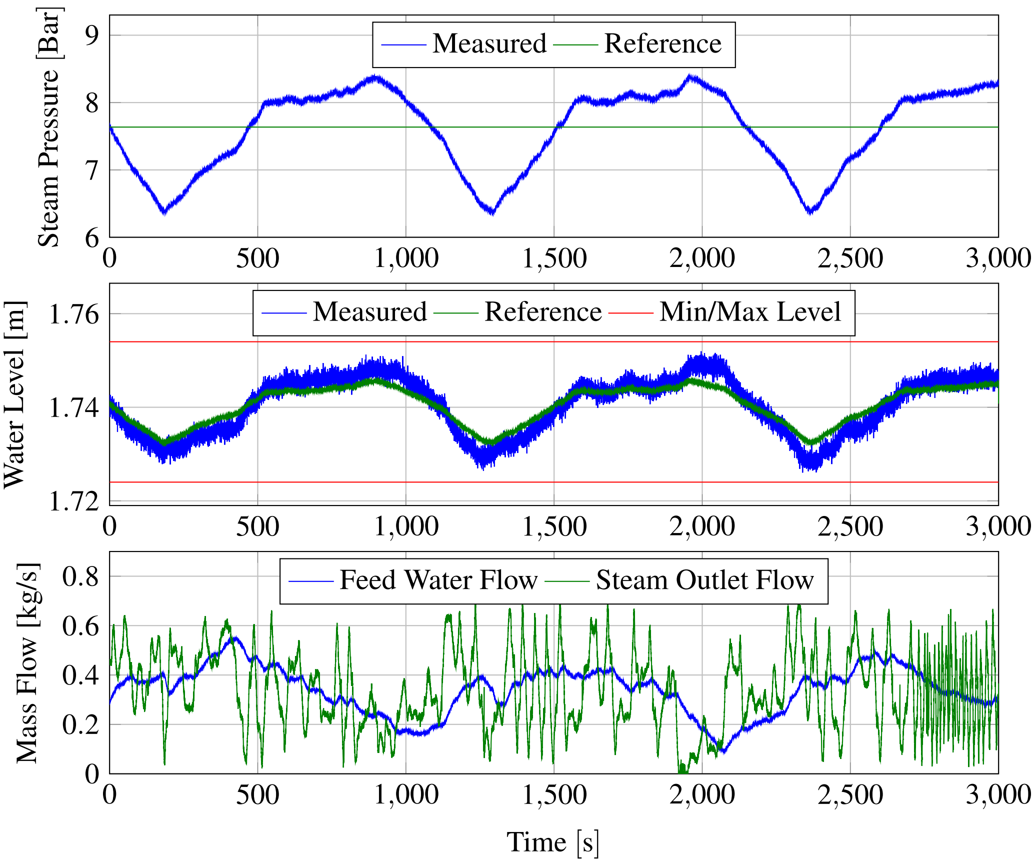

Figure 6.11: The simulated MISO feed water controller with pressure feed forward.

6.2.7 The Complete MISO Feed Water Controller

In this subsection, an overview and description of the complete MISO feed water controller is given. The controller states equals

$$x_c(n) = [x_{\text{sys}}(n) \quad x_i(n)]^T = [\delta p_s \quad \delta V_w \quad \delta L_{w,e}(n)]^T, \tag{6.33}$$

while the controller is governed by

$$\hat{x}_c(n+1) = \begin{bmatrix} \mathcal{A}_{\text{sys}} & 0 \\ \mathcal{B}_i \mathcal{C}_{sys} & I \end{bmatrix} \hat{x}_c(n) + \begin{bmatrix} \mathcal{B}_{\text{sys}} \\ 0 \end{bmatrix} u(n) + \begin{bmatrix} \mathcal{O}_{\text{sys}} \\ 0 \end{bmatrix} \hat{e}(n), \tag{6.34a}$$

$$u(n) = -\begin{bmatrix} \mathcal{F}_{\text{sys}} & \mathcal{F}_i \end{bmatrix} x_c(n) \tag{6.34b}$$

$$\hat{y}_e(n) = [C_{\text{sys}} \quad 0]\, \hat{x}_c(n) \text{ and} \tag{6.34c}$$

$$\hat{e}(n) = y_e(n) - \hat{y}_e(n). \tag{6.34d}$$

Additionally, from the pressure feed forward design the following reference network was established according to

$$y_e(n) = \mathcal{F}_{\text{FF}}\, y_{\text{sys}}(n). \tag{6.34e}$$

For clarity, this controller is depicted on Figure 6.12 and has the form:

$$\begin{aligned} \left[\begin{array}{c} \hat{x}_c(n+1) \\ \hline u(n) \end{array}\right] &= \left[\begin{array}{c|c} \mathcal{A} & \mathcal{B} \\ \hline \mathcal{C} & 0 \end{array}\right] \left[\begin{array}{c} \hat{x}_c(n) \\ \hline y_{\text{sys}}(n) \end{array}\right] \\ &= \left[\begin{array}{cc|c} \mathcal{A}_{\text{sys}} - \mathcal{B}_{\text{sys}}\mathcal{F}_{\text{sys}} - \mathcal{O}_{\text{sys}}\mathcal{C}_{\text{sys}} & -\mathcal{B}_{\text{sys}}\mathcal{F}_i & \mathcal{O}_{\text{sys}}\mathcal{F}_{\text{FF}} \\ \mathcal{B}_i\mathcal{C}_{\text{sys}} & I & 0 \\ \hline -\mathcal{F}_{\text{sys}} & -\mathcal{F}_i & 0 \end{array}\right] \left[\begin{array}{c} \hat{x}_c(n) \\ \hline y_{\text{sys}}(n) \end{array}\right] \end{aligned} \tag{6.35}$$

This completes the MISO feed water controller design, which will be used to design the SISO feed water controller in the following section.

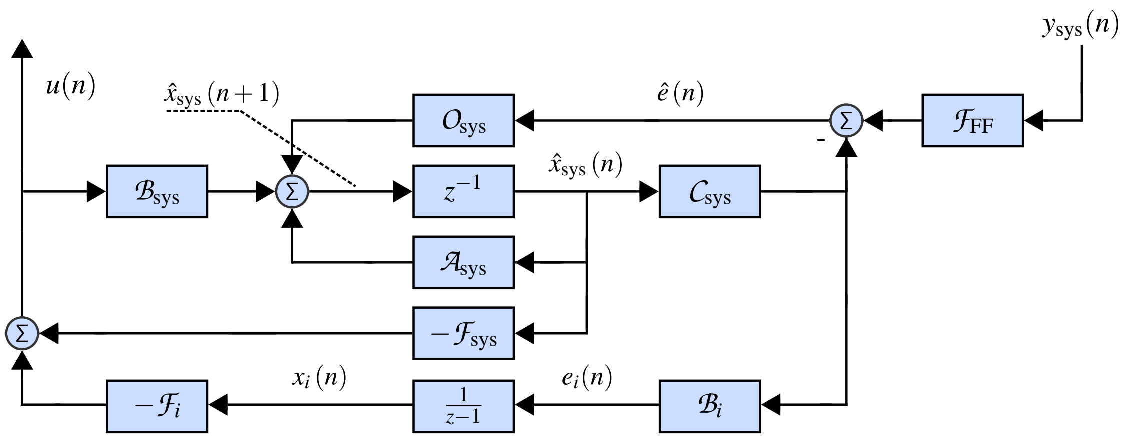

Figure 6.12: Block diagram of the complete MISO feed water controller. Note that $\frac{1}{z-1}$ is a short hand writing of the integrator loop, with $x_i(n)$ as its output and $e(n)$ as its input.

6.3 SISO Feed Water Controller Design

In this section, a SISO feed water controller is designed based on the MISO feed water controller. The intention is to reduce the MISO feed water controller to a standard PID class controller, as described in Section 6.1 (Introduction).

The MISO feed water controller states is described by $x_c(n) = [x_{\text{sys}}(n) \quad x_i(n)]^T$, which is related to the measured output through

$$\underbrace{\begin{bmatrix} \delta p_s(n) \\ \delta L_w(n) \end{bmatrix}}_{y_{\text{sys}}(n)} = \underbrace{\begin{bmatrix} C_{\text{sys},\,p_s} & 0 \\ 0 & C_{\text{sys},\,L_w} \end{bmatrix}}_{C_{\text{sys}}} \underbrace{\begin{bmatrix} \delta p_s(n) \\ \delta V_w(n) \end{bmatrix}}_{x_{\text{sys}}(n)}. \tag{6.36}$$

However, as the SISO feed water controller does not have access to the pressure measurement, which reduce (6.36) to (6.37). The strategy is to approximate the observer states $x_{\text{sys}}(n)$ from a single measurement $y_{\text{sys, siso}}(n)$. This can be done through the pseudo inverse denoted by †, which results in (6.38). Note that no information can be recovered about the steam pressure δp_s from the level measurement, which makes sense. As a consequence, the pressure feed forward term is not a part of this controller, which is expected to decrease the controllers steadiness.

$$\underbrace{\delta L_w}_{y_{\text{sys, siso}}(n)} = \underbrace{\begin{bmatrix} 0 & C_{\text{sys},\,L_w} \end{bmatrix}}_{C_{\text{sys,siso}}} \underbrace{\begin{bmatrix} \delta p_s(n) \\ \delta V_w(n) \end{bmatrix}}_{x_{\text{sys}}(n)} \tag{6.37}$$

$$x_{\text{sys}}(n) \approx C^{\dagger}_{\text{sys,siso}} y_{\text{sys, siso}}(n) = \begin{bmatrix} 0 \\ C^{-1}_{\text{sys},\,L_w} \end{bmatrix} y_{\text{sys, siso}}(n) \tag{6.38}$$

Applying (6.38) to the MISO feed water controller given by (6.35), produce a PI class controller as desired, which is governed by (6.39b). It has the proportional term $-\mathcal{F}_{\text{sys},V_w} C^{-1}_{\text{sys},L_w}$ and the integral term $-\mathcal{F}_i$.

$$\begin{bmatrix} x_i(n+1) \\ \hline u(n) \end{bmatrix} = \left[\begin{array}{c|c} I & \mathcal{B}_i C_{\text{sys}} C^{\dagger}_{\text{sys,siso}} \\ \hline -\mathcal{F}_i & -\mathcal{F}_{\text{sys}} C^{\dagger}_{\text{sys,siso}} \end{array}\right] \begin{bmatrix} x_i(n) \\ \hline y_{\text{sys,siso}}(n) \end{bmatrix} \tag{6.39a}$$

$$= \left[\begin{array}{c|c} 1 & 1 \\ \hline -\mathcal{F}_i & -\mathcal{F}_{\text{sys},V_w} C^{-1}_{\text{sys},L_w} \end{array}\right] \begin{bmatrix} x_i(n) \\ \hline y_{\text{sys,siso}}(n) \end{bmatrix} \tag{6.39b}$$

Where

$$\mathcal{F}_{\text{sys}} = \begin{bmatrix} \mathcal{F}_{\text{sys},p_s} & \mathcal{F}_{\text{sys},V_w} \end{bmatrix} \text{ and } \mathcal{B}_i = \begin{bmatrix} 0 & 1 \end{bmatrix}$$

Using this controller, the response as depicted on Figure 6.13 is obtained, which is very close to the MISO feed water controller without pressure feed forward. This will become more clear in the following section where the controllers are evaluated.

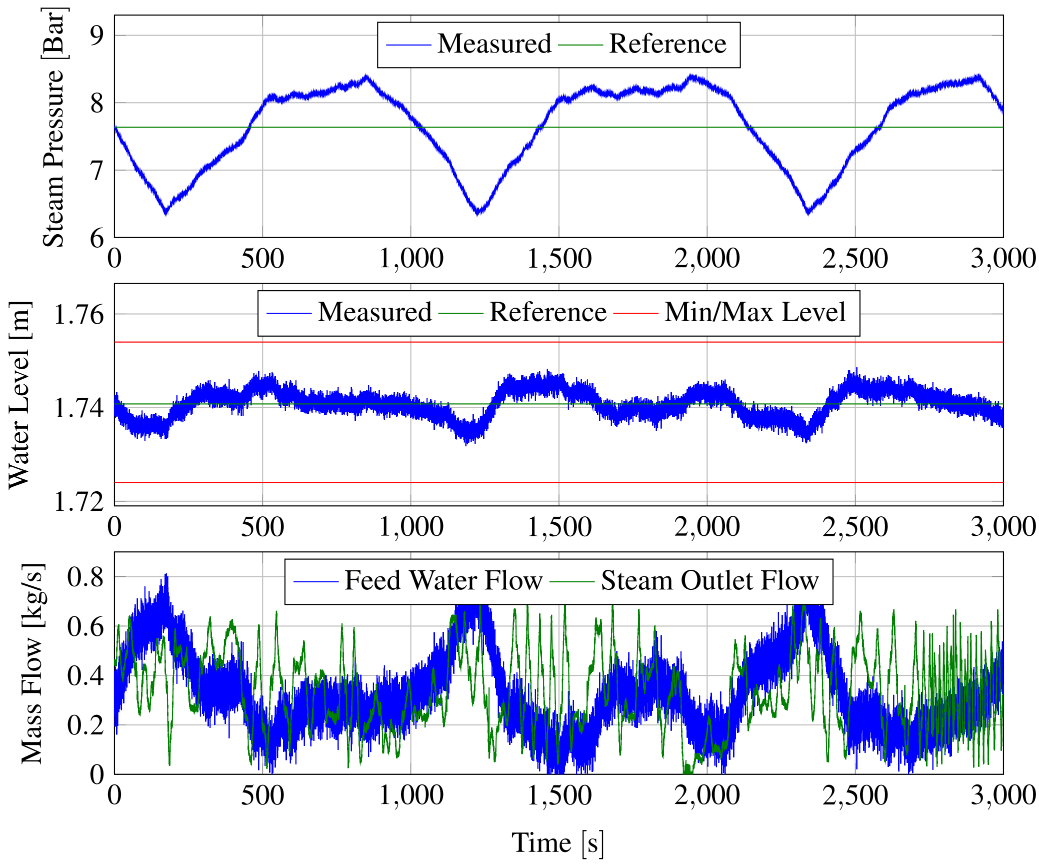

Figure 6.13: The simulated SISO feed water controller.

6.4 Controller Evaluation

In this section the developed controllers will be evaluated based on the performance criteria specified in Section 6.1 (Introduction).

The steam outlet flow $\dot{m}_s$ is scaled by 50%, 100% and 150% to evaluate the steadiness cost function for different steam outlet levels. This is primarily to evaluate the controllers ability to adapt to changing operating conditions. On Table 6.1 the steadiness cost of the SISO, MISO and MISO controller with feed forward (MISO+FF) is depicted. The reasons for comparing the SISO controller and MISO controller is to show that they produce very similar results. However, the MISO controller with feed forward clearly produce the best overall steadiness of the three different controllers, despite changing steam outlet demand levels.

Controller	**Steam Demand** [e-3]		
	50%	100%	150%
SISO	22.3	24.5	20.8
MISO	14.4	12.2	11.9
MISO+FF	1.9	2.7	2.8

Table 6.1: The steadiness cost for the developed controllers calculated using (6.1b). Lower cost indicate better ability to keep the control input steady.

On Figure 6.14 the feed water control signal and $\dot{m}_{s,\text{mean},N_s}$ is depicted for the three tests, which gives additional insight of the water level trend as well as the controllers ability to track it. Note that the MISO controller with feed forward is more consistent, as indicated by the steadiness. Furthermore, without feed forward the controllers tend to saturate at lower steam demands, which inevitably leads to larger feed water bursts. From a practical standpoint this is not desired as this leads to a large amount of start and stop cycles for the pump, which in turn decreases its lifespan. Furthermore, please notice that the primary difference between the SISO and MISO controller is additional noise and a phase shift from the observer.

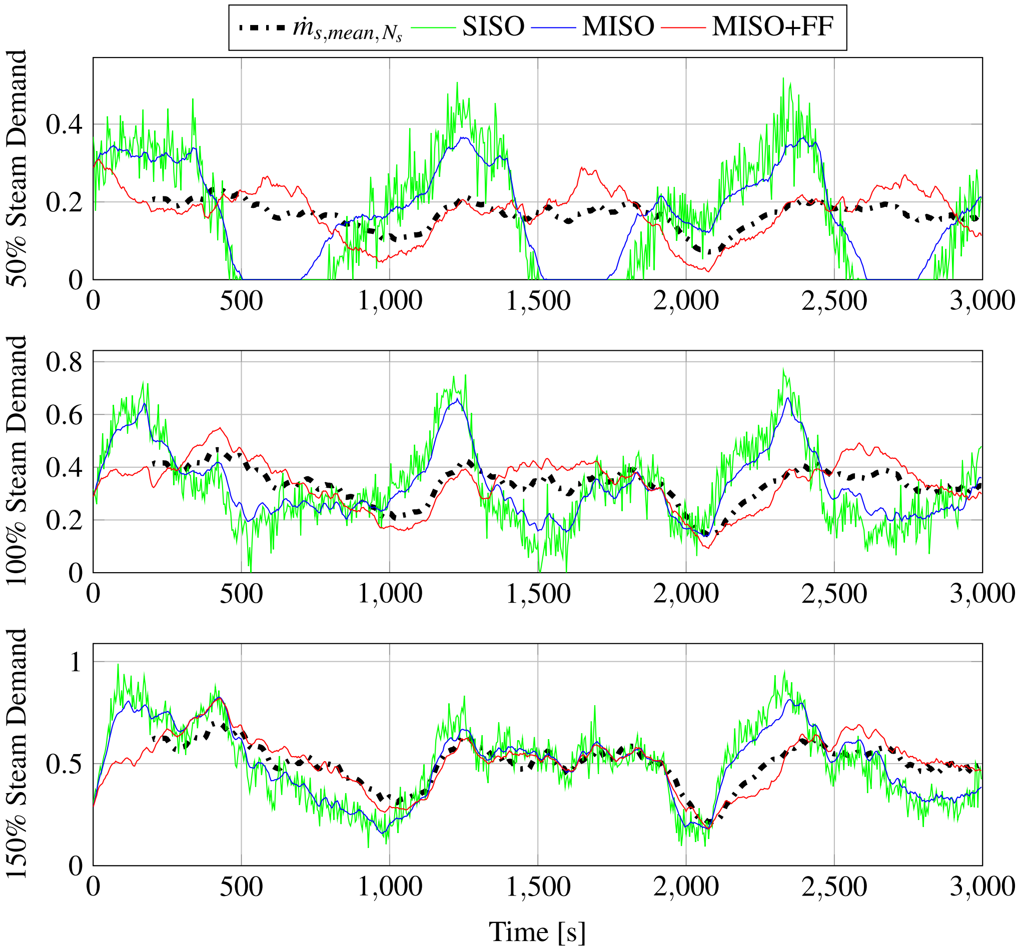

Figure 6.14: Feed water flow with different steam demands with the different controllers. All the values are feed water flows, which has the unit kg/s.

The next demand which need to be considered is the "Min/Max Level" has been satisfied for the different controllers. On Figure 6.15 the water levels of the different controllers are displayed, which shows that the MISO controller with feed forward has larger level variations than the other controllers as expected. However, this controller is very close to violating the "Min/Max Level", as a consequence of applying the pressure feed forward. This can be demonstrated by comparing the MISO+FF controller with the MISO controller, which produce a more stable water level. Based on this, the MISO+FF controller still produce an acceptable level control, given the fact that a 150% steam outlet demand is very unlikely for the Danish Crown steam boiler, based on the measurement series.

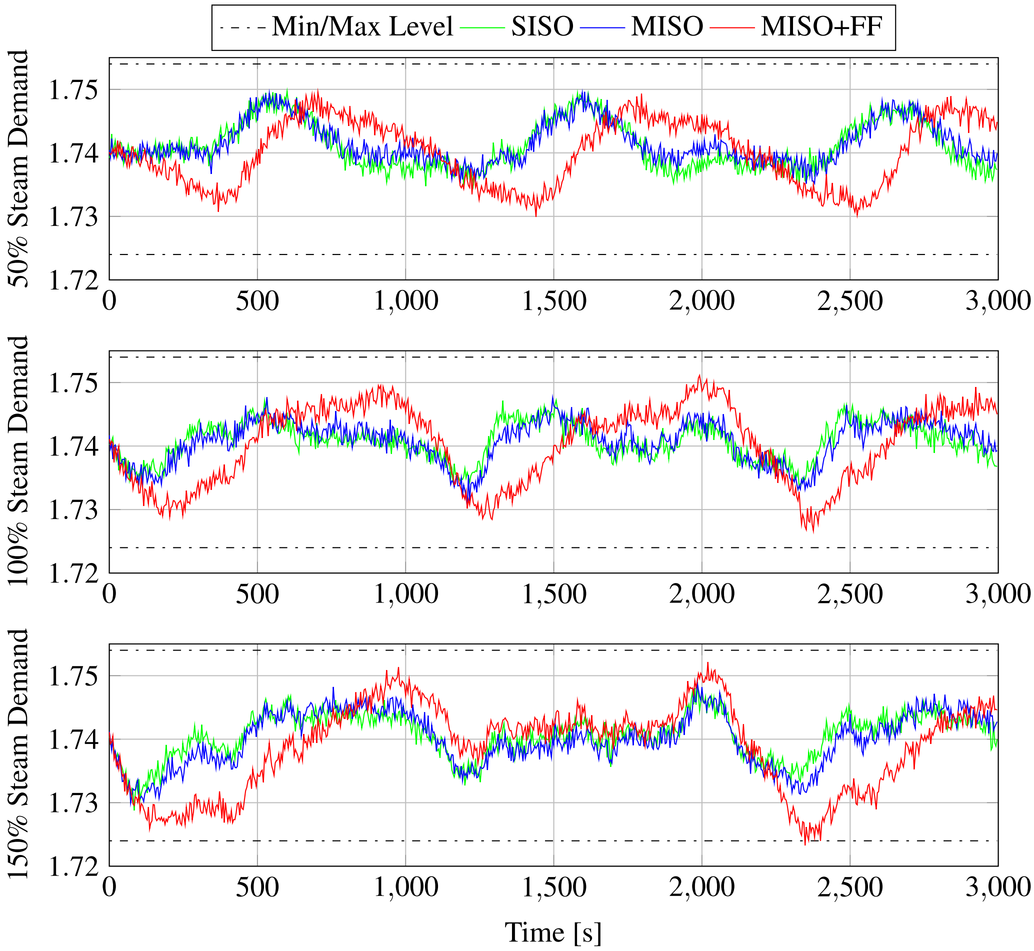

Figure 6.15: Water level with different steam demands with the different controllers.

Lastly, the feedback law eigenvalues are located at $\{0.99923, 0.99943 \pm 0.00056483j\}$, while the observer eigenvalues are located at $\{0.83221, 0.98995\}$. In continuous time these poles roughly translate to $\{-0.0061231, -0.0045405 \pm 0.0045212j\}$ for the feed back law and $\{-1.4693, -0.080786\}$ for the observer. This shows that the observer eigenvalues are considerably faster than the controller eigenvalues, which is considered good practice in traditional observer based controller design.

6.5 Stepwise Commissioning Design

In this section the stepwise commissioning design based on the developed method described in Chapter 2 is carried out for the two designed feed water controllers. For clarity, the developed controllers consist of the PI feed water controller developed in Section 6.3 and the MISO feed water controller with pressure feed forward (MISO+FF) developed Section 6.2. The developed sequential stepwise commissioning method is restated in Definition 6.2 for convenience from Section 2.5 (Sequential Stepwise Commissioning Strategy).

Definition 6.2 (Sequential Stepwise Commissioning)
Let $\mathbb{S}^-$ be the set of all real, rational, stable and proper transfer function matrices of appropriate dimensions in continuous or discrete time. Similarly, let $\mathbb{S}$ be the set of all real, rational and proper transfer function matrices of appropriate dimensions in continuous or discrete time.

The stepwise commissioning of the n stabilizing controllers $\mathcal{K} = \{K_1, ..., K_n\}$ with the plant $P \in \mathbb{S}$ is governed by

$$K_{\text{SSC}}(\gamma_1, ..., \gamma_n) = K_0 + \left(\sum_{i=1}^{n} [\gamma_i \; (K_i - K_0) \star (P \star K_0)] \right) \star [-(P \star K_0)] \tag{6.40}$$

where $K_0 \in \mathbb{S}^-$ is any stabilizing controller. The transition parameters $\gamma_i \in [0;1]$ is selected according to (6.41).

$$\gamma_j = 1 - \gamma_{j \to k} \tag{6.41a}$$

$$\gamma_k = \gamma_{j \to k} \tag{6.41b}$$

$$1 = \sum_{i=1}^{n} \gamma_i \tag{6.41c}$$

To ease up the notation for state space controllers, the state space notation given by Definition 6.3 is used.

Definition 6.3 (State Space Shorthand Notation)
Let the discrete time state space system G be described by

$$x(n+1) = \mathcal{A}x(n) + \mathcal{B}u(n) \text{ and} \tag{6.42}$$

$$y(n) = \mathcal{C}x(n) + \mathcal{D}u(n). \tag{6.43}$$

The shorthand notation for this system is given by

$$G \stackrel{\text{ss}}{=} \left[\begin{array}{c|c} \mathcal{A} & \mathcal{B} \\ \hline \mathcal{C} & \mathcal{D} \end{array} \right]. \tag{6.44}$$

The controller that is desired to be used in the sequential stepwise commissioning are the two controllers $\mathcal{K} = \{K_{\text{PI}}, K_{\text{MISO+FF}}\}$, which are restated with the proper input in (6.45).

$$K_{\text{PI}} \stackrel{\text{ss}}{=} \left[\begin{array}{c|cc} 1 & 0 & 1 \\ \hline -\mathcal{F}_i & 0 & -\mathcal{F}_{\text{sys},V_w} \mathcal{C}^{-1}_{\text{sys},L_w} \end{array} \right] \tag{6.45a}$$

$$K_{\text{MISO+FF}} \stackrel{\text{ss}}{=} \left[\begin{array}{cc|c} \mathcal{A}_{\text{sys}} - \mathcal{B}_{\text{sys}}\mathcal{F}_{\text{sys}} - \mathcal{O}_{\text{sys}}\mathcal{C}_{\text{sys}} & -\mathcal{B}_{\text{sys}}\mathcal{F}_i & \mathcal{O}_{\text{sys}}\mathcal{F}_{\text{FF}} \\ \mathcal{B}_i \mathcal{C}_{\text{sys}} & I & 0 \\ \hline -\mathcal{F}_{\text{sys}} & -\mathcal{F}_i & 0 \end{array} \right] \tag{6.45b}$$

The plant P is not stable, as it has a pole in zero as described in Subsection 5.4.2 (Linearization). For this reason, the initial controller K_0 is selected as a proportional controller with proportional term equal to that of the PI controller, which equals

$$K_0 \overset{\mathrm{ss}}{=} \left[\begin{array}{c|c} & \\ \hline 0 & \mathcal{F}_{\mathrm{sys},V_w} C^{-1}_{\mathrm{sys},L_w} \end{array}\right]. \tag{6.46}$$

This controller can be shown to stabilize the plant P. Applying Definition 6.2 results in the stepwise sequential controller

$$K_{\mathrm{SSC}}(\gamma) = K_0 + [(1-\gamma)(K_{\mathrm{PI}} - K_0) \star (P \star K_0) + \gamma (K_{\mathrm{MISO+FF}} - K_0) \star (P \star K_0)] \star [-(P \star K_0)], \tag{6.47}$$

where γ is the transition parameter. Note that γ is used instead of $\gamma_{\mathrm{PI}\rightarrow\mathrm{MISO+FF}}$ and governs the transition between K_{PI} and $K_{\mathrm{MISO+FF}}$. This controller is calculated using the state space algebra described in Section A.1 (State Space Algebra) and is not stated as it gives no additional insight to its performance. Similar to the example made in Section 2.7 (Stepwise Commissioning Example) a simulation of the transition will be carried out along with how the singular values and pole-zeros change throughout the transition.

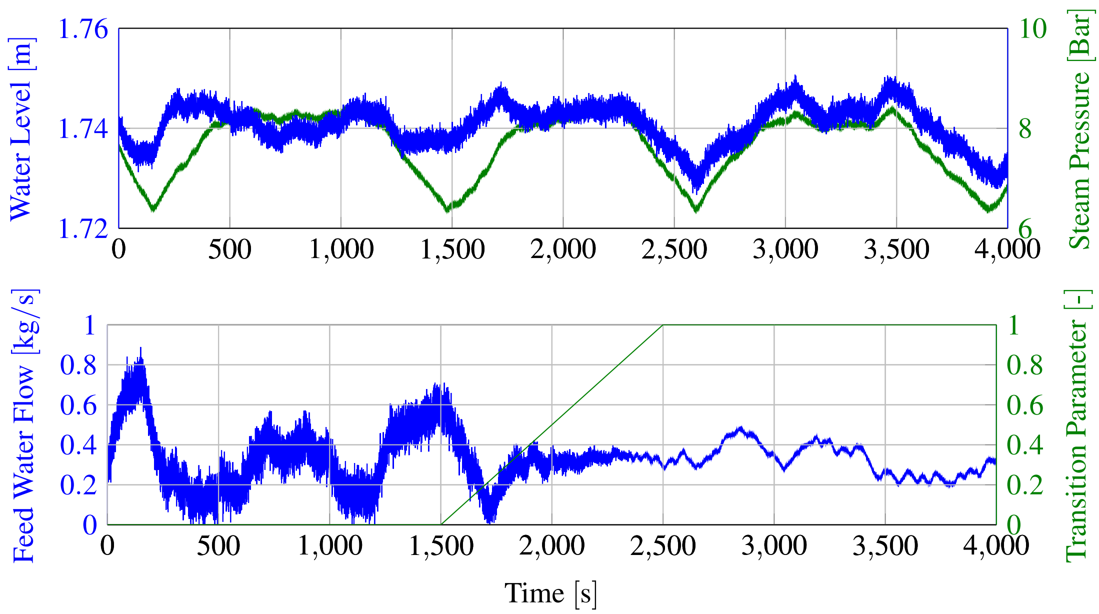

Figure 6.16: Stepwise Commissioning simulation of the MISO feed water controller from the PI feed water controller.

On Figure 6.16 a simulation with $K_{\mathrm{SSC}}(\gamma)$ and the nonlinear plant is carried out. The PI controller is active for the first 1500 seconds, where the transition takes place over a period of 1000 seconds. In the last 1500 seconds the MISO+FF controller is active. Notice how the controllers output behavior changes gradually and in a controlled manner, exactly as desired. Furthermore, note that a transition time of 1000 seconds has been selected to illustrate that the transition happens in a controlled fashion despite large steam pressure variations. The characteristics of this transition is that at $\gamma \approx 20\%$ the water level starts to follow the pressure feed forward reference. Then the feed water flow gradually becomes less noisy until the MISO+FF controller appears to be dominant at $\gamma \approx 80\%$.

To demonstrate that faster transition speeds also produce acceptable results, a transition time of 50 seconds can be depicted on Figure 6.17. Similar to the previous transition, the output changes in a smooth but faster fashion.

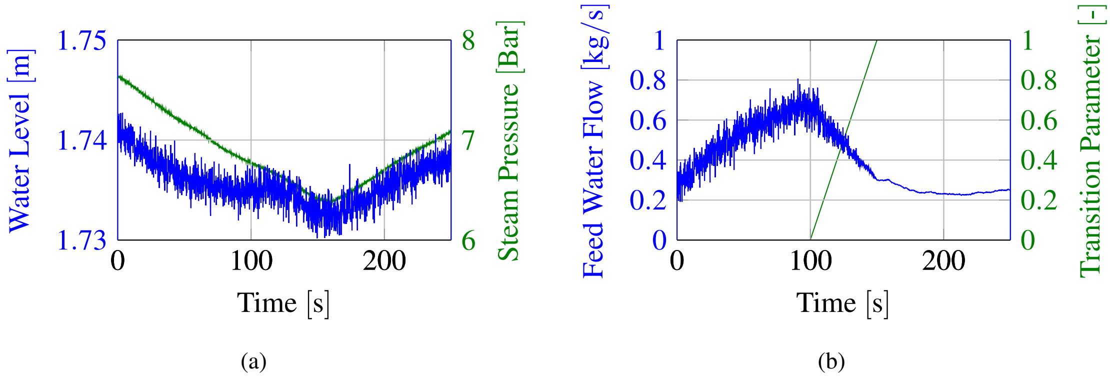

Figure 6.17: Fast Stepwise Commissioning simulation of the MISO feed water controller from the PI feed water controller.

On Figure 6.18 the singular values of the plant and controller in open loop, $PK_{SSC}(\gamma)$, is depicted for the transition parameter $\gamma \in [0;1]$. The top plot depicts how the singular values are related to the water level changes throughout the transition. The magnitude after 10^{-2} Hz is significantly decreased, which is caused by the observer. Additionally, the bottom plot shows that the singular value related to the steam pressure is nonexistent. This makes sense, as the feed water controller is not designed to stabilize the steam pressure and naturally has little influence on the steam pressure.

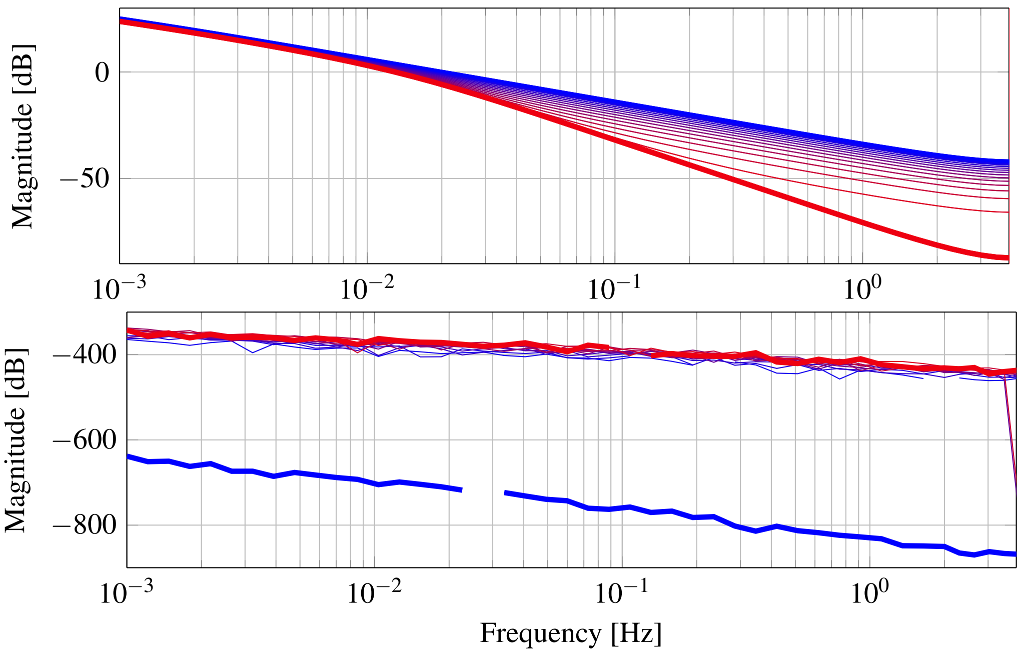

Figure 6.18: Singular values of the open loop system denoted by $PK_{SSC}(\gamma)$ for $\gamma \in [0;1]$. The transition is color coded and move from blue (PI) to red (MISO) as γ goes from 0 to 1.

On Figure 6.19 the pole-zero movement throughout the transition is depicted. As the pole-zero movements are very subtle, the green boxes indicate the moving poles and zeros for clarity. Furthermore, it might appear like the system contains unstable poles due to the axis scaling, but it does not. This figure supports that the output changes in a predictable fashion, as observed on Figure 6.16 and Figure 6.17. It also suggest that the largest difference between the two controllers is the pressure feed forward reference, given the subtle pole-zero changes.

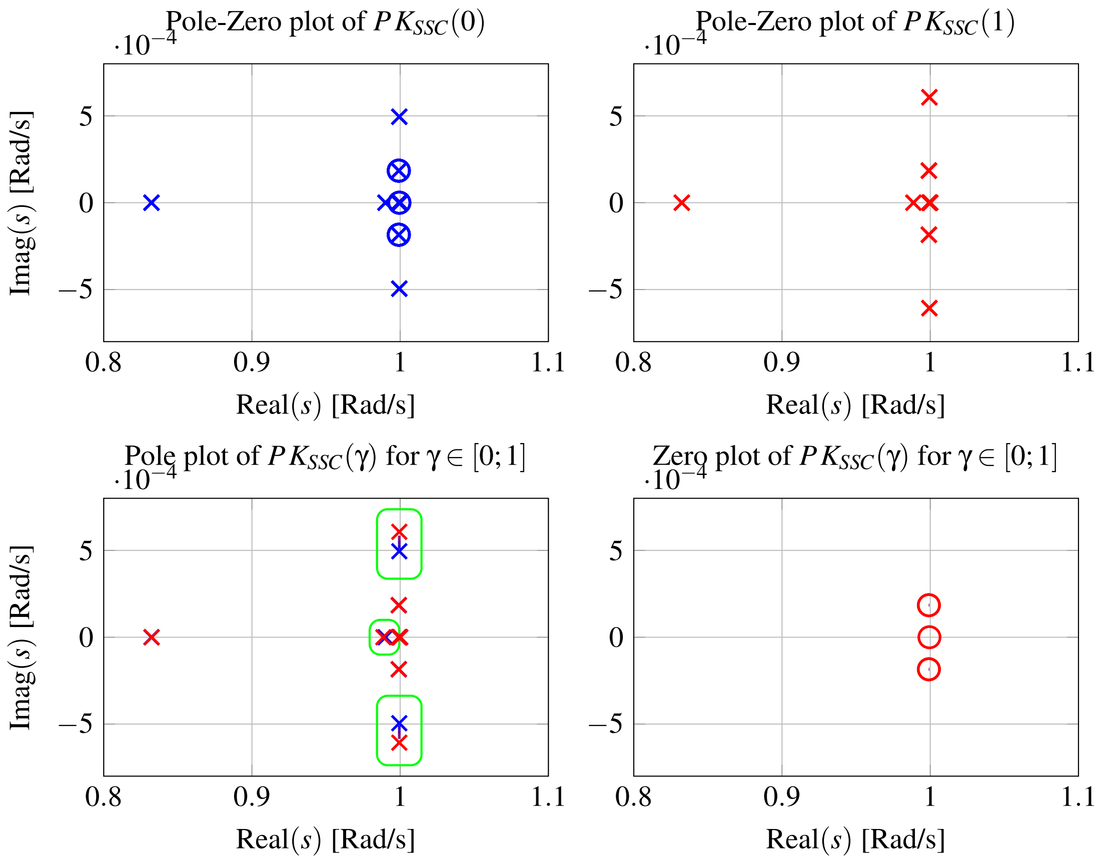

Figure 6.19: Top plots: The Pole-Zero plot of $PK_{\mathrm{SSC}}(0)$ and $PK_{\mathrm{SSC}}(1)$. Bottom plots: The pole and zero movement of $PK_{\mathrm{SSC}}(\gamma)$ as γ goes from 0 to 1. Once again, K_{PI} is denoted by blue and $K_{\mathrm{MISO+FF}}$ by red.

This concludes the stepwise commissioning design of the two feed water controllers. Now the experimental results obtained will be described.

Chapter 7

Experimental Results

7.1 Introduction

The primary purpose of the test at Danish Crown in Sønderborg is to test the stepwise commissioning strategy described in Chapter 2 (Stepwise Commissioning Design). For this purpose two controllers was developed in Chapter 6 (Stepwise Commissioning Design), both of which has the purpose of keeping the Feed Water flow steady as it is expected to improve the operating conditions of the deaerator as explained in Subsection 4.2.3 (Benefits of adopting a MISO boiler feed control strategy). The stepwise commissioning method has been applied to these controllers, which results in a stepwise commissioning controller. Additionally, the temperature of the feed water is an indicator of the deaerators ability to remove dissolved gases from the feed water, as explained in Section 4.1 (Description of the Steam Boiler System).

This means that it is interesting to investigate the performance of the two controllers, the transition between the two controller through the stepwise commissioning and the temperature of the feed water. On Figure 7.1 the expected test setup is depicted, which permits these questions to be answered. The stepwise commissioning controller (SCC) measures the steam pressure with the pressure sensor (PS) and the water level with the level sensor (LS) and controls the feed water pump, which is necessary for the designed controller. Additionally, the feed water temperature is measured by the temperature sensor (TS), which is mounted on the outside of the feed water pipe. All of these components uses the industrial 4-20mA current signal standard. For more information about the sensors and the control platform, a manual written by Grundfos is available at the CD at `[Data Sheets/ControllerDocumentation.pdf]`.

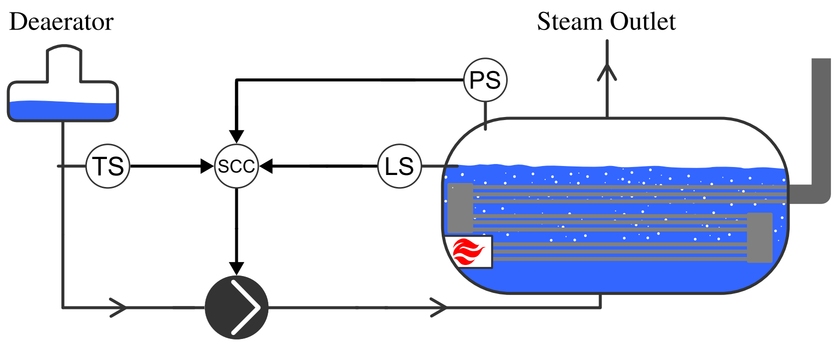

Figure 7.1: The expected Danish Crown test setup.

The Danish Crown steam boiler is not highly accessible, which means that no more than a single test was expected to be conducted. It is not highly accessible due to the fact that a test session requires co-ordination with Grundfos, as they provide an experienced boiler systems technician, and Danish Crown, as they provide access to the steam boiler. Additionally, there is a logistical challenge as Danish Crown is located in Sønderborg and the controller is developed in Aalborg, which requires around 300 km of travel. For these reasons, it is desired to be sure that the controller has the desired behavior before the actual test and a lab test setup has been developed, which is explained in Section 7.2 along with the controller itself. Afterwards the test results obtained will be described in Section 7.3. Additionally, keep in mind that the controllers cannot be tuned on site at the Danish Crown steam boiler as the alloted time does not allow for this.

7.2 Controller and Lab Test Setup

In this section the controller and the lab test setup is described. The controller is supplied by Grundfos, while the lab test setup is developed in this project as a way of verifying that the different components of the controller has the desired behavior, before the actual test at Danish Crown.

The controller is made up of two mayor components, which consists of an PLC and a μ-controller as depicted on Figure 7.2. The μ-controller is named "Beaglebone Black" and has an arm-based processor which runs the embedded Linux distribution called Debian. It is more than capable of running the controller, which is written in C++ and has an array of high level interfaces, of which Ethernet is used for the communication with the host computer and the PLC. The PLC is a modular unit which houses different input/output, which can be interfaced to through the Modbus TCP protocol. For this reason, the libmodus c library is used which implements the Modbus TCP protocol. Further information about this library can be found at [Raimbault, 2015].

The controller code is available on the CD at `[Controller Code/]`. The code specific to the stepwise controller code is generated with Matlab Coder, which can convert matlab code into c/c++ code. Hence, the controller code is included for inspiration for future projects and will not be described further.

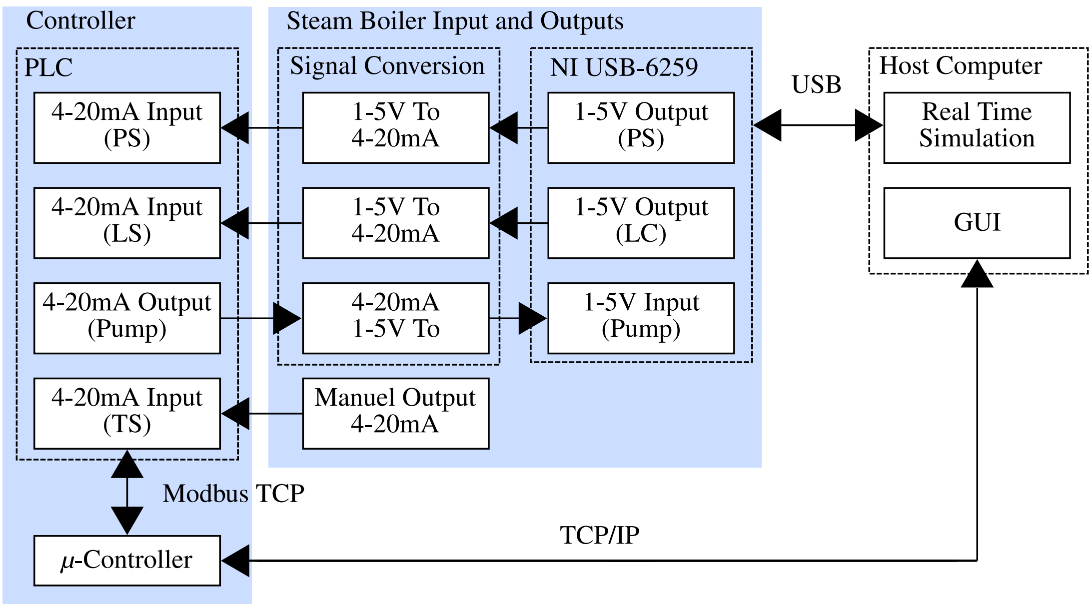

Figure 7.2: The controller and the Lab Test Setup structure.

The lab test setup is desired to behave like the Danish Crown Steam Boiler and runs the nonlinear simulation model in real time, which is described in Subsection 5.3.7 (The System Identification Results). To emulate the expected Steam Boiler input and output interfaces depicted on Figure 7.1, an USB National Instruments data acquisition unit (NI USB-6259) is used to read and emit voltages. This device is supported by the Matlab Data Acquisition interface, which is described in detail at [MathWorks, 2015]. The voltage outputs of the pressure and level sensor are converted to 4-20mA signals through a converter from a 1-5v interface, while the 4-20mA pump reference output is converted to a voltage through a resistor. Additionally, the feed water temperature sensor is emulated through a manually configurable device, as this sensor is not a part of the real time simulation. This allows the test setup to emulate the Danish Crown steam boiler and verify that the entire controller has the desired behavior.

In Section B.4 (Stepwise Commissioning Test of the Test Setup) a test, which shows that the stepwise commissioning controller has the desired behavior on the lab test setup. Additionally, a safety controller was developed, which would overwrite the stepwise commissioning controller in case the specified water level bounds are violated and is specified and tested in Section B.5.

It was discovered rather late in the project that the feed water pump was not flow controlled, but speed controller instead. Hence, the pump curve is used to give a relationship between the pump speed and the feed water flow in the following subsection.

7.2.1 Pump Output Flow Curve

The feed water pump at the Danish Crown steam boiler was found to not be flow controlled as previously assumed, but speed controlled instead. For this reason, the pump curve established in Section B.1 (Faulty pressure difference argument) will be used to give a qualified guess of the output flow in terms of the pump speed n. By solving for the feed water flow $\dot{m}_{fw}$ in (B.2)

$$\dot{m}_{fw} = \frac{a_1 n + \sqrt{4 a_0 a_2 n^2 + a_1^2 n^2 - 4 a_2 \Delta P}}{2 a_2} \tag{7.1}$$

is obtained, which states that the feed water flow $\dot{m}_{fw}$ it is a function of the pump speed n and the pressure difference over the pump ΔP.

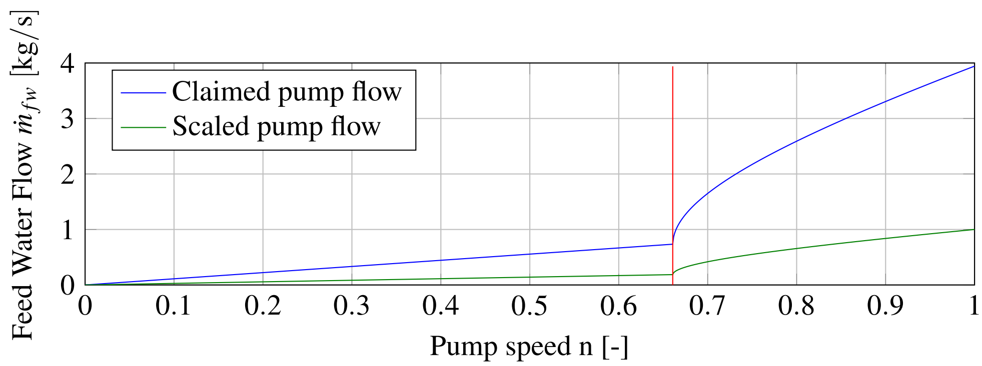

Figure 7.3: The feed water flow as a function of the pump speed for the feed water pump with $\Delta P = 7$ Bar.

The pressure difference over the pump ΔP is approximated by assuming that the steam pressure p_s is at the pump outlet and that there is around 1 bar of pressure at the pump inlet. Hence, $\Delta P \approx p_s - 1$ Bar. Using (7.1) the blue trace on Figure 7.3 is obtained with $\Delta p = 7$ Bar. The red vertical line indicates when the pump cannot produce enough pressure to push water into the steam boiler as it has an one way valve.

The linear blue trace to the left of the red bar allows the controller to utilize the entire speed range, in case the pump curve is invalid. Furthermore, to compensate for the fact that this pump model has been found to overestimate the feed water flow, it is compensated for by scaling it as depicted by the green trace on Figure 7.3. The validity of this approach will be revisited later.

Keep in mind that it is considered bad practice to use a pump when it does not move any water, as it can lead to overheating of the water at the pump impeller, which decreases the lifespan of the pump. Additionally, if this is found to be the case during the test at the Danish Crown steam boiler, it can easily be turned off in the controller code. Special attention must be given to this during the test.

7.3 Results from the Danish Crown Steam Boiler

This section contains the results and thoughts related to the test conducted at Danish Crown in Sønderborg at the 29th of may 2015. It has to be stated that a previous attempt was made the 26th of may 2015, but it had to be aborted as the pump could not be reconfigured using the available configuration tool. On Figure 7.5 a picture displays the steam boiler during the test.

A stepwise commissioning test similar to the one depicted on Figure 6.16 in Section 6.5 (Stepwise Commissioning Design) has been conducted on the steam boiler system. Now the aspects mentioned in Section 7.1 (Introduction) will be discussed.

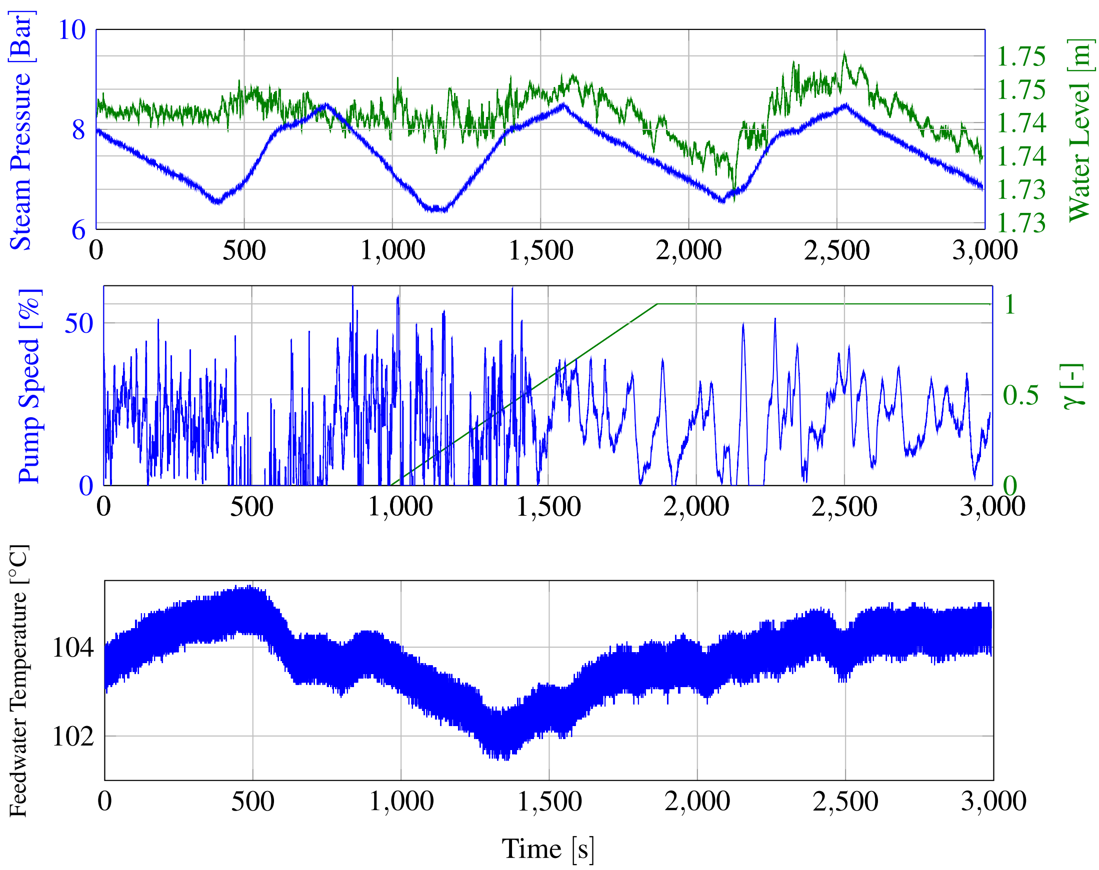

Figure 7.4: Stepwise Commissioning over a 15 minute time period on the Danish Crown Steam Boiler using the developed controllers.

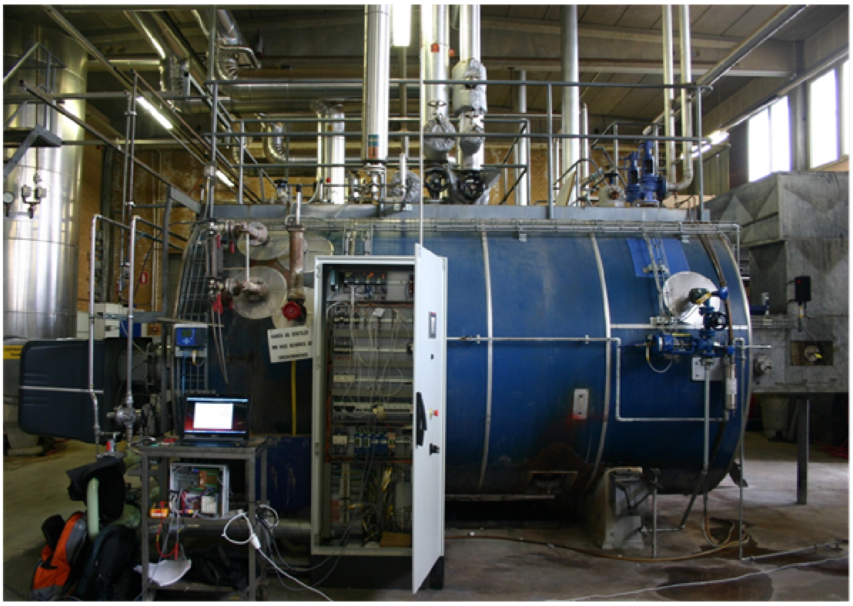

Figure 7.5: The Danish Crown steam boiler during the test.

Evaluation of the Controllers

The PI controller is active for the first 1000 seconds while the MISO controller with pressure feed forward (MISO+FF) is active for the last 1100 seconds on Figure 7.4. Common for the two controllers is that the control signal is very unsteady, which is neither the expected or desired behavior. This is suspected to be caused by the feed water pump not having the expected behavior and has a significantly higher gain than expected, which will be further specified in Subsection 7.3.1 (Issues and Considerations).

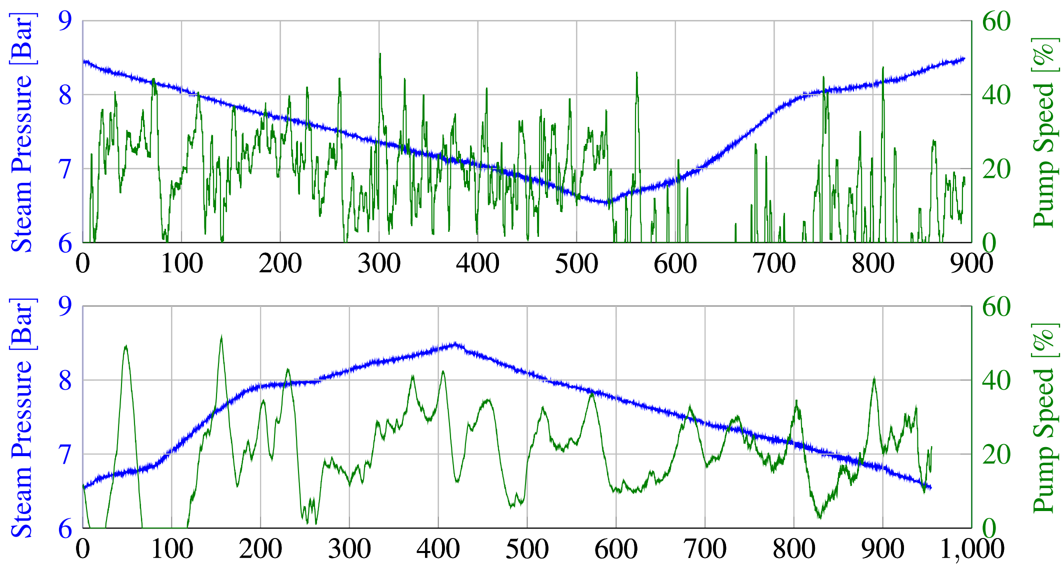

Figure 7.6: Top Plot: One burner cycle with the PI controller. Bottom Plot: One burner cycle with the MISO+FF controller.

Even though both controllers has quite unsteady control signal, the control signal of the MISO+FF controller is significantly more steady compared to the PI controller. One reason which explains this is the pressure feed forward, which is supported by the fact that the PI controllers behavior depends on the steam pressure. This is illustrated on the top plot of Figure 7.6, where the mean PI controllers pump speed is 20.6% when the burner is off and only 5.7% when the burner is on. Additionally, the mean pump speed for the MISO+FF controller is 20.5% when the burner is on and 19.7% when the burner is off. The specifics of how the pump speed on average can be higher with the MISO+FF controller might be caused by the pump operating without moving water some of the time or a higher steam outlet flow throughout the burner cycle.

The Stepwise Commissioning

Despite the unsteady control signal, the stepwise commissioning of the two controllers occurs in a gradual fashion as desired, which is depicted on the middle plot of Figure 7.4. The first signs of the MISO+FF controller appears at $\gamma \approx 25\%$, which is about 5% slower than the simulation in Section 6.5 (Stepwise Commissioning Design), as the feed water pump stops to track the water level reference generated by the pressure feed forward. Shortly after, the output starts to become less noisy and more consistent. At around $\gamma \approx 70\%$ the MISO+FF controller appear to be dominant, which is 10% earlier than the transitional behavior depicted on Figure 6.16 in Section 6.5 (Stepwise Commissioning Design). This behavior is consistent with faster transition speeds, but due to the unsteady control signal nothing conclusive can be said for transition speeds below 6 minutes, as the main indicators of the transition is the water level behavior, how noisy and steady the control signal is.

For instance, on Figure 7.7 the stepwise commissioning from the PI controller to the MISO+FF controller is occurring at around 100 seconds, which shows almost the same behavior in reverse. At $\gamma \approx 70\%$ the control signal starts to become gradually more noisy and at $\gamma \approx 35\%$ the water level straightens up and becomes less steady, which is very close to the transition behavior for the 15 minute transition. Similarly, a transition back to the MISO+FF controller is depicted at 500 seconds, which has the exact same behavior as the 15 minute transition with the same indicators. As a result, the stepwise commissioning method is considered a success, despite the unsteady controllers.

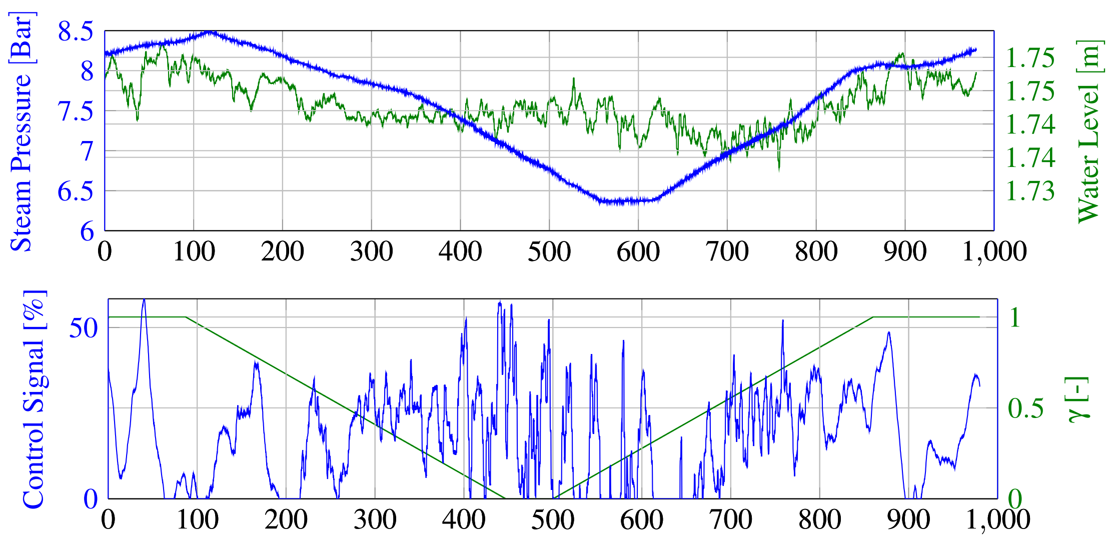

Figure 7.7: Stepwise Commissioning with a 6 minute transition time from the MISO+FF controller to the PI controller and back again to the MISO+FF controller.

The Feed Water Temperature

Furthermore, a sample of the past on/off feed water controller was also carried out, which is depicted on Figure 7.8 and shows an average temperature close to that of the developed controllers. It has to be stated that this measurement was taken after the stepwise commissioning tests, which allow for the possibility that the deaerator did not have the time to time settle prior to the readings. However, similar temperatures was observed before the stepwise commissioning tests, which suggest that this is rather unlikely.

During the visit at Danish Crown it was observed that the temperature controller in the deaerator is on/off controlled and activates approximately 1-2 times per hour. Consequently, this means that it is hard to tell if the feed water temperature has increased as a consequence of using the developed controllers.

Additionally, the temperature of the feed water is higher than expected compared to the data used for the parameter identification in Section 5.3, which on average was in the vicinity of 85 °C. The feed water temperature in Figure 7.6 is around 104 °C for both the on/off and the developed controllers. This temperature change is most likely caused by the deaerators controller being changed. Hence, it cannot be concluded that a flow controlled feed water controller improves the performance of an on/off controlled deaerator.

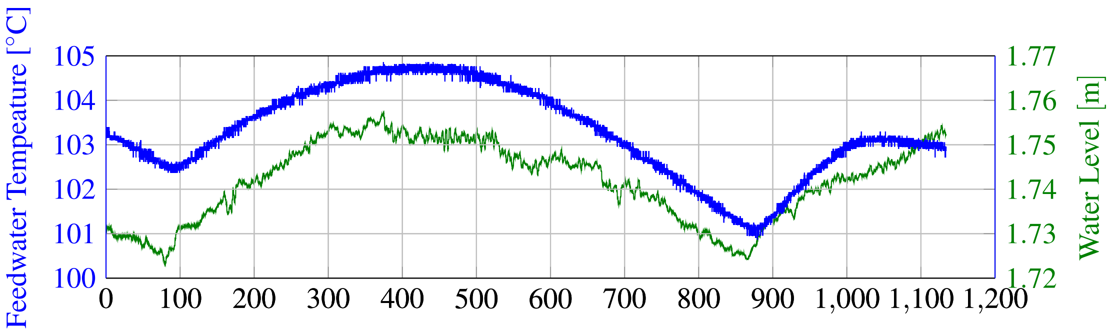

Figure 7.8: The measured feed water temperature of two feed water cycles.

7.3.1 Issues and Considerations

Some issues and considerations regarding the Danish Crown steam boiler is described in this section. The aim is to describe some aspects, which must be taken into consideration if future tests is to be conducted with a similar configuration.

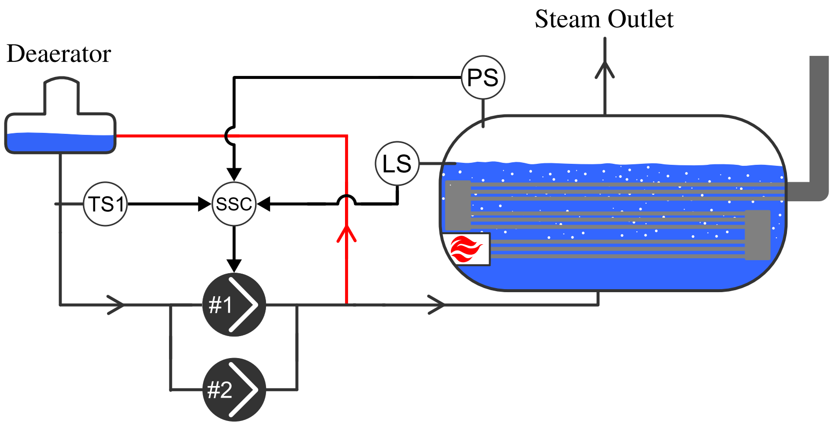

Figure 7.9: The expected Danish Crown test setup with additional observed elements.

An additional backup pump is installed. As depicted on Figure 7.9 two feed water pumps are installed in parallel and is individually capable of controlling the water level in on/off mode. It was possible to run pump #2 while pump #1 was reconfigured to be compatible with the stepwise commissioning controller. That being said, pump #2 had not been used for years, but with proper supervision it is considered both a responsible and convenient solution for reconfiguring pump #1 while the steam boiler is in operation.

On Figure 7.10 a picture of the two pumps are depicted at Danish Crown, where the pump on the left is pump #1 and the pump on the right is #2.

Figure 7.10: The two installed feed water pumps.

The 4-20mA pump interface on pump #1 does not work. Instead a 0-10V signal was used, by converting the current signal into a voltage through a resistor.

Pump #1 still depends on the on/off signal to run. Pump #1 was configured to run according to an external set-point signal, which is active only when it receives the on signal from the on/off controller. To easier understand how this works, the on/off controller use the percentile water level between highest permissible water level (HWL) and lowest permissible water level (LWL), which is described in Subsection 4.1.1 (Safety and Regulations). It is configured to start at a water level of 40% and turn off at 60%, which means that it is not possible to exceed a water level of 60% using the external set-point. Additionally, a warning alarm will sound if the water level reaches 30% water level, which gives plenty of time to activate pump #2 as a backup solution.

Pump #1 could not be configured to control the pump speed. The external set-point determines how much of the maximum pressure the pump should produce, as opposed to the pump speed as expected. This can explain why the set-point never reached the required 66% , which is when the pump should start to pump water into the boiler drum. Additionally, the gain of this type of input signal must therefore be higher and is considered one of the reason for the unsteady control signal.

A bypass valve is open after the pump-outlets. As depicted on Figure 7.9 by the red line, a bypass valve is open which permit the feed water to return to the deaerator. This is a quite peculiar configuration, as it is not normally used in an on/off feed water configuration. That being said, it explains why only around 25% of the expected feed water enters the boiler drum, as discussed in Section B.1 (Faulty pressure difference argument). It has to stated that this pipe is significantly smaller in diameter compared to the pipe leading to the steam boiler drum.

Additionally, it was possible to limit the maximum speed of the pump, which showed that the pump could not keep up with the feed water demand at 70% speed. When maximally limited to 75% speed, the pump could still meet the feed water demand which means that the scaled pump curve described in Subsection 7.2.1 (Pump Output Flow Curve) is not completely wrong, which shows that feed water should enter the boiler drum at 66% pump speed when the steam boiler pressure is at 8 Bar.

Pump #1 is over-dimensioned. Assuming that the bypass valve is closed and that the pump curve depicted in Subsection 7.2.1 (Pump Output Flow Curve) is accurate. Then it is not possible to keep the pump in continuous operation with an average steam outlet flow of 0.289 [kg/s] when the lowest possible outlet flow is around 0.7 [kg/s]. As a matter of fact, the bypass valve actually helps in this regard, but the exact effect is still unknown. For this reason, it is considered advisable to use a less powerful pump in the future, which is capable of operating in the range around the operating point.

This concludes the test at the stepwise commissioning Danish Crown steam boiler and is the end of the experimental results.

PART III

DISCUSSION

Chapter 8

Conclusion

The objective of this chapter is to answer the problem statement stated in Section 1.4 (Project Outline):

> **Is it possible to perform a sequential MIMO controller activation of a MIMO system, from a SISO controlled system using the Youla-Kucera parameterization?**

To answer the above question, a stepwise commissioning method based on the Youla-Kucera parameterization (YKP) has been developed. It allows for the gradual transition between any two controllers amongst a set of stabilizing controllers in a controlled manner while guaranteeing nominal stability. The only additional requirements imposed is that it requires a plant model and any additional stable and stabilizing controller. The developed method has the benefit of having a fixed reference structure, which require no additional design considerations besides the transition speed. This method makes it possible to perform a sequential MIMO controller activation on a MIMO system from a SISO controlled system. Furthermore, an example of the stepwise commissioning of a generic MIMO system has been carried out to investigate the underlying dynamics of the transition.

To test if this method holds in practice a case study has been carried out, which focuses on feed water control of a steam boiler at Danish Crown located in Sønderborg. This limits the controller to be a MISO controller and a single input multiple output (SIMO) plant and not a multiple input multiple output (MIMO) controller and plant. A system model developed in a previous student project has been adopted and a parameter identification has been carried out, which is based on data gathered at the Danish Crown steam boiler in the same student project. The difficulties of feed water control has been investigated along with the underlying steam boiler model principles.

The desired feed water controller behavior was determined, which consists of keeping the feed water flow steady and the water level within specified bounds. An optimal observer based MISO feed water controller was designed based on these desired behaviors. Additionally, it was discovered that a steadier feed water flow could be archived by accounting for pressure variations through a pressure feed forward reference. A PI controller was developed by reducing the developed MISO feed water controller to a PI controller, which makes the performance of the two controllers comparable. The stepwise commissioning method was applied on the MISO and PI feed water controller and the specifics of the transition was investigated.

The developed stepwise commissioning controller was implemented on a physical controller, which was verified to have the desired behavior on a lab test setup. The lab test setup uses the steam boiler model to emulate the steam boiler behavior and has the expected physical interface as the Danish Crown steam boiler. An actual test on the real steam boiler at Danish Crown has been carried out, which showed that the designed controllers did have poor performance, as the feed water pump was configured differently than expected. It also showed that the feed forward term improved the controllers steadiness as expected. Additionally, the stepwise commissioning of the MISO controller from the PI controller had almost the same characteristics as in simulation and is therefore considered a success.

Chapter 9

Perspective

This chapter is divided into two sections of which the first section discuss the perspective of the stepwise commissioning method and the second section discuss the perspective of the Steam Boiler case study.

9.1 The Stepwise Commissioning Method

The developed stepwise commissioning method has no considerations regarding robustness to parameter deviations and only considers the stability with nominal system parameters. As the developed method is model-based it would be interesting to determine how robust the transition is to parameter deviations. This question originates from the fact that the characteristics of the transition changed slightly during the test on the real system compared to the simulation. This begs the question of how accurate the model needs to be.

It is equally interesting to investigate if certain types of model errors leads to worse transition results than others. This question originates from the fact that it is possible to initialize the controller before the transition takes place, which allows it to take place in a controlled manner. Consequently, this means that the inactive controllers operate in open loop with information about the real system as input, while it controls a simulated version of the system model.

The practical aspects of this project has only considered a SIMO system and still needs to be tested if the theory scales well with larger systems in practice. It also begs the question whether a performance criteria can be established that can determine the quality of the transition. This is motivated by the fact that no such criteria has been determined in this project, which means that the results is partly free to interpretation. Additionally, this would allow for the design of a detection algorithm, which could abort the transition if the system stability or a performance criteria is violated.

Additionally, the burner controller was determined to be an on/off controller, which is a nonlinear type controller. With this in mind, it could be interesting to determine if the proposed method also has applications for nonlinear systems, as it is known that a nonlinear version of the YKP exists. One place to start could be [Paice and Moore, 1990], which describes the nonlinear YKP.

In classical control theory, bumbles transfer is usually used to archive similar results to the developed method as mentioned in Chapter 1 (Introduction). But it has not been determined if the proposed method produce better results than bumbles transfer, as the focus has primarily been on establishing and testing the concept.

Additionally in Chapter 1 (Introduction) it was suggested that the transition itself could be used as a tuning parameter. In retrospect, this is still a possibility as two controllers, with different bandwidth or some other performance parameter, could be used to characterize a range of controllers. This could potentially lead to easier tunning of MIMO controllers, as controller reconfiguration can be carried out in real time during deployment.

9.2 The Steam Boiler Case Study

When designing the MISO feed water controller, a steam outlet flow estimator was also designed, which was abandoned as it did not produce good steam outlet estimates without the burner signal. This could be included if the burner signal was included as well. However, it would also be possible to determine this signal through multi-model estimation, which essentially selects the model that produce the smallest estimation error amongst a set of models. This approach would be ideal, given the fact that the burner only has a known set of inputs, which is off, half- and full power.

Additionally, some improvements should be made at the Danish Crown steam boiler to make it more suitable for a flow controlled feed water configuration. First of all, the pump is over-dimensioned compared to the steam outlet demand, as the lowest theoretical feed water flow is double the flow of the operating point. For this reason, a smaller pump should be installed which permits continuous operation without hitting actuator saturations. Based on the steadiness test conducted in Section 6.4 (Controller Evaluation) with 100% steam demand, a pump that can operate in the range of 0.2-0.7 kg/s would be ideal for the Danish Crown steam boiler. This would allow both the MISO and MISO+FF controller to avoid actuator saturations under normal operating conditions.

The effects of the opened bypass valve during the test in Danish Crown should be further investigated before additional tests are conducted. It could be especially interesting if this lowers the feed water flow in a predictable way, which would make continuous feed water control easier with over-dimensioned pumps.

Lastly, even though it was not determined if a continuous feed water strategy improves the performance of an on/off controlled deaerator, it does not mean that the same is true for a continuous controlled deaerator.

Bibliography

Anderson, 1998. Brian D. O. Anderson. *From Youla-Kucera to Identification, Adaptive and Nonlinear Control*. Automatica, 34, 1485–1506, 1998.

Antoniou and Lu, 2007. A. Antoniou and W.-S. Lu. *Practical Optimization - Algorithms and Engineering Application*. Springer, 2007.

Bendtsen, Trangbæk, and Stoustrup, 2013. Jan Dimon Bendtsen, Klaus Trangbæk, and Jakob Stoustrup. *Plug-and-Play Control - Modifying Control Systems Online*. IEEE TRANSACTIONS ON CONTROL SYSTEMS TECHNOLOGY, VOL. 21, NO. 1, JANUARY 2013, pages 79–93, 2013.

Flemming Christensen, Februar 2012. Flemming Christensen. *Reflektion/refraktion vs. bølgelængde*, 2012. Vejledermøde i grupperum.

Franklin, Powel, and Emami-Naeini, 2010. Gene F. Franklin, J. David Powel, and Abbas Emami-Naeini. *Feedback Control of Dynamic Systems*. Pearson, sixth edition, 2010. ISBN 978-0-13-500150-9.

Grundfos. Centrifugalpumpen, 2006. URL `https://dk.grundfos.com/content/dam/danish/industries-solutions/centrifugalpumpen_samlet.pdf`.

Grundfos, 2012. Grundfos. *Boiler Feed Manual*. page 30, 2012.

Holmgren, 2007. Magnus Holmgren. *xSteam*, 2007. URL `http://www.mathworks.com/matlabcentral/fileexchange/9817-x-steam--thermodynamic-properties-of-water-and-steam`.

Khalil, 2002. Hassan K. Khalil. *Nonlinear Systems*. 2002.

Knudsen, 2004. Morten Knudsen. *Experimental modelling of dynamic systems*. page 104, 2004.

Sanjay Lall, 2010. Sanjay Lall. *Realization Theory*. Stanford University, 2010. URL `http://lall.stanford.edu/svn/engr207c_2010_to_2011_autumn/data/realization_2008_11_15_03.pdf`.

MathWorks, 2015. MathWorks. *Data Acquisition Toolbox*, 2015. URL `http://se.mathworks.com/products/daq`.

Mortensen, Moelbak, Andersen, and Pedersen, 1998. Jan H. Mortensen, Tommy Moelbak, Palle Andersen, and Tom S. Pedersen. *Optimization of boiler control to improve the load-following capability of power-plant units*. Control Engineering Practice 6 (1998), pages 1531–1539, 1998.

Paice and Moore, **1990**. A.D.B. Paice and J.B. Moore. *On the Youla-Kucera parametrization for nonlinear systems*. Systems & Control Letters, Volume 14, Issue 2, 121–129, 1990.

Bjarni Geir Pétursson. Boiler Feed System - Modelling and Control Analysis. Semester project, Aalborg University - School of Information and Communication Technology, January 2015.

Raimbault, **2015**. Stéphane Raimbault. *libmodbus.org*, 2015. URL `http://libmodbus.org/`.

Ole Sørensen and Palle Andersen. Optimal Control, February 2010.

Åström and Bell, **1999**. Karl J. Åström and Rod Bell. *Drum-Boiler dynamics*. Automatica 36(2000) 363-378, pages 363–378, 1999.

Sugie and Ono, **1989**. Toshiharu Sugie and Toshiro Ono. *On doubly coprime factorizations*. Linear Algebra and its Applications, 122–124, 681–696, 1989.

Vedsted, **2008**. Roy Vedsted. *Kedel- og maskinpasser*. Erhvervsskolernes Forlag, 5 edition, 2008. ISBN 978-87-7881-998-7.

Appendix A
Supplements to the Stepwise Commissioning

A.1 State Space Algebra

This section is based on the state space shorthand notation which is defined by:

Definition A.1 (State Space Shorthand Notation)
Let the discrete time state space system G_i be described by

$$x_i(n+1) = \mathcal{A}_i x(n) + \mathcal{B}_i u(n) \text{ and} \tag{A.1}$$
$$y_i(n) = \mathcal{C}_i x(n) + \mathcal{D}_i u(n). \tag{A.2}$$

The shorthand notation for this system will be given by

$$G_i \stackrel{\text{ss}}{=} \left[\begin{array}{c|c} \mathcal{A}_i & \mathcal{B}_i \\ \hline \mathcal{C}_i & \mathcal{D}_i \end{array}\right]. \tag{A.3}$$

In the following, state space algebra will be stated based on [Lall, 2010, pp. 8-9]. To give a notion of how state space algebra can be implemented in matlab, the corresponding matlab command will be stated using state space objects. State space objects are defined by matlab according to the function

$$G_i \stackrel{\text{ss}}{=} \texttt{ss}\left(\mathcal{A}_i, \mathcal{B}_i, \mathcal{C}_i, \mathcal{D}_i, T_s\right), \tag{A.4}$$

where T_s is the sample time of the discrete time system matrices $\mathcal{A}_i$, $\mathcal{B}_i$, $\mathcal{C}_i$ and $\mathcal{D}_i$.

State Space Addition

$$G_1 + G_2 \stackrel{\text{ss}}{=} \left[\begin{array}{cc|c} \mathcal{A}_1 & 0 & \mathcal{B}_1 \\ 0 & \mathcal{A}_2 & \mathcal{B}_2 \\ \hline \mathcal{C}_1 & \mathcal{C}_2 & \mathcal{D}_1 + \mathcal{D}_2 \end{array}\right] \qquad \text{[Matlab: } G_1 + G_2\text{]} \tag{A.5}$$

State Space Subtraction

$$G_1 - G_2 \stackrel{\text{ss}}{=} \left[\begin{array}{cc|c} \mathcal{A}_1 & 0 & \mathcal{B}_1 \\ 0 & \mathcal{A}_2 & \mathcal{B}_2 \\ \hline \mathcal{C}_1 & -\mathcal{C}_2 & \mathcal{D}_1 - \mathcal{D}_2 \end{array}\right] \qquad \text{[Matlab: } G_1 - G_2\text{]} \tag{A.6}$$

State Space Series Connection

$$G_1G_2 \overset{\text{ss}}{=} \left[\begin{array}{cc|c} \mathcal{A}_1 & \mathcal{B}_1\mathcal{C}_2 & \mathcal{B}_1\mathcal{D}_2 \\ 0 & \mathcal{A}_2 & \mathcal{B}_2 \\ \hline \mathcal{C}_1 & \mathcal{D}_1\mathcal{C}_2 & \mathcal{D}_1\mathcal{D}_2 \end{array}\right] \qquad \text{[Matlab: } \texttt{series}(G_1,G_2)\text{]} \tag{A.7}$$

State Space Inverse If $\mathcal{D}$ is invertible then

$$G^{-1} \overset{\text{ss}}{=} \left[\begin{array}{c|c} \mathcal{A}-\mathcal{B}\mathcal{D}^{-1}\mathcal{C} & -\mathcal{B}\mathcal{D}^{-1} \\ \hline \mathcal{D}^{-1}\mathcal{C} & \mathcal{D}^{-1} \end{array}\right] \qquad \text{[Matlab: } \texttt{inv}(G)\text{]} \tag{A.8}$$

can be used. If $\mathcal{D}$ is left invertible, then the pseudo inverse, denoted by †, equals

$$G^{-1} \overset{\text{ss}}{=} \left[\begin{array}{c|c} \mathcal{A}-\mathcal{B}\mathcal{D}^{\dagger}\mathcal{C} & -\mathcal{B}\mathcal{D}^{\dagger} \\ \hline \mathcal{D}^{\dagger}\mathcal{C} & \mathcal{D}^{\dagger} \end{array}\right]. \tag{A.9}$$

State Space Feedback The common state space feedback loop, using the $\star$-operator, equals

$$G_1 \star G_2 \overset{\text{ss}}{=} \left[\begin{array}{cc|c} \mathcal{A}_1-\mathcal{B}_1\mathcal{C}_2D^{-1}\mathcal{C}_1 & -\mathcal{B}_1\mathcal{D}_2+\mathcal{B}_1\mathcal{C}_2D^{-1}\mathcal{D}_1\mathcal{C}_2 & \mathcal{B}_1-\mathcal{B}_1\mathcal{D}_2D^{-1}\mathcal{D}_1 \\ \mathcal{B}_2D^{-1}\mathcal{C}_1 & \mathcal{A}_2-\mathcal{B}_2D^{-1}\mathcal{D}_1\mathcal{C}_2 & \mathcal{B}_2D^{-1}\mathcal{D}_1 \\ \hline D^{-1}\mathcal{C}_1 & -D^{-1}\mathcal{D}_1\mathcal{C}_2 & D^{-1}\mathcal{D}_1 \end{array}\right]$$

$$\text{[Matlab: } \texttt{feedback}(G_1,G_2)\text{]} \tag{A.10}$$

with $D^{-1}=(I+\mathcal{D}_1\mathcal{D}_2)^{-1}$. Another common feedback construction is

$$(I+G)^{-1} \overset{\text{ss}}{=} \left[\begin{array}{c|c} \mathcal{A}-\mathcal{B}(I+\mathcal{D})^{-1}\mathcal{C} & \mathcal{B}(I+\mathcal{D})^{-1} \\ \hline -(I+\mathcal{D})^{-1}\mathcal{C} & (I+\mathcal{D})^{-1} \end{array}\right]. \quad \text{[Matlab: } \texttt{feedback}(\texttt{eye}(\texttt{length}(G.A)),G)\text{]} \tag{A.11}$$

Appendix B
Supplements to the Danish Crown Boiler Case Study

B.1 Faulty pressure difference argument

In this section, the argument claiming that the pressure difference over the feed water pump cannot be used to estimate the feed water flow is established. The preliminaries are described in Subsection 4.2.1, but specifically the pump head equation (4.1) is needed. It is restated and equals

$$H = \frac{p_{\text{outlet}} - p_{\text{inlet}}}{\rho g} = \frac{\Delta p}{\rho g}. \tag{B.1}$$

The pump curve for the feed water pump for the Danish Crown Boiler is depicted on the next page. The intention is to make an approximate model of the pump curve at 100% pump speed. A least square fit is made through the model according to (B.2), which can be described in terms of H by employing (B.1) and equals (B.3). This model is supplied by Grundfos.

$$\begin{aligned} \Delta p &= -a_2\,\dot{m}^2 + a_1\,\dot{m}\,n + a_0\,n^2 && \text{(B.2)}\\ &= H\,\rho\,g && \text{(B.3)} \end{aligned}$$

Where $\dot{m}$ is the flow [kg/s] and n [-] is the pump speed in percentage. Selecting arbitrary points are $\{(100\,\text{m},\ 12.5\,\text{m}^3/\text{h}),\ (120\,\text{m},\ 11\,\text{m}^3/\text{h}),\ (140\,\text{m},\ 9.2\,\text{m}^3/\text{h}), (160\,\text{m},\ 6\,\text{m}^3/\text{h})\}$ gives the linear system described by the left side of (B.4), of which the parameters can be solved for by employing the pseudo inverse (†) as described by the right side of (B.4).

$$\rho\,g \begin{bmatrix} \dot{m}_1 \\ \dot{m}_2 \\ \dot{m}_3 \\ \dot{m}_4 \end{bmatrix} = \begin{bmatrix} -\dot{m}_1^2 & \dot{m}_1\,n & n^2 \\ -\dot{m}_2^2 & \dot{m}_2\,n & n^2 \\ -\dot{m}_3^2 & \dot{m}_3\,n & n^2 \\ -\dot{m}_4^2 & \dot{m}_4\,n & n^2 \end{bmatrix} \begin{bmatrix} a_2 \\ a_1 \\ a_0 \end{bmatrix} \Rightarrow \begin{bmatrix} a_2 \\ a_1 \\ a_0 \end{bmatrix} = \begin{bmatrix} -\dot{m}_1^2 & \dot{m}_1\,n & n^2 \\ -\dot{m}_2^2 & \dot{m}_2\,n & n^2 \\ -\dot{m}_3^2 & \dot{m}_3\,n & n^2 \\ -\dot{m}_4^2 & \dot{m}_4\,n & n^2 \end{bmatrix}^{\dagger} \begin{bmatrix} \dot{m}_1 \\ \dot{m}_2 \\ \dot{m}_3 \\ \dot{m}_4 \end{bmatrix} \rho\,g = \begin{bmatrix} 1.13 \\ 2.5 \\ 14.6 \end{bmatrix} \tag{B.4}$$

Solving for $\dot{m}$ results in (B.5). Applying this equation on the measured dataset and integrating the calculated feed water flow throughout the day gives a total of 62.2 m^3 of feed water. To put this into perspective, 16.5 m^3 is known to enter the boiler system throughout the day, which makes the calculated feed water result roughly 3.8 times larger than expected. For this reason, the pump model cannot be used to recover the feed water from the pressure difference measurement Δp.

$$\dot{m} = \frac{2a_1 n + \sqrt{4\,a_0\,a_2\,n^2 + a_1^2\,n^2 - 4\,a_2\,\Delta p}}{a_2} \tag{B.5}$$

Company name:	Lenntech BV - lenntech.com
Created by:	info@lenntech.com
Phone:	+31 15 2610900
Fax:	+31 15 2616289
Date:	-

96512570 CRE 10-16 50 Hz

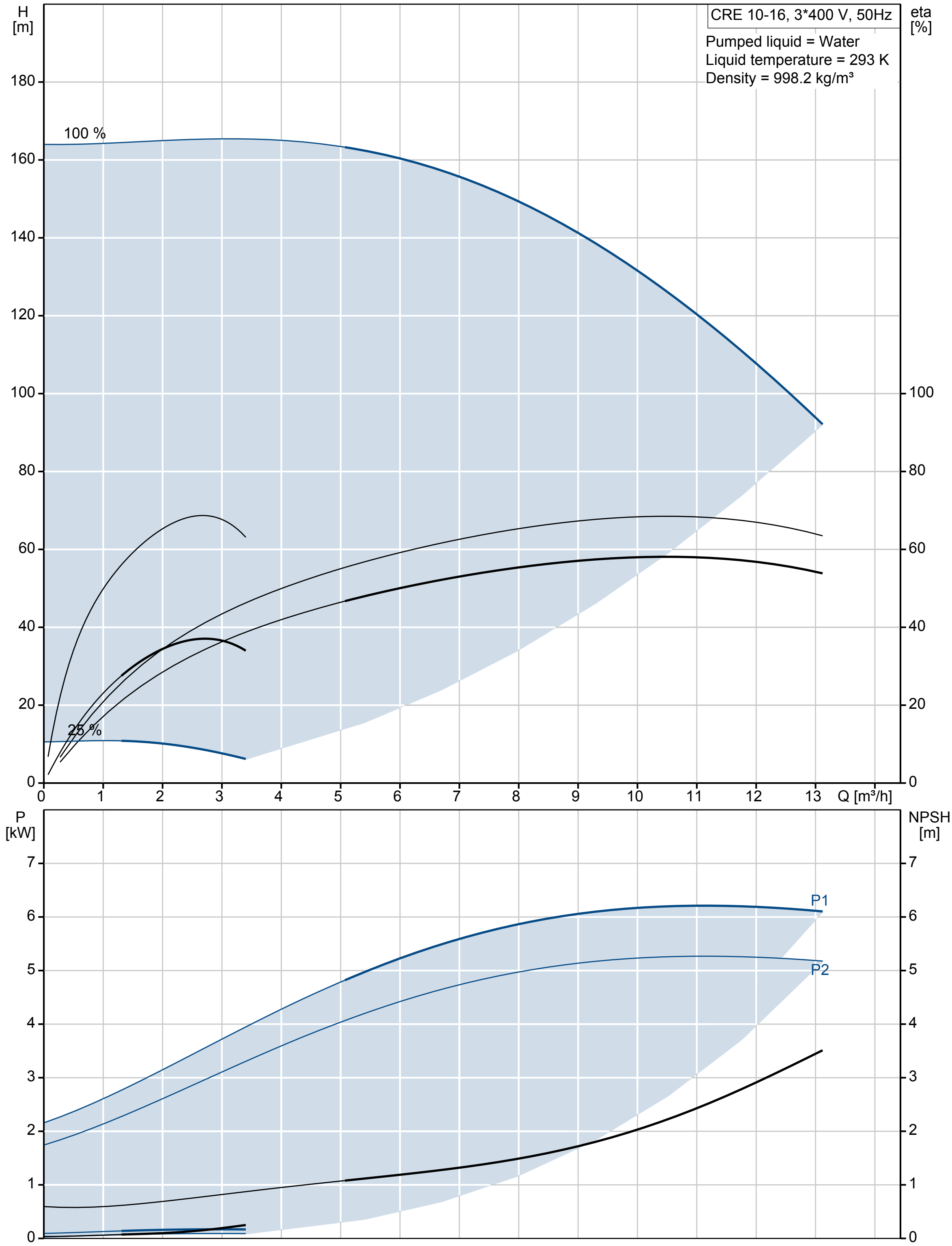

Printed from Grundfos CAPS [2013.03.059]

5/8

B.2 Linearization of the Steam Boiler dynamics

In this section, a strategy for linearizing the system dynamics described in Subsection 5.3.7 (The System Identification Results) is described. It is on the form of (B.6). The linearization will be carried out using a first order Taylor expansion, as described by Definition B.1.

$$J(x)\dot{x} = H(x,u,d) \tag{B.6}$$

Where

$x \in \mathbb{R}^n$ is the system states.
$u \in \mathbb{R}^m$ is the system input.
$d \in \mathbb{R}^k$ is the system disturbance.
$J(x) \in \mathbb{R}^{n\times n}$ is an invertible matrix.
$H(x,u,d) \in \mathbb{R}^n$ is a vector.

Definition B.1 (First Order Taylor Expansion)
Eulers notation for differentiation is adopted, and for simplicity the operating points is written into it, such that

$$D_a f(a_o, b_o) = \left.\frac{df(a,b)}{da}\right|_{a_o,b_o}. \tag{B.7}$$

A first order Taylor expansion of the multivariable function $f(a,b)$ in a_o and b_o is given by:

$$f(a,b) \approxeq f(a_o,\, b_o) + \left.\frac{\partial f(a,\, b)}{\partial a}\right|_{a_o,\, b_o}(a-a_o) + \left.\frac{\partial f(a,\, b)}{\partial b}\right|_{a_o,\, b_o}(b-b_o) \tag{B.8}$$

$$\approxeq f(a_o,\, b_o) + D_a f(a_o,\, b_o)(a-a_o) + D_b f(a_o,\, b_o)(b-b_o) \tag{B.9}$$

Solving for $\dot{x}$ get the system on the proper form and equals

$$\dot{x} = J^{-1}(x)H(x,u,d). \tag{B.10}$$

A first order Taylor expansion in the operating points x_o, $\dot{x}_o$, u_o and d_o is carried out using Definition B.1, and equals

$$\begin{aligned}\dot{x} \approxeq\ & J^{-1}(x_o)H(x_o,\, u_o,\, d_o) + D_x\left[J^{-1}(x_o)H(x_o,\, u_o,\, d_o)\right](x-x_o) + \ldots \\ & J^{-1}(x)D_u H(x_o,\, u_o,\, d_o)(u-u_o) + J^{-1}(x_o)D_d H(x_o,\, u_o,\, d_o)(d-d_o)\end{aligned} \tag{B.11}$$

where

$$D_x\left[J^{-1}(x_o)H(x_o,\, u_o,\, d_o)\right] = D_x J^{-1}(x_o)H(x_o,\, u_o,\, d_o)(x-x_o) + J^{-1}(x_o)D_x H(x_o,\, u_o,\, d_o).$$

As the system is in equilibrium at the operating point, hence $\dot{x} = J^{-1}(x_o)H(x_o,\, u_o,\, d_o) = 0$ reduces the system to

$$\dot{x} \approxeq J^{-1}(x_o)\, D_x H(x_o,\ u_o,\ d_o)\,(x - x_o) + J^{-1}(x_o)\, D_u H(x_o,\ u_o,\ d_o)\,(u - u_o) + \ldots$$
$$J^{-1}(x_o)\, D_d H(x_o,\ u_o,\ d_o)\,(d - d_o)\,.$$

A change of variable according to

$$\delta x = x - x_o, \tag{B.12a}$$
$$\delta \dot{x} = \frac{d\,(\delta x)}{dt} = \frac{d\,(x - x_o)}{dt} = \dot{x}, \tag{B.12b}$$
$$\delta u = u - u_o \text{ and} \tag{B.12c}$$
$$\delta d = d - d_o \tag{B.12d}$$

where δ indicate small signal values, results in

$$J(x_o)\delta\dot{x} = D_x H(x_o,\ u_o,\ d_o)\delta x + D_u H(x_o,\ u_o,\ d_o)\delta u + D_d H(x_o,\ u_o,\ d_o)\delta d. \tag{B.13}$$

Solving for $\delta\dot{x}$ gives the linearized small signal version of (B.6) and its associated linear system matrices, according to:

$$\delta\dot{x} = \underbrace{J^{-1}(x_o) D_x H(x_o,\ u_o,\ d_o)}_{\mathcal{A}_c(x_o,\ u_o,\ d_o)}\delta x + \underbrace{J^{-1}(x_o) D_u H(x_o,\ u_o,\ d_o)}_{\mathcal{B}_{c,u}(x_o,\ u_o,\ d_o)}\delta u + \underbrace{J^{-1}(x_o) D_d H(x_o,\ u_o,\ d_o)}_{\mathcal{B}_{c,d}(x_o,\ u_o,\ d_o)}\delta d \tag{B.14}$$

Where

$\mathcal{A}_c\,(x_o,\ u_o,\ d_o) \in \mathbb{R}^{n\times n}$ is the continuous time state transition matrix.
$\mathcal{B}_{c,u}\,(x_o,\ u_o,\ d_o) \in \mathbb{R}^{n\times m}$ is the continuous time input matrix.
$\mathcal{B}_{c,d}\,(x_o,\ u_o,\ d_o) \in \mathbb{R}^{n\times k}$ is the continuous time disturbance input matrix.

B.3 Linearization of the Steam Boiler Measurement Equations

In this section, the measurement equations described in Subsection 5.2.2 (Measurement Model) are linearized using Definition B.1. The measurement equation has the shape of (B.15), and is linearized using the same approach as the system dynamics in Section B.2.

$$y = h(x) \tag{B.15}$$

Where

$y \in \mathbb{R}^l$ is the measurement vector
$h(x) \in \mathbb{R}^l$ is a vector of measurement equations
$x \in \mathbb{R}^n$ is the state vector

Applying Definition B.1 to (B.15) gives

$$y \approx \underbrace{h(x_o)}_{y_o} + D_x h(x)(x - x_o). \tag{B.16}$$

Where

x_o is the operating point of the states

y_o is the operating point of the measurement

A change of variable according to

$$\delta y = y - y_o = y - h(x_o) \text{ and} \tag{B.17}$$

$$\delta x = x - x_o \tag{B.18}$$

gives the linearized small signal system

$$\delta y = \underbrace{D_x h(x_o)}_{C_c(x_o)} \delta x. \tag{B.19}$$

Where

$C_c(x_o) \in \mathbb{R}^{n \times l}$ is the continuous time output matrix.

B.4 Stepwise Commissioning Test of the Test Setup

In this section a stepwise commissioning test conducted on the lab test setup described in Section 7.2 is described. This is primarily to make sure that the controller works as intended before the real test at danish crown. Additionally, it uses the inverse of the pump curve described in Subsection 7.2.1 (Pump Output Flow Curve). On Figure B.1 a stepwise commissioning test as simulated in Section 6.5 (Stepwise Commissioning Design) has been carried out on the test setup. It confirms that the controller has the desired performance. It is not considered a problem that the burner cannot keep up with the steam outlet demand from 1200 seconds and onwards, as it still allows the controller switching to be validated.

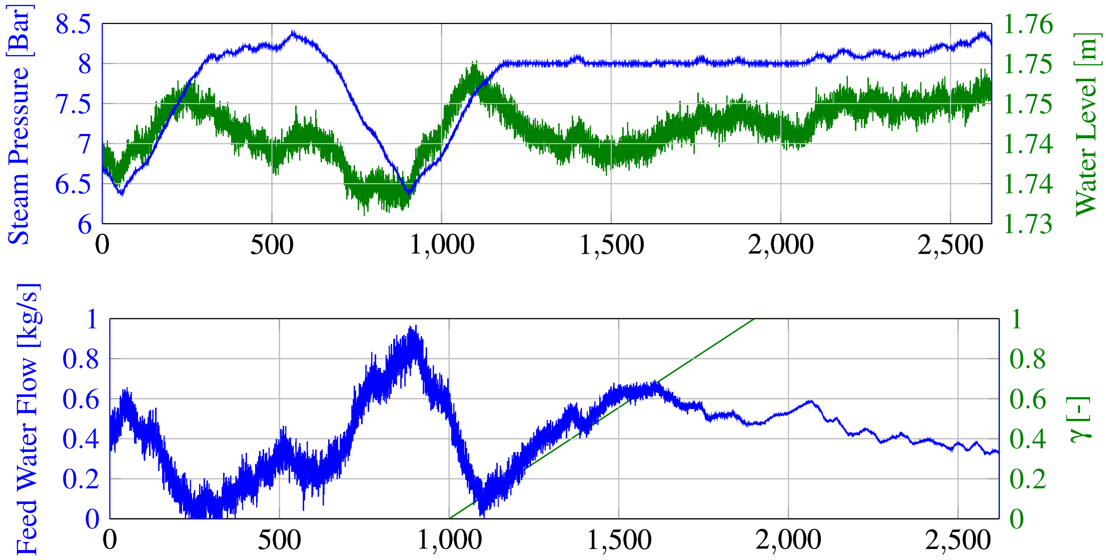

Figure B.1: A stepwise commissioning on the lab test setup with a transition time of 15 minutes with the physical controller.

B.5 Safety Controller

In this section the safety controller is described and tested, which will overwrite the output of the developed controllers in case the water level bounds are not satisfied. The purpose is to guarantee that the water level is between two specified bounds and will be implemented as a hysteresis like controller, similar to the current feed water controller.

Thee water levels are important to the safety controller, which are the lower and upper water level bounds and the operating water level. If the water level drops below the lower water level, then the pump turns completely on until the water level exceed the operating water level. Additionally, if the water level exceed the upper water level, then the pump turns completely off until the water level drops below the operating water level.

On Figure B.2 a test is depicted where the positive and negative water level bound is violated.

Lower Safety Bound Test For the first 600 seconds the pump is manually turned completely off and the water level continuous to drop until the lower safety bound is violated. This is indicated by the Safety Controller State has the value -1 and the control signal turns completely on until the water level reaches the operating water level at around 700 seconds.

Upper Safety Bound Test At around 750 seconds the feed water input is manually completely turned on, which leads to the upper safety bound being violated at around 1100 seconds. This is indicated by the Safety Controller State has the value 1 and the control signal turns completely off until the water level reaches the operating water level at around 1500 seconds.

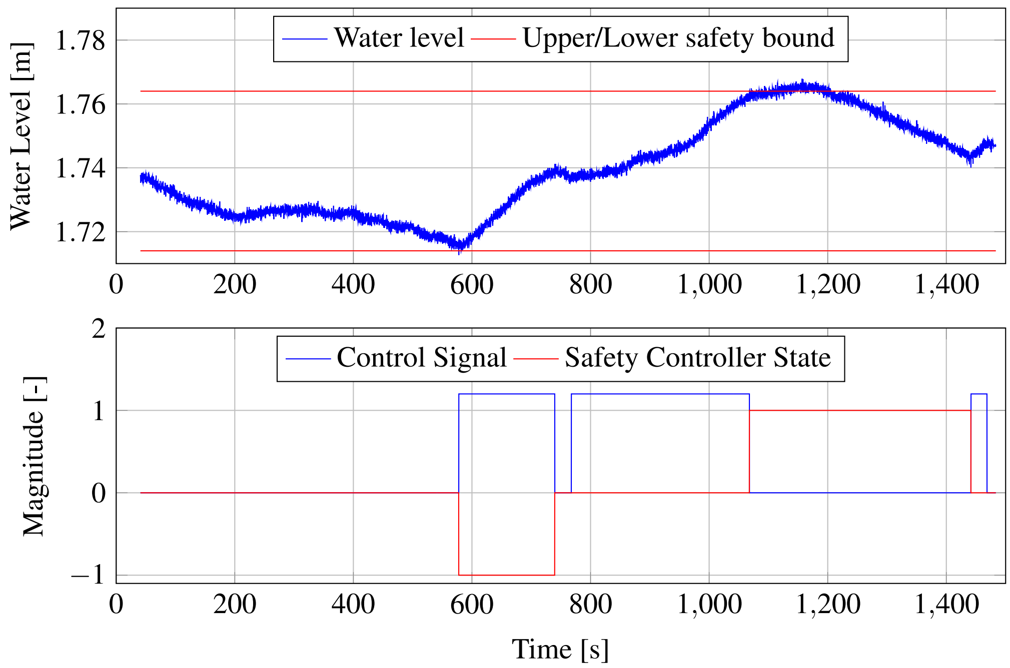

Figure B.2: Safety controller test.

Appendix C

Attached CD

Datasheets

Digital Copy of this Report

Measurement logs